Cape Peninsula
University of Technology

X-Band Antenna Design for Nano-Satellite Applications

by

Sinamandla Mvuyisi Maqina

Thesis submitted in fulfilment of the requirements for the degree

Master of Engineering: Electrical Engineering

in the Faculty of Engineering

at the Cape Peninsula University of Technology

Supervisor: Prof R Lehmensiek

Bellville
March 2018

Declaration

I, Sinamandla Mvuyisi Maqina, declare that the contents of this dissertation/thesis represent my own unaided work, and that the dissertation/thesis has not previously been submitted for academic examination towards any qualification. Furthermore, it represents my own opinions and not necessarily those of the Cape Peninsula University of Technology.

……

SM Maqina
Bellville
March 2018

Acknowledgements

I would like to thank my family, for the opportunity that they have given me to study at the Cape Peninsula University of Technology, for their encouragement, love and support during the period of my studies. I wish to extend my great appreciation to my supervisor, Professor Robert Lehmensiek for the invaluable support and guidance throughout the research project.

Special thanks go to my fellow colleagues for their help, availability, and co-operation in the completion of this project.

Abstract

This research report discusses feasible designs of conformal antennas that provide a proof of concept for the French South African Institute of Technology's future needs. The design is to be used in forthcoming space missions and the intention is to mount the antenna on the surface of a spacecraft. Hence, a low profile is mandatory along with good circular polarisation radiation characteristics. Microstrip patch antennas have been chosen for this purpose simply because they have low profile and conform to most structures, thus fulfilling the requirements stated above. All the designs that are featured in this thesis were modelled and validated using the electromagnetic simulation software FEKO and prototypes were built and tested. The simulations and measured results are supplemented by theory.

Sometimes it can be challenging to design and develop an antenna that fulfils the required performance goals given the size and weight restrictions that are specified for nano-satellite technology. Therefore, the first phase of this project finds a good balance between the criteria set for CubeSat platforms and antenna performance. The second phase is validation. Single patch antennas and a sequential rotated patch array were designed, built and tested. The sequential rotated patch array offers considerable improvements in performance when compared to single patch antennas. For instance, the 3 dB axial ratio bandwidth increased to 9.6 % from 2 % when a sequential rotated array was used.

The CubeSat normally flies in the inclined regions of the low Earth orbit (LEO). This area has high-energy auroral electron fluxes, in which the high-density electrons build up on ungrounded surfaces of spacecraft and cause discharge arcing. The discharge can affect the satellite operation and, in the worst case, cause permanent damage to the components. A mitigation technique by means of a bleeding path provides a quick route to ground and the space-qualified material that is used will ensure that the antenna is robust enough to survive this.

Contents

List of Figures

List of Tables

Glossary and acronyms

Definitions

1U is one unit (10 cm cube).

CubeSat is the type of nano-satellite that uses a 1U standard size and form factor.

Nano-satellite weighs between 1-10 kilograms.

X-band section of electromagnetic spectrum with frequency range between 8 GHz to 12 GHz.

Acronyms

ADCS: Attitude Determination and Control System

AR: Axial Ratio

COTS: Commercial Off-The-Shelf

DST: Department of Science and Technology

F'SATI: French South African Institute of Technology

LEO: Low Earth Orbit

LHCP: Left Hand Circular Polarisation

NRF: National Research Foundation

PERT: Project Evaluation and Review Technique

RHCP: Right Hand Circular Polarisation

SMA: Sub-Miniature Type A connector

SMP: Sub-Miniature Push on connector

TMM: Thermal Microwave Material

VSWR: Voltage Standing Wave Ratio

XANT: X-Band Antenna

XTX: X-Band Transmitter

Chapter 1

Introduction

1.1 Background

The French South African Institute of Technology (F'SATI) based at the Cape Peninsula University of Technology (CPUT), in Bellville, is one of the institutions in South Africa that plays an active role in promoting space related programmes, which involve community outreach and CubeSat platforms. The programme is aimed at the development of human capital in space science and technology, which Africa as a whole is lacking. Postgraduate students also benefit from this initiative, which sees them obtaining an MSc degree in Satellite Systems Engineering through Ecole Supérieure d'Ingénieurs en Electronique et Electrotechnique (ESIEE) University based in France. The programme has a backing from the Department of Science and Technology (DST) and the National Research Foundation (NRF).

FSATI is in the process of developing an X-band transmitter (XTX) and an X-band antenna (XANT). The student role in this development is to investigate the technical feasibility of conformal antennas that can be applicable for space use and adhere to the CubeSat form factor. The concept of nano-satellites was developed in 1999 and since then there has been a growing interest from the academia, public, and private sectors in utilising the miniaturised satellites to conduct scientific experiments and space exploration. These satellites are small in size, for example, a 1-Unit (1U) satellite is a 10 cm cube with a net weight of about 1.1 kg. CubeSats' standard sizes and form factor are shown in Figure 1-1 below.

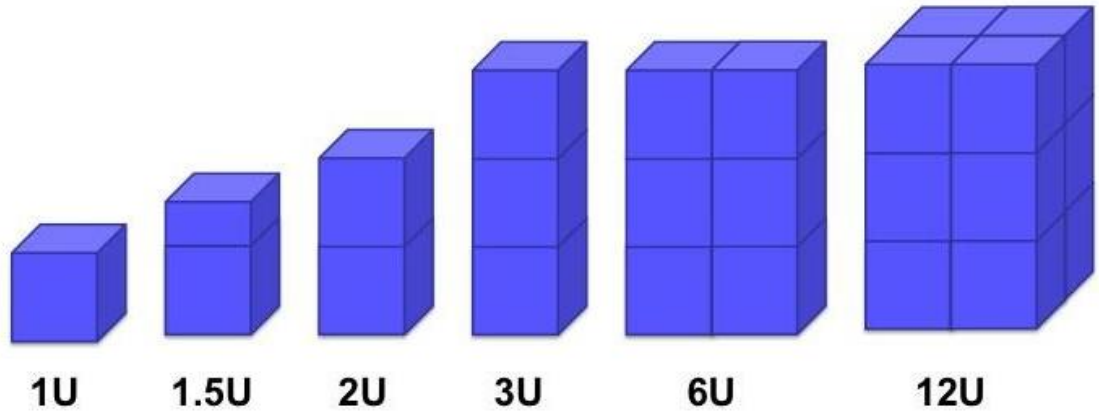

Figure 1-1: CubeSat standard form factors (Adapted from NASA, 2016)

The reduction in size comes with many challenges as it limits the technology that can be used and the weight of the satellite becomes a limiting factor. These satellites however, normally cost a lot less when compared to conventional satellites. They can also be built in a very short period of time and the cost of getting them into space is reduced significantly. This makes the CubeSat platform favourable.

It is also important to study the environment in which the satellite orbits. This will provide a better understanding about effects the space environment has on exposed materials so that mitigation measures can be considered at an early stage of the design process. This in turn ensures the robustness of the components or materials used while maintaining optimal performance. The space environment factors include space radiation, material outgassing, and temperature variations (Huang, 2006:41).

1.2 Statement of the research problem

The miniaturisation of satellites to meet the CubeSat standards limits the size, cost, and weight of the spacecraft. This further limits the technology that can be used. Thus, the main challenge is to satisfy the required performance necessary for a successful space mission given the constraints in size, weight, and cost.

1.3 Research questions

The following questions were used to provide a guideline for this research:

- How these limiting factors mentioned in section 1.2 are going to be balanced?
- What type of antenna geometry can provide the best possible results?
- How is space an extreme environment?
- What is a suitable material needed to ensure the robustness of the antenna in space?

1.4 Objectives of the research

- The main objective of this research project is to study and design a suitable X-band antenna that conforms to the CubeSat form factor.
- The antenna should be compact and lightweight.
- It should also be compatible with a 50 Ω system.

1.5 Methodology

The methodology that made this research work to be effective, convenient, and efficient is illustrated in Figure 1-2. The initial step was to conduct a literature study on relevant sources such as books on antennas, journals, course notes, and personal interviews with people who have a great hands-on experience in antennas. This has helped in the formulation of an idea on the type of antenna to use, as there has been a great study on antennas for the past decades. Once the idea is known, the proposed antenna is designed, modelled, and simulated using the electromagnetic (EM) simulation software package FEKO[1]. The software has different solvers that could be used depending on the type of problem, so before commencing with simulations, there would be a need to associate the problem at hand to a suitable solver.

Furthermore, the modelling or simulation results should be able to give an insight on the expected performance of the prototype. However, its accuracy could only be determined after the simulated results are compared to the measured results. If the simulated results yield the expected performance, then the antenna will be prototyped to realise the results.

[1] https://www.feko.info

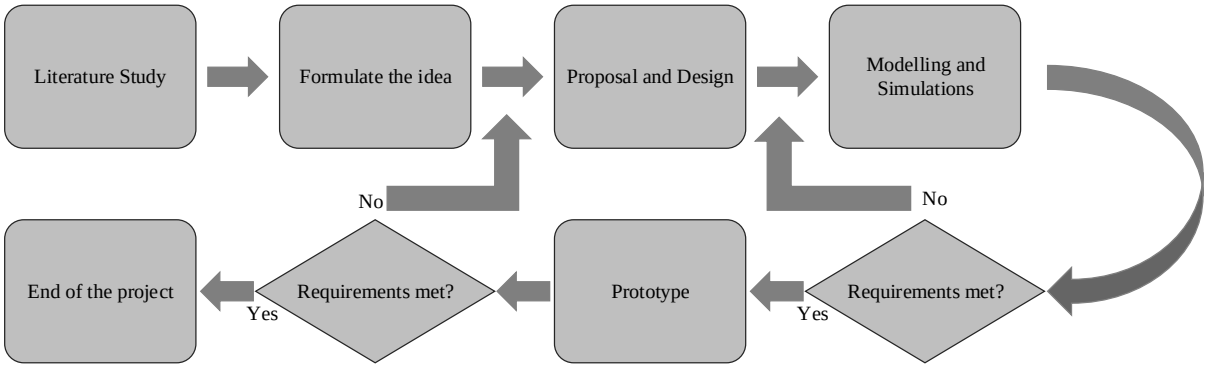

Figure 1-2: Work structure

1.6 Delineation

The scope of this study on antennas suitable for space use will be limited to microstrip antennas. These antennas have a low profile, which suits the intended application, but they provide low gain and narrow bandwidth. Thus, this research concentrates on optimising the bandwidth, matching and axial ratio. Different shapes and feeding mechanisms will also be looked at for comparison.

1.7 Significance of the research

The study into technical feasibility of X-band antennas would facilitate the growing need of transmitting at higher frequencies. It will also provide a proof of concept for future antenna development at F'SATI.

1.8 Expected outcomes

- Antenna topologies or prototypes, which are supported by design guidelines and theory.

1.9 Outline of the thesis

This thesis is divided into five chapters as is shown in Figure 1-3.

Chapter 1 provides a general background about the institution, methodology, the significance of this research work and the expected outcomes. It also highlights the focal point and the

challenges that have been faced by the CubeSat enthusiasts since the miniaturised version of the conventional satellites began.

Chapter 2 this chapter mainly focuses on technical theory relating to antennas. Performance parameters such as bandwidth, directivity, efficiency, gain, and polarisation are presented in this section. Microstrip patch antennas are discussed here and different feeding techniques are looked at with the intent to study each effect on antenna performance so that a definitive and systematic decision could be made.

Chapter 3 this section of work provides an analysis of the simulation results. Design models and explanations on decisions taken regarding suitable antenna materials are presented here.

Chapter 4 the prototype is presented here. The measured results are analysed and compared to the simulated results in order to verify the accuracy of the models.

Chapter 5 presents conclusions and recommendations.

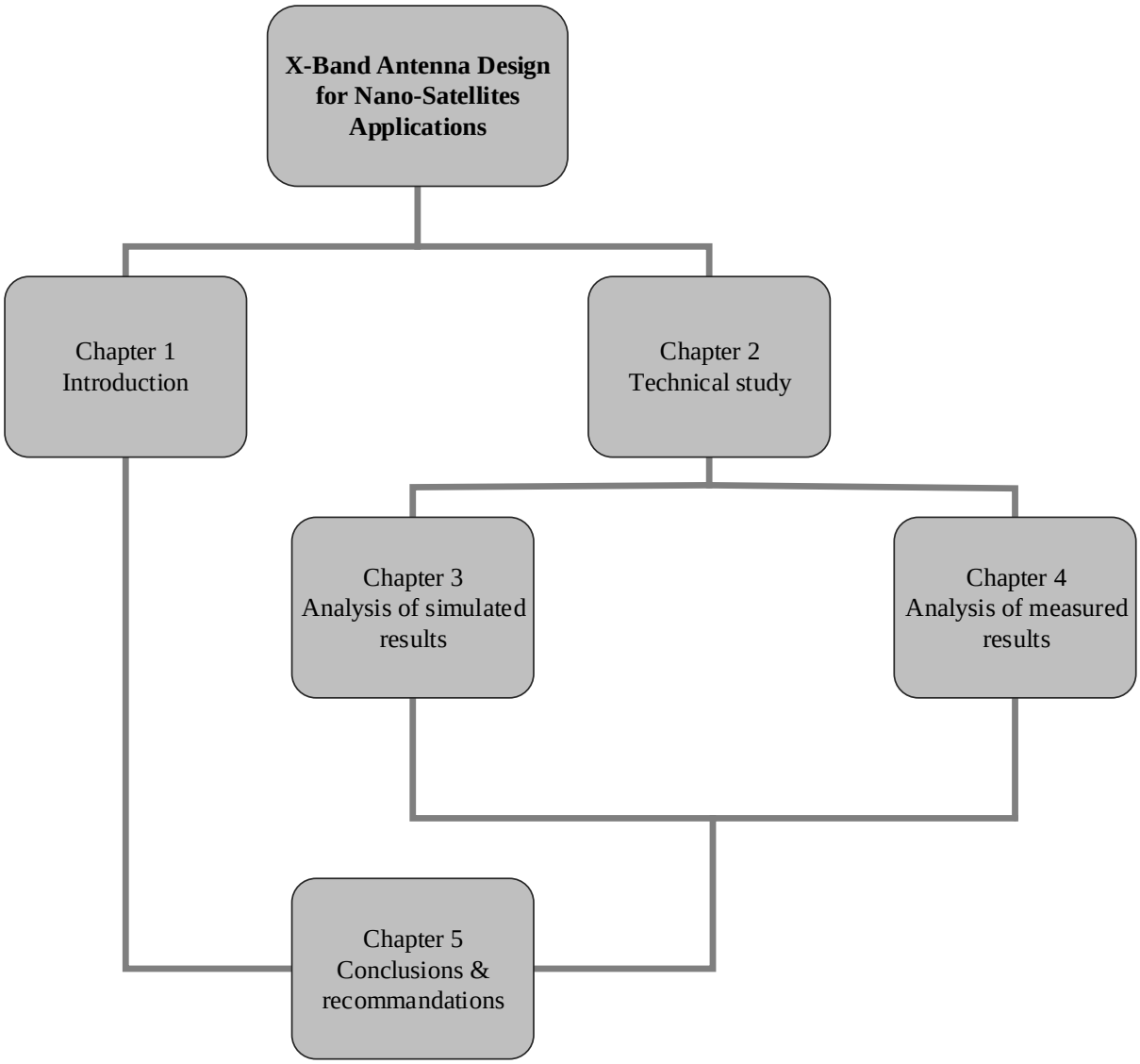

Figure 1-3: Research structure

Chapter 2

Technical Study

2.1 General overview

Space missions are heavily dependent on communication systems in order to relay information between Earth and spacecraft. Without communication, there would be no space explorations or missions. Figure 2-1 shows a space communication link.

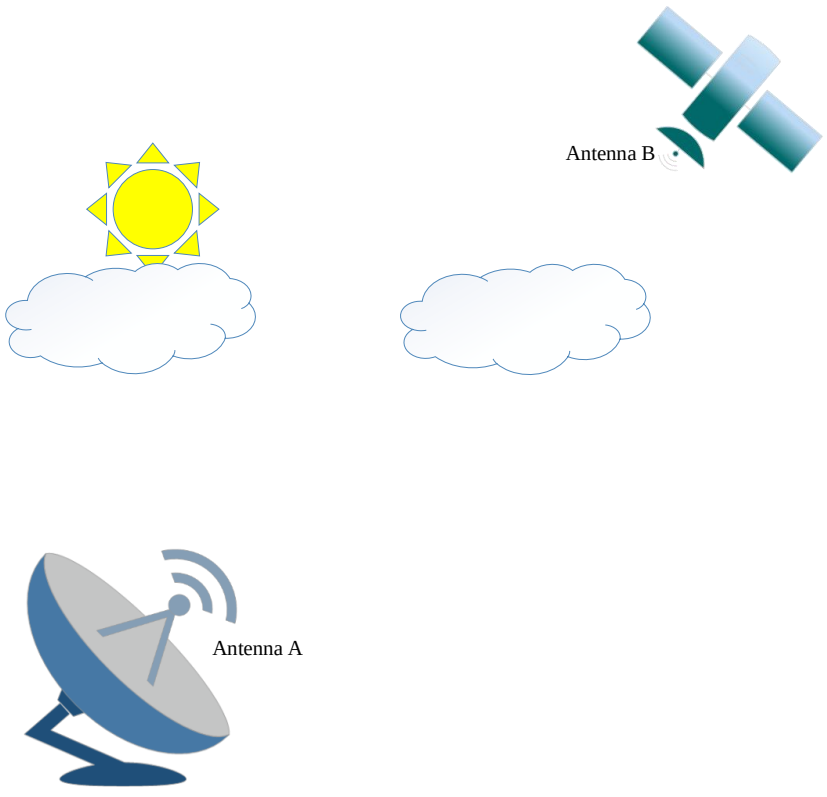

Figure 2-1: Space communication link

From this figure, it can be seen that the information sent from either ends of this communication link, is propagated through free space. In wireless communication, antennas are at the forefront, and are regarded as transducers. They are able to convert electrical energy into electromagnetic (EM) waves during transmission and are also able to convert EM waves into electrical signals during reception. The popular antenna types in nano-satellites are deployable and non-deployable conformal antennas. Figure 2-2 presents examples of deployable and non-deployable conformal antennas mounted on a 1U CubeSat form factor.

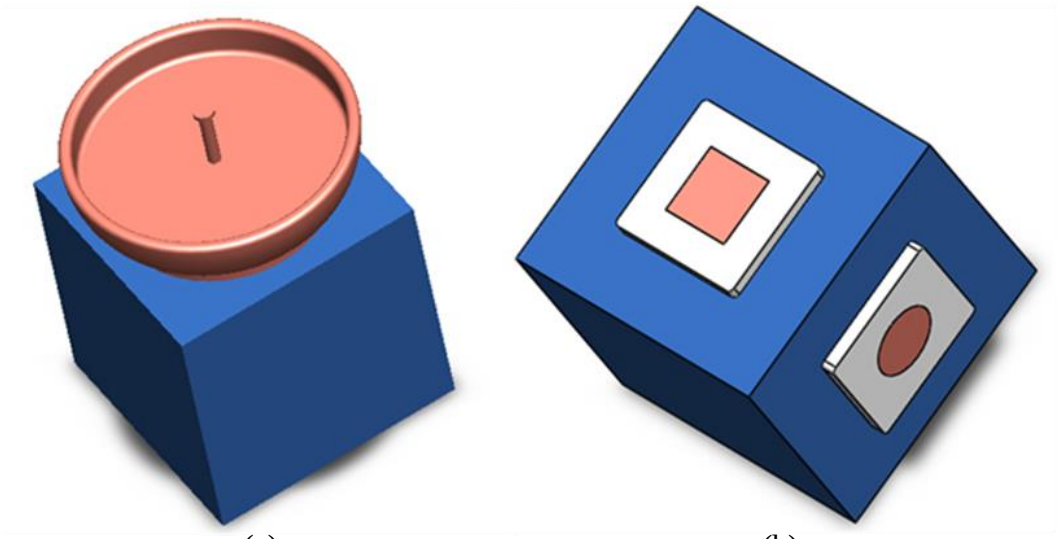

(a) (b)

Figure 2-2: Popular antenna types on a 1U CubeSat: (a) Deployed antenna (b) conformal antennas

Deployable antennas may require sophisticated mechanisms that occupy a certain volume of the CubeSat. Such systems usually add more costs to the satellite program, and there are potential risks involved. For example, the mission will not commence if the antenna fails to deploy. The non-deployable antennas on the other hand can be made to conform to the structure of the satellite and can occupy small volumes. According to Farr and Henderson (2014:26), there is a great need for low profile antenna designs to mate with the surface of the satellite as much as there is growing need for deployable antennas. The scope of this thesis will be limited to conformal antennas.

One type of conformal antenna is the patch antenna. This antenna is simple, has an extremely low profile, is conformable to different structures, and can be made into a variety of shapes. The microstrip antenna as shown in Figure 2-3 below is made from a metallic patch placed on top of a grounded substrate material that provides mechanical support (Jackson, 2007). The drawback of patch antennas is their low gain and narrow bandwidth (Balanis, 2005:811). Nonetheless, there are ways to mitigate some of these challenges like using different feeding mechanisms, thicker substrates, the use of substrate with lower permittivity or array to obtain higher gain. Furthermore, it is necessary to study the effects of the environment in which the antenna is going to operate, to ensure that the material used survives the conditions when exposed.

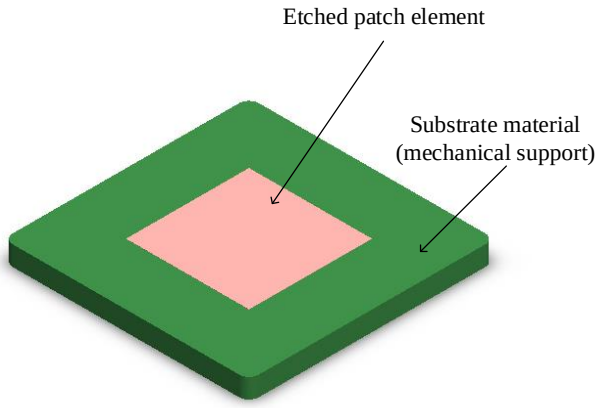

Figure 2-3: Basic microstrip patch antenna

In summary, this chapter will discuss antenna properties and highlights the space environmental factors that may affect antenna performance and durability.

2.2 Antenna properties

According to Balanis (2005:27), it is not necessary to specify all antenna properties in order to get a complete description of the antenna performance as some parameters are interrelated. A microstrip antenna as shown in Figure 2-3 will be the subject of this study and the bandwidth, directivity, radiation efficiency, input impedance and polarisation are the parameters that are discussed in this section.

2.2.1 Directivity and Gain

The manner in which the antenna concentrates its energy in one direction as compared to other directions is one of the most important aspects in antennas theory (Stutzman & Thiele, 2013:50). Antennas are categorised into three types namely: isotropic, directional and omni-directional. Figure 2-4 below shows some of the radiation patterns.

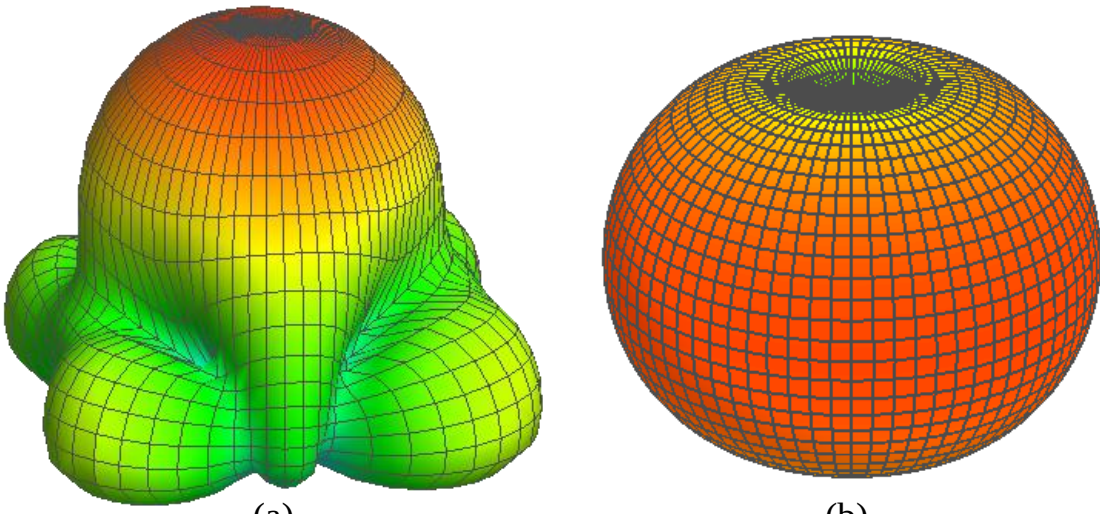

(a) (b)

Figure 2-4: Three dimensional antenna radiation patterns: (a) Directional (b) Omni-directional

An isotropic antenna is described as the antenna type that emits energy equally in all directions. This type of antenna is not realisable but it is often used as the reference antenna for expressing the directive properties of the physical antenna (Balanis, 2005:33). The directional antennas as the name suggests are antennas, which radiate energy more efficiently in some directions in reference to other directions. These types of antennas can have a narrow beamwidth, which means that energy can be diverted in that particular direction for farther distances or stronger communication links. However, as the beamwidth narrows, the coverage area reduces and side lobes, which may present radiation in undesired directions, begin to form. Consequently, the antenna will need to point in the direction of desired coverage, which can be challenging for a low cost CubeSat that has a limited attitude determination and control system (ADCS). A compromise needs to be made between signal quality and coverage. Omni-directional (hemispherical) antennas can provide such trade-off, as they are directional in one plane and constant in another (Balanis, 2005:33).

Directivity of an antenna is the ratio of radiation intensity (U) obtained in a main direction (θ, φ) from the antenna to the radiation intensity of an isotropic antenna (U_{iso}) as given in equation 2-1. (See Figure 2-5 for the coordinates system). Corresponding to directivity is gain, which takes into account the losses, and can be described as the ratio of radiation intensity in a given direction to the radiation intensity that would be achieved if the input power of the antenna were radiated isotropically (Balanis, 2005:66). This gain does not include the losses due to mismatch. Thus, the realised gain ($G_{realised}$) as given in equation 2-2 includes mismatch losses and can be express in terms of directivity.

$$D = \frac{U}{U_{iso}} = \frac{4\pi U}{P_{rad}} \qquad 2\text{-}1$$

$$G_{realised} = \left(1 - |S_{11}|^2\right)\eta D \qquad 2\text{-}2$$

Where:

D denotes the directivity

P_{rad} is the total radiated power.

η is the radiation efficiency and

S_{11} reflection coefficient expressed in a linear scale

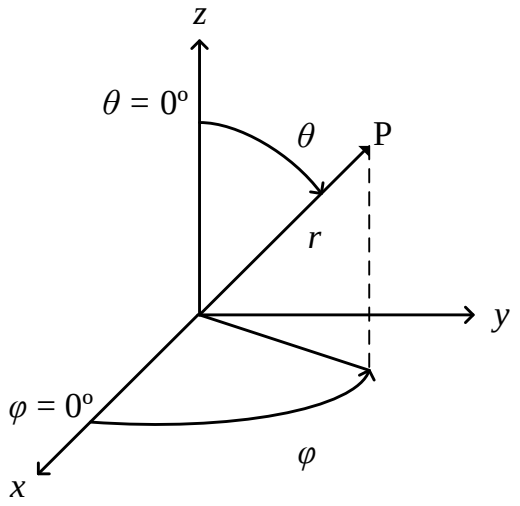

Figure 2-5: Antenna measurement coordinate system

2.2.2 Polarisation

In satellite communication, propagation effects such as polarisation rotation can affect the performance of a communication system. The interaction of radio waves with electrons in the ionosphere may alter the polarisation of these waves (Ippolito, 1999). This effect is often called Faraday's rotation and is not a concern for circularly polarised fields. The antenna can be linearly, circularly, or elliptically polarised and can be determined by plane of the electric fields (*E* fields). In general, polarisation is defined by three parameters namely: axial ratio, tilt angle and sense of rotation (Garg, Bhartia, Bahl, & Ittipiboon, 2001:493). These parameters are not all always applicable; it depends on the type of polarisation. For example, axial ratio for linearly polarised fields is equal to zero and tilt angle defines the orientation.

Since the antenna is for space use, only circular polarisation will be considered. The conditions needed to satisfy circular polarisation whether it is right hand or left hand are listed below. These conditions are taken from *Antenna Theory Analysis and Design* (Balanis, 2005).

- The fields must have two orthogonal linear components.
- The components must have the same magnitude.
- The two components must have a time-phase difference of odd multiples of 90°.

Ideally, the receiving antenna polarisation should match the polarisation of the incoming waves. This however is not always the case as the polarisation is likely to be mismatched and as a result, the maximum amount of power will not be extracted from the incoming waves because of polarisation losses (Balanis, 2005:76). Polarisation loss factor can be used as the figure of merit to determine how much power the receiving antenna can extract from the incoming waves given the angle between the two vectors. If for example the linearly polarised vectors are considered, and the first scenario is when they are perfectly aligned, all the power will be transferred to the antenna however if there is an angle between the vectors there will be losses and the worst case is when the angle is 90°. This is illustrated in Figure 2-6 and Table 2-1 summarises the polarisation losses in a communication link.

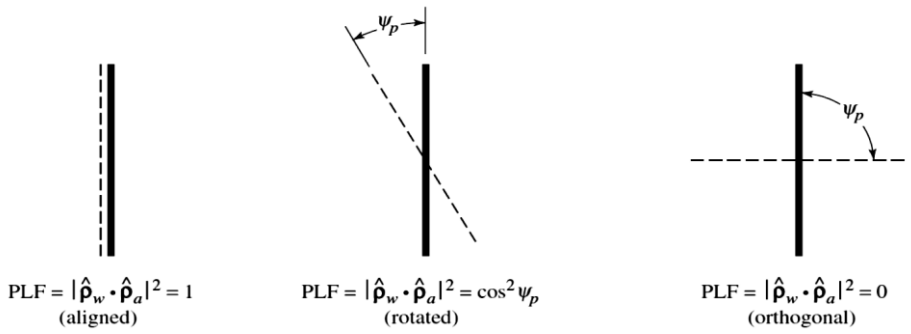

Figure 2-6: Polarisation loss factor of a wire antenna (Adapted from Balanis, 2005)

Table 2-1: Losses due to polarisation mismatch (Reckeweg & Rhohner, 2015:8)

Polarisation of a transmitting antenna	Polarisation of a receiving antenna	Losses [dB]
Vertical	Vertical	0
Vertical	45°	3
Vertical	Horizontal	∞
Horizontal	Horizontal	0
Vertical	Circularly	3
Left hand side circularly	Left hand side circularly	0
Left hand side circularly	Right hand side circularly	∞

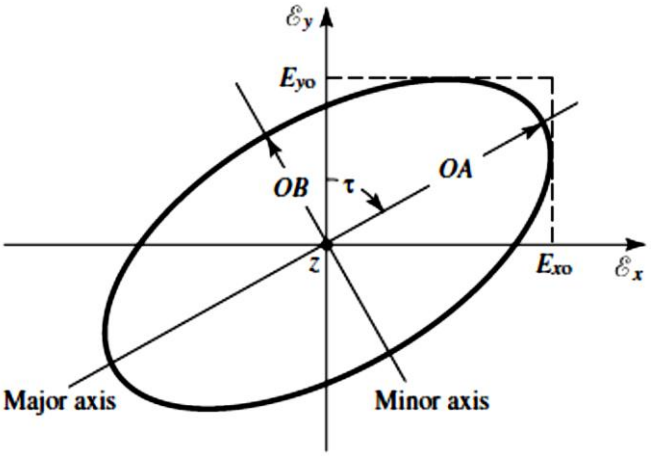

Figure 2-7: Rotation of a plane electromagnetic wave (Adapted from Balanis, 2005)

With reference to Figure 2-7, an axial ratio (AR) is the ratio of major axis to the minor axis of the polarisation ellipse and it can be used as a measure of circular polarisation purity. In practice, it is difficult to obtain perfect circularly polarised fields and, in most cases, fields are usually elliptical. Thus, the major axis divided by minor axis of this ellipse is used to determine the axial ratio as given in equation 2-3. Since a circle has the major axis equal to the minor axis, the axial ratio should be equal to 1 or 0 dB.

$$\mathrm{AR} = \frac{\text{Major axis}}{\text{Minor axis}} \qquad 2\text{-}3$$

2.2.3 Input impedance

Input impedance is one of the significant parameters of an antenna. In a general form, the input impedance is complex, that is, it contains both the real and imaginary (reactive) parts, and it is a function of frequency. This impedance, presented at the input port of an antenna (see Figure 2.8), is given in equation 2-4. The real part takes into account radiation resistance and the loss resistance. According to Reckeweg and Rhohner (2015:14), radiation resistance is spatially dependent thus when specified it is imperative to indicate its location on the antenna.

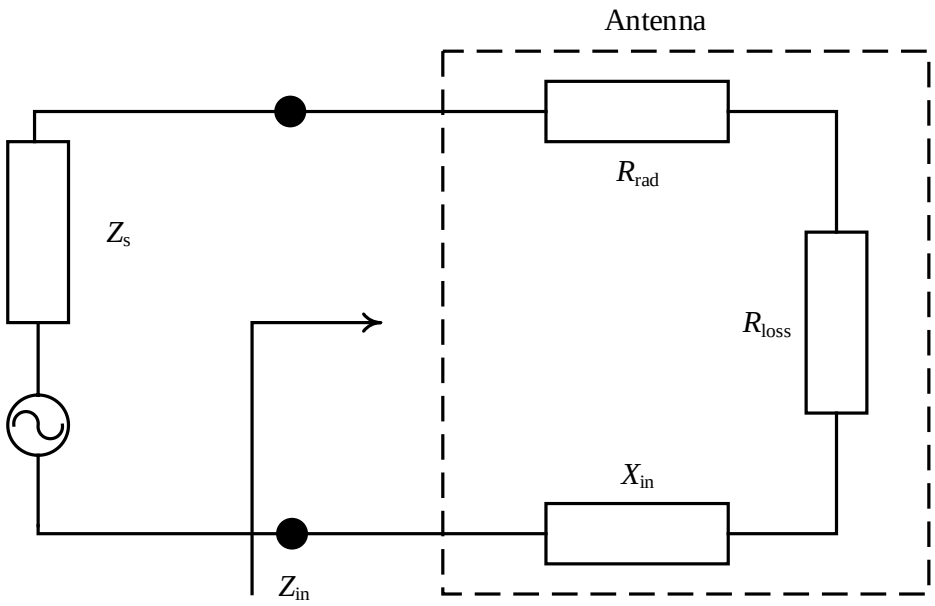

Figure 2-8: Equivalent circuit diagram of a transmitting antenna

$$Z_{in} = (R_{rad} + R_{loss}) \pm jX_{in} \quad \Omega \qquad 2\text{-}4$$

For maximum power transfer, the input impedance must be equal to the conjugate of the source impedance. An ideal case is to have the input impedance at resonance equal to the system characteristic impedance, which is normally 50 Ω. Sometimes it can be challenging to obtain this and for better matching, the impedance can be transformed to the system characteristic impedance by the use of matching networks or impedance transformers. From equation 2-5, it can be seen that if the input impedance is complex and not equal to the system characteristic impedance, then the matching will be poor. Proper matching ensures maximum power transfer and minimum reflection. The input impedance can also be influenced by the geometry of the antenna and the feeding techniques (Balanis, 2005:85). Table 2-2 below, summarises the parameters that determine the degree of matching.

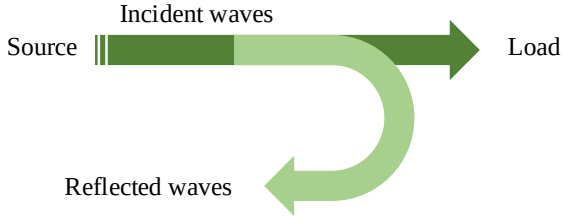

Figure 2-9: Representation of incident and reflected power waves due to impedance mismatch

$$\Gamma = \frac{Z_{in} - Z_0}{Z_{in} + Z_0} \qquad 2\text{-}5$$

Table 2-2: Comparison of reflection coefficient, VSWR, and return loss

Parameter	Good	Moderate	Bad
Γ	0	0.33	1
Voltage Standing Wave Ratio (VSWR)	1	2	∞
Return Loss [dB]	∞	10	0

2.2.4 Radiation efficiency

A radiating antenna receives power from a source and radiates it into space; hence, the ratio of the radiated power to the input power is referred to as radiation efficiency (Balanis, 2005:854). The efficiency includes losses at the feeding point of the antenna and losses due to the physical structure. These losses are mismatch losses, conduction and dielectric or material losses. Mathematically, the radiation efficiency is defined by equation 2-6 (Garg *et al*, 2001:285).

$$\eta = \frac{P_{rad}}{P_{rad} + P_c + P_d + P_{sw}} \qquad 2\text{-}6$$

Where:

P_{rad} is the radiated power

P_c is the conduction losses

P_d is the dielectric losses and

P_{sw} is the surface wave

Equation 2-6 does not include mismatch losses and according to (Narbudowicz, 2013:11) the total efficiency includes mismatch losses as given by equation 2-7.

$$\eta_{total} = \left(1 - |S_{11}|^2\right)\eta \qquad 2\text{-}7$$

The power dissipated in low loss substrates at microwave frequencies is usually insignificant (Garg *et al*, 2001:285), thus, the dielectric and conduction losses can be neglected. Figure 2-10 shows a plot of radiation efficiency of a rectangular patch antenna as a function of frequency for different substrate materials. The substrate thickness is kept constant at 1.52 mm for all the materials to compare the influence of substrate permittivity on efficiency. From this figure, it can be deduced that the efficiency decreases with increasing substrate dielectric. This is because substrates with higher dielectric constant contain the electric fields, that is, they reduce the amount of fringing fields (Garg *et al*, 2001:287).

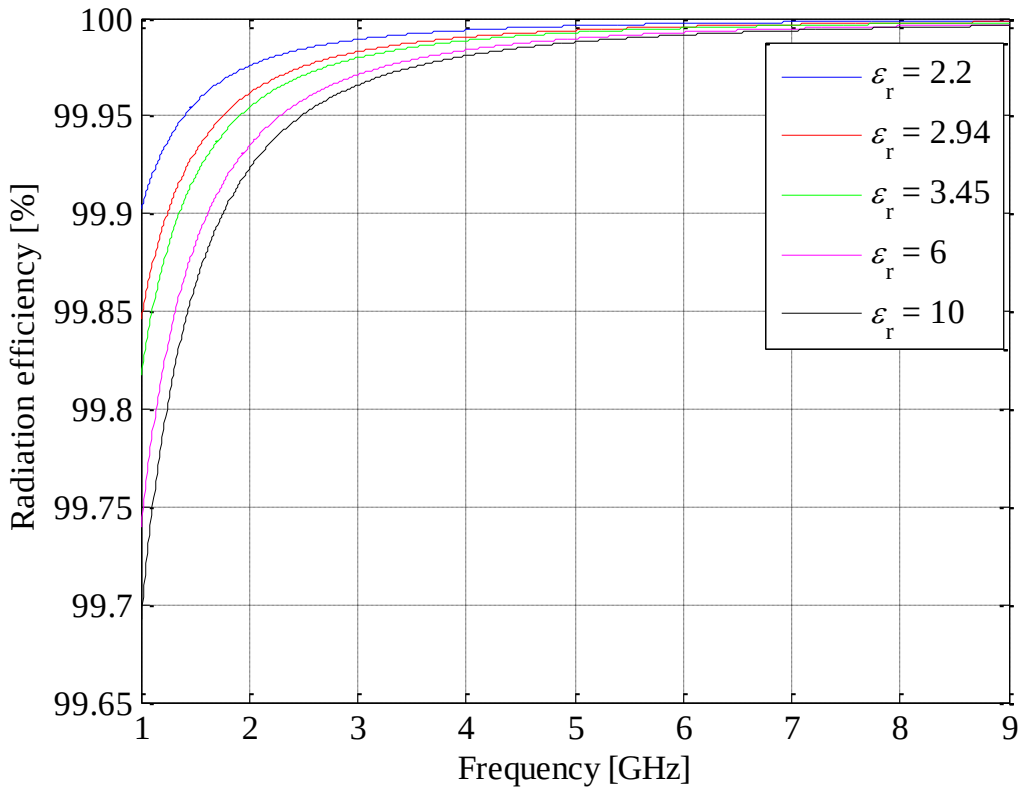

Figure 2-10: Radiation efficiency of a rectangular patch antenna versus frequency for substrate height (*h* = 1.52 mm)

Figure 2-11, shows efficiency as a function of height for five different substrate materials. The plots are generated from the equations presented by Jackson and Alexopoulos (1991:407). From this figure, it can be seen that substrates with low dielectric constant are more efficient than

substrates with higher dielectric constants. Also, the efficiency decreases with increasing substrate thickness.

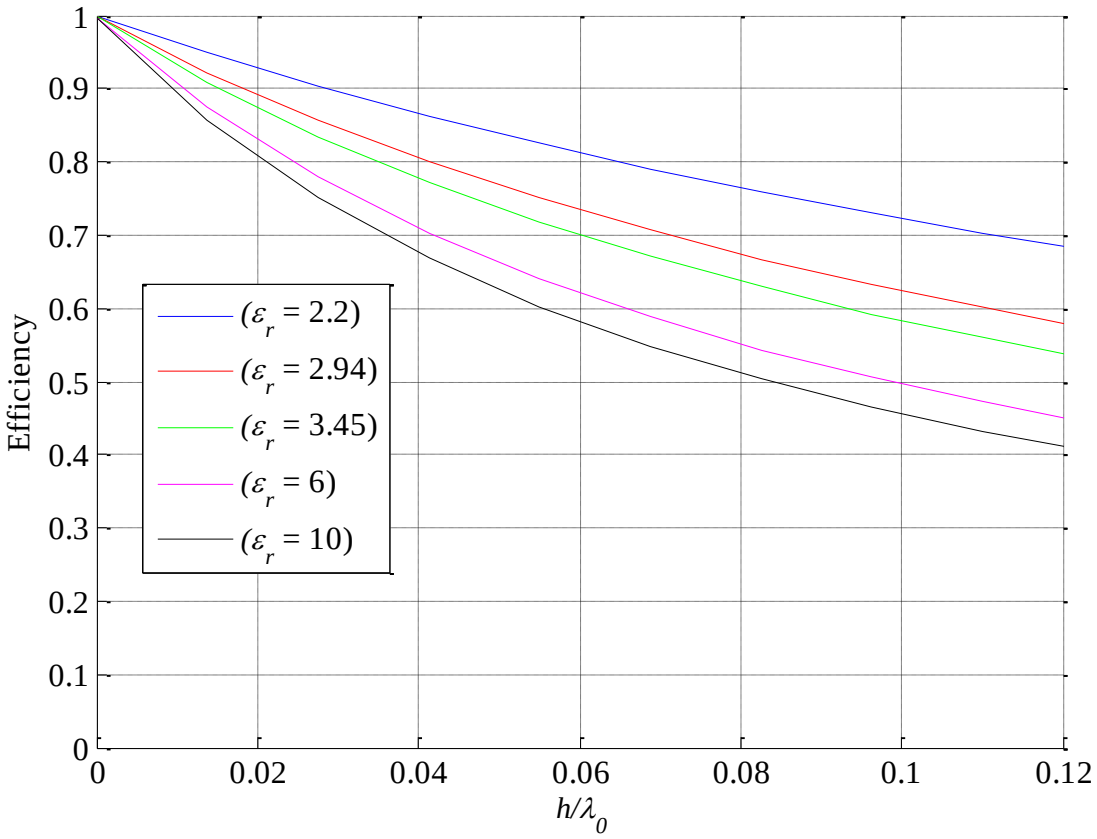

Figure 2-11: Efficiency versus substrate thickness at 8.25 GHz

The surface waves can degrade the radiation efficiency since their power increases with increasing substrate thickness. They are always present because their dominant mode has a cut-off frequency equal to zero. The power transferred into the surface waves does not contribute to the desired radiated power, but it is diffracted at the edge of the substrate as illustrated in Figure 2-12, resulting in spurious radiation (Kristensson, Waller & Dernery, 2001:1). According to Jackson *et al* (1993), surface wave excitation may result in an increase of mutual coupling between distant antenna elements (in arrays) since the decay is slower with radial distance compared to the space wave radiation.

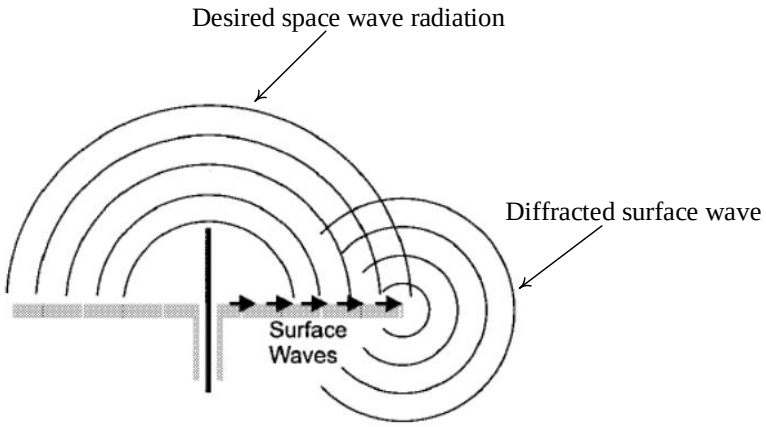

Figure 2-12: Illustration of surface waves (Adapted from D. Sievenpiper, L. Zhang, R. F. Broas, N. G. Alexopolous & E. Yablonovitch, 1999)

Fortunately, there are ways to minimise the effects of surface waves. The techniques include the use of thicker foam as a substrate material, or the substrate may be cut in such a way that it does not extend beyond the patch etching, or the periodic structure may be etched around the patch to form an electromagnetic band gap (Jackson, 2007) or the use of peripheral chokes.

2.2.5 Bandwidth

Antenna bandwidth is one of the fundamental properties of the antenna. It defines the range of frequencies over which the antenna can fulfil the specified requirements (Balanis, 2005:70). According to Pozar (1995), the specification of an antenna may involve a number of parameters; thus, it is important to specify the criteria used when antenna bandwidth is mentioned. For instance, antenna gain, beamwidth, and polarisation can be categorised as pattern bandwidth while input impedance and radiation efficiency are associated with impedance bandwidth (Balanis, 2005:70). The pattern bandwidth considers a single frequency point and one cut plane at a time whereas the impedance bandwidth examines the range of frequencies.

In the case of microstrip patch antennas, the bandwidth is a function of substrate thickness and permittivity; this is shown by equation 2-8 (Milligan, 2005:294). According to this equation, the bandwidth (BW) increases with the substrate thickness (h) and low permittivity (ε_r) assuming that the ratio of width (W) to length (L) of the patch is fixed.

$$BW = \frac{16 C_1 phW}{3\sqrt{2}\eta \varepsilon_r \lambda_0 L} \qquad 2\text{-}8$$

Where:

$$C_1 = 1 - \frac{1}{n^2} + \frac{0.4}{n^4}$$

n is the index of refraction

p is the ratio of patch radiated power to the total power produced by the corresponding patch surface current

Factors associated with feeding techniques can limit the achievable bandwidth. For example, in a coaxial fed microstrip patch antenna, the inductance increases with increasing coaxial probe length and this will result in an inductive input impedance that is not desirable. In most antennas, frequency points with a –10 dB or VSWR $\leq$ 2 are normally taken as a point of reference for impedance bandwidth. Feeding mechanisms and their effects on the performance of the antenna are discussed in the last sections of this chapter. Different techniques to increase antenna bandwidth have been suggested in *Antenna Engineering Handbook by Volakis* (2007). Jackson and Alexopoulos (1991) have demonstrated that approximate formulas can be used to provide insight on how the substrate material parameters influence the performance of a microstrip patch antenna. Figure 2-13 below shows a plot of a bandwidth versus substrate thickness (*h*) normalised to free space wavelength (λ_0). According to this figure, substrates with higher dielectric constants have a narrow bandwidth. This is because fields are contained closer to the substrate resulting in higher *Q* values. The *Q* factor is determined by the ratio of energy stored to the energy dissipated.

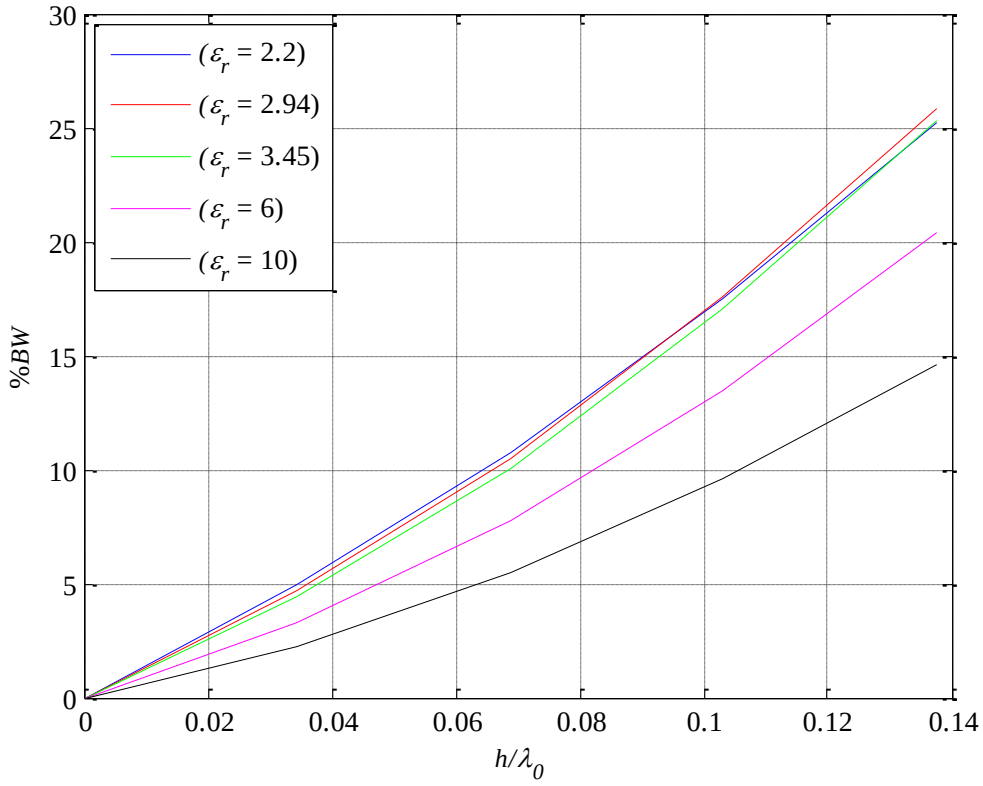

Figure 2-13: Bandwidth versus substrate thickness

2.3 Environment factors

Most nano-satellites fly in the low Earth orbit where material used to make up the antenna is likely to be exposed to radiation, temperature variations, material outgassing, and internal charging. In order to mitigate the effects of these environmental factors whilst ensuring that the antenna performs optimally, the material used as the support structure should meet most if not all the criteria needed for space applications. The effects of space environment are discussed below.

2.3.1 Material outgassing

Space is a high vacuum environment. According to Huang (2006:42), outgassing can cause a material to lose its mass in the form of gases or volatile condensable matter when subject to vacuum. Because of this phenomenon, the material may lose its mechanical and electrical properties. A low outgassing criterion is a necessity for space applications. Materials with total mass loss (TML) greater than 1% and collected volatile condensable material (CVCM) greater

than 0.1% are not recommended for use in space applications (Huang, 2006:43). Material companies such as Rogers Corporation have developed substrate materials that fulfil the conditions set for outgassing, which means that such materials can be used in space applications.

2.3.2 Radiation exposure

Space radiation originates from different sources. A continuous exposure of material to radiation may cause damages, which can also affect its electrical characteristics. Consequently, the material for space applications should be able to retain its properties when exposed to radiation.

2.3.3 Temperature variations

Wide temperature variations can affect both the physical and electrical properties of a substrate material. For instance, if the material is exposed to extremely high temperatures, which is likely to happen in space vacuum, it tends to soften which leads to expansion. Performance parameters that are dependent on material thickness may be altered and this may compromise the performance. Temperature insensitive material like Thermal Microwave Material (TMM) has been developed to minimise the effects of large temperature changes.

2.3.4 Internal charging

In low Earth orbit, the density of plasma is high and is most likely to prevent the charging effects on the surface of the spacecraft by providing charged particles, which will introduce neutralising currents (Martin, 1991). However, internal charging may occur when the satellite is flying over inclined regions such as the polar regions, where there is a high-energy auroral electron flux, which can accumulate within dielectric materials and ungrounded conductors. If the charge accumulation exceeds the breakdown voltages of the material then an internal electrostatic discharge (arcing) occurs, charges may be discharged to nearby conductors or sensitive components and this may lead to soft anomalies or permanent damages. A perfect example is a case of a patch antenna, which is etched on a substrate material and protrudes on the satellite structure. If the dielectric material used accumulates charges to a point where it reaches a breakdown, it can discharge to a nearby conductor (patch) which is connected to a coaxial cable leading to the sensitive components and result in glitches or destruction of the circuitry. Mitigation of charge accumulation can be

obtained by providing a bleeding path in order for the charges to be spread all over the spacecraft or the use of thin and static dissipative (leaky) dielectric material so that the charges can reach ground faster (Garrett, 2011).

2.4 Microstrip patch antennas

Microstrip patch antennas are probably the most common type of conformal antennas used in low cost satellite applications. Unlike some other types of antennas, patch antennas are generally low profile, lightweight, low cost, and conformable, thus making them more favourable. However, single patch microstrip antennas are generally known to have narrow bandwidth and lower gain, which may not be sufficient for some applications. As a result, increasing the bandwidth is one of the primary objectives of this research work. In addition, patch antennas can be made into a variety of shapes; in which some are illustrated in Figure 2-14 and can be manufactured as a single element or an $n \times m$ array.

Figure 2-14: Popular shapes of microstrip patch antennas: (a) Square (b) Rectangular (c) Circular

Antennas can have their fields configured in a manner that could make them be linearly polarised, circularly polarised, or elliptically polarised. The study of this research is focused on antennas suitable for space applications meaning that their fields should be immune to Faraday's rotation. A circularly polarised antenna is the suitable type for space use and it will be studied in detail.

2.4.1 Circularly polarised microstrip patch antenna

The patch elements shown in Figure 2-14 can primarily radiate linearly polarised fields if they are fed on the central axis without any modifications being made on them (Balanis, 2005:859). Circular polarisation requires that the patch antenna be fed with signals of equal magnitude that have a 90º phase difference. This can be achieved by a single feed, dual, or multiple feeds with each method presenting its own challenges or limitations.

2.4.1.1. Single fed microstrip antennas

Single pin feeding mechanism is possibly the simplest method that is used to excite the two orthogonal modes required to establish circular polarisation. The excitation of these modes depends on the feed point location and the geometry of the patch antenna. Some examples are shown in Figure 2-15 below.

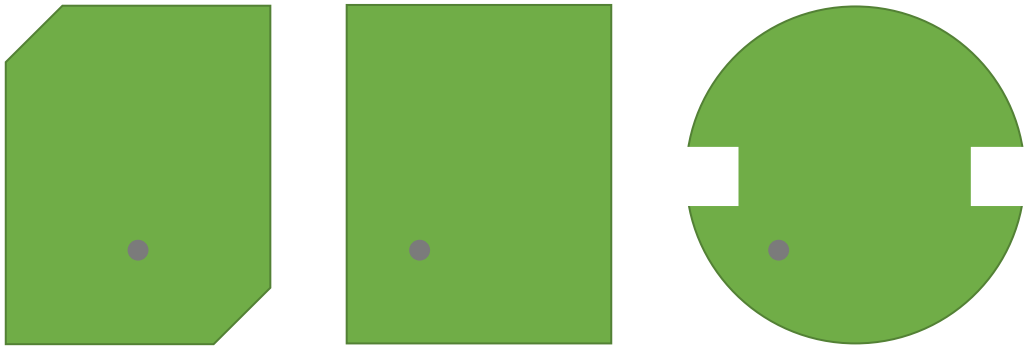

Figure 2-15: Classical shapes of singly fed microstrip patch antennas

Circular polarisation can be achieved by cutting the diagonal opposite corners of the rectangular or square patch antenna. For this antenna type, which is commonly referred to as the *corner trimmed* or *truncated* patch antenna, the two orthogonal modes are generated when it is fed on the central axis. This configuration allows one mode to be excited whilst the other one is excited by the perturbations (Narbudowicz, 2013:16), that is, the resonant frequency of the mode along the cut corners can be tuned by carefully selecting the value of the perturbed area. Furthermore, the direction of polarisation is dependent on the diagonal corners that are cut.

In the illustrations depicted below, a linearly polarised square patch antenna is first considered to demonstrate typical field configurations. Equations 2-9 and 2-10 (Balanis, 2005:830) are used to calculate the dimensions of the patch and resonant frequency respectively. From equation 2-10, it can be deduced that the modes along the cavity have a half wavelength cycle variation.

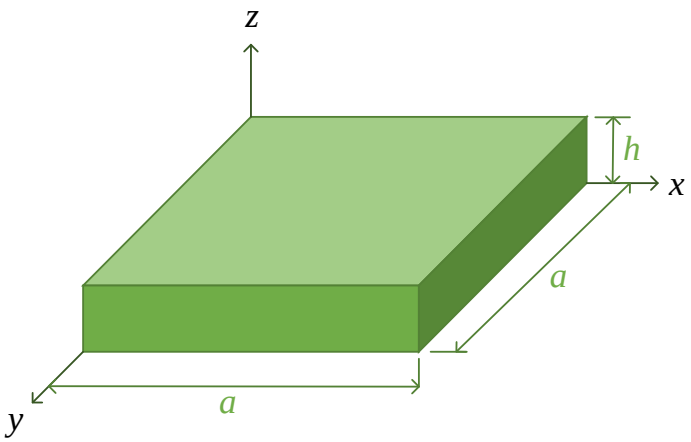

Figure 2-16: Cavity model of a microstrip patch antenna

$$a = \frac{c_0}{2 f_r \sqrt{\varepsilon_r}} \quad \text{mm} \qquad \text{2-9}$$

$$f_{10} = \frac{c_0}{2a\sqrt{\varepsilon_r}} \quad \text{Hz} \qquad \text{2-10}$$

Where:

c_0 is the speed of light

f_{10} fundamental frequency

ε_r substrate dielectric constant and

a patch antenna dimensions

The cavity model presented in Figure 2-16 can be represented by radiating and non-radiating slots of width a and height h as depicted in Figure 2-17 (Garg *et al*, 2001:79). The equivalent current densities (M) on the radiating slots have the same magnitude and phase (Balanis, 2005:842) whereas the non-radiating slots have opposing currents.

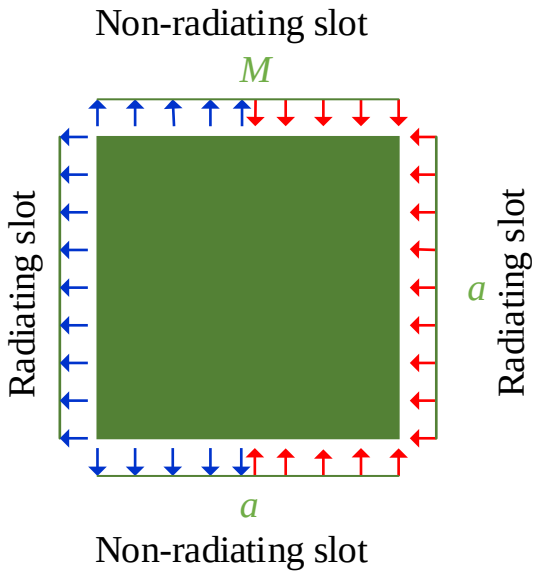

Figure 2-17: Electric field configuration of a square patch antenna for a TM_{10} mode

Comsol multiphysics[2] modelling software was used to illustrate the structure of electric field components in a square patch antenna for TM_{10} modes (refer to Figure 2-18). The electric field component can be approximated by:

$$E_z = E_0 \cos\left(\frac{\pi}{a}x\right) \quad \text{V/m} \qquad 2\text{-}11$$

Where:

E_0 is the electric field intensity on the magnetic walls in a cavity

E_z is the electric field vector in the z direction and

x is the direction of field variation with the cavity

[2] https://www.comsol.com/comsol-multiphysics

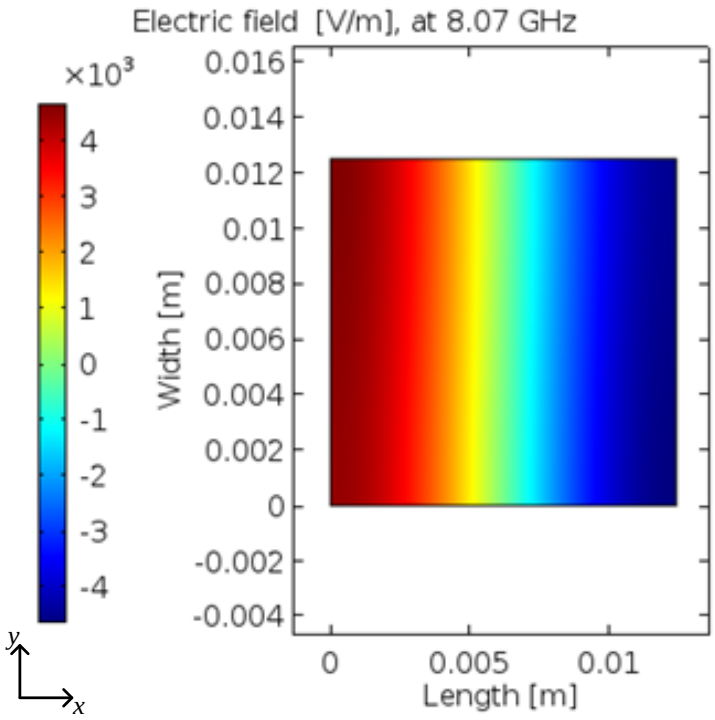

Figure 2-18: Electric field configuration for a TM_{10} mode

Figure 2-18 depicts the TM_{10} mode field configuration for a linearly polarised square patch antenna, which is identical to the four-slot model of Figure 2-17. Since the patch is symmetrical or has equal sides, the TM_{10} and TM_{01} are degenerate modes. According to Garg *et al*, (2001:496), the modifications on the corners can detune the degenerates of a symmetrical patch antenna. In reference to Figure 2-19, frequency f_1 can be detuned such that at the operating frequency f_0, the fields are equal and orthogonal (Garg, *et al*., 2001:496). The side with cut corners is shorter consequently; the resonant frequency f_1 will be slightly higher as compared to f_2.

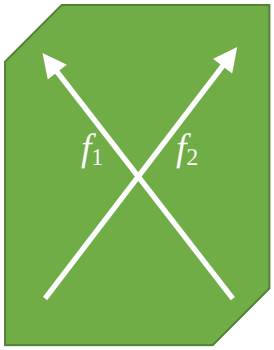

Figure 2-19: Orthogonal modes of a singly fed truncated patch antenna

Figure 2-20 below shows a Comsol multiphysics model of electric field configurations in a truncated patch antenna. From this figure, it can be observed that the frequency on the diagonal that is not cut is equal to the resonant frequency of the square model shown in Figure 2-18. However, the perturbation annuls the fields structure presented in the square model, hence the fields are now diagonal.

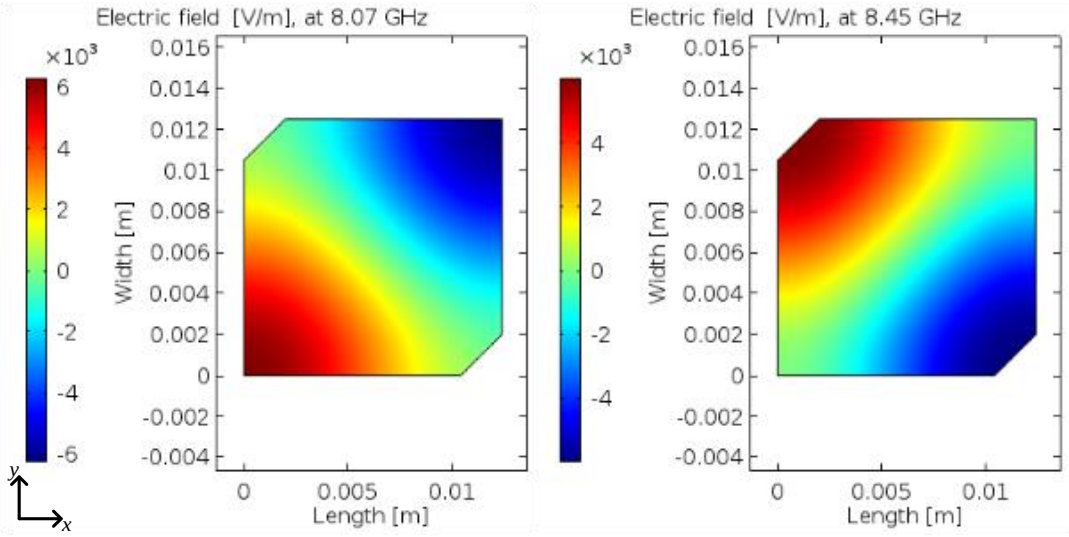

Figure 2-20: Comsol multiphysics model of a truncated square patch (ΔS = 4 mm^2): (a) Mode at f_2 (b) Mode at f_1

In the case of a nearly square or square patch antenna, the modes are excited by placing the feeding point along the diagonal axis and according to Kumar and Ray (2003:321), the dimensions of the patch antenna should have the ratio that ranges from 1.01 to 1.1 depending on the substrate material. Equation 2-12 (Balanis, 2005:862) defines this ratio, which is derived from the energy perturbation method.

$$b = a\left(1+\frac{1}{Q_t}\right) \quad \text{mm} \qquad 2\text{-}12$$

Where:

$$Q_t = \frac{1}{\tan(\delta_{eff})}$$

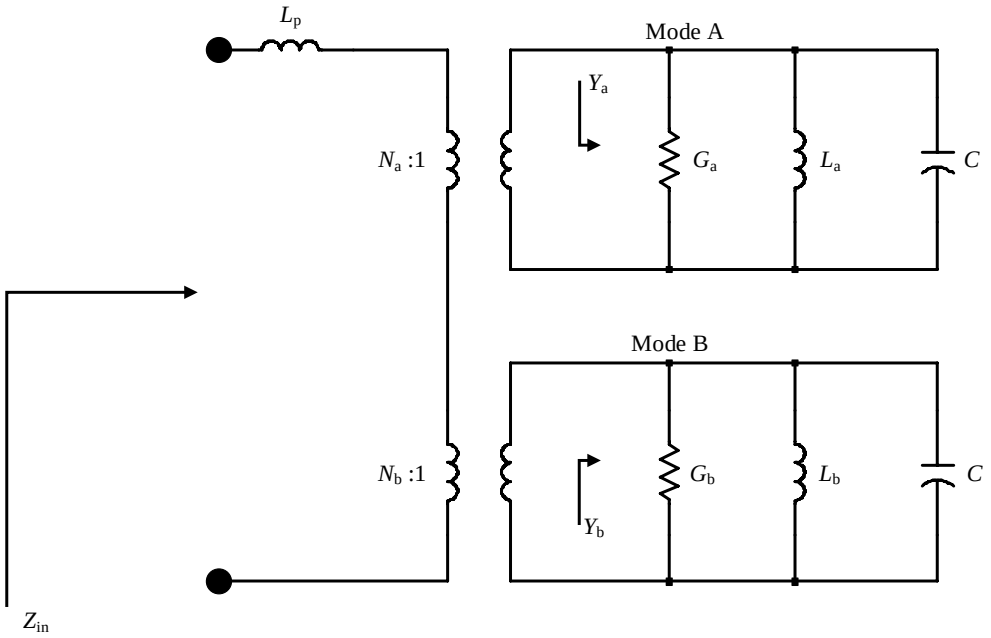

Figure 2-21: Equivalent circuit for a nearly square circularly polarised patch antenna

Figure 2-21 shows the equivalent circuit for a nearly square patch antenna (James & Hall, 1989:229). At resonant frequency, the two modes denoted as Mode A and Mode B have conjugate impedances, as a result; the patch input impedance will be inductive due to the inductive properties (L_p) of the feeding probe (Nascimento & Lacava, 2011). The rectangular patch antenna is normally used to compensate for the probe's inductive reactance since it establishes capacitive reactance (Nascimento & Lacava, 2011). The frequencies of Mode A and Mode B can be determined by equation 2-13(a, b).

$$f_A = f_0\sqrt{1+\frac{1}{Q_t}} \text{ Hz} \qquad \text{2-13a}$$

$$f_B = \frac{f_0}{\sqrt{1+\frac{1}{Q_t}}} \text{ Hz} \qquad \text{2-13b}$$

Where: $f_0 = \sqrt{f_A f_B}$ Hz

Once more, the sense of polarisation depends on the axis chosen. For instance, if the element is fed from the lower left corner towards the upper right corner then the left hand circular polarisation can be established.

The circular patch antenna like other geometries that were discussed is fed on the axis, which is 45º in reference to the notches on diametrically opposite points. If an ellipse is used, then the feed pin is place 45º along central axis. The main disadvantage with a single feed method is the axial ratio that rapidly degrades as the frequency is swept from the resonant frequency because of the conditions required for circular polarisation can no longer be respected.

2.4.1.2. Dual or multiple feeds microstrip patch antenna

The circular polarisation in a dually fed patch antenna requires an external feeding network that either is integrated into the patch structure or is connected directly to the 50 Ω points on the patch. For the integrated type, the patch must first be matched to the feeding networks using impedance transformers, as shown in Figure 2-22. Amongst the common networks used is the T-junction/Wilkinson power divider with one arm extended by 90º and a branch-line coupler. This configuration has a fairly larger axial ratio and VSWR bandwidths when compared to the single fed antenna but it requires more space. Various studies have been conducted for realising patch antennas with wider bandwidth, and these include the use of multiple feeding points, the sequentially rotated arrays, dual feed planar multiple-resonators and stacked patch antennas (Garg, *et al*., 2001:524).

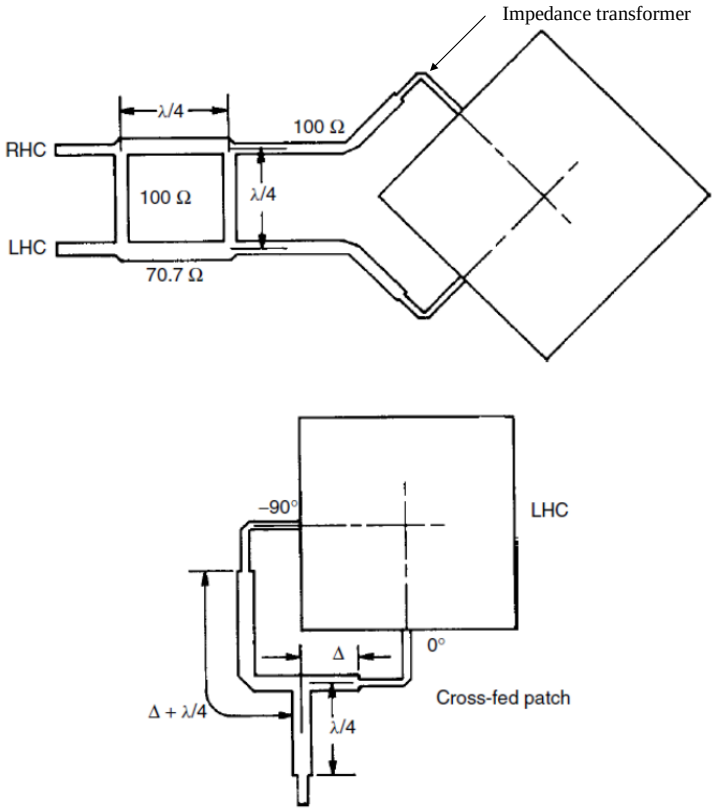

Figure 2-22: Integrated patch antenna with dual feed (Adapted from Milligan, 2005:317)

The use of multiple feeds such as four feeding points (see Figure 2-23) may yield a significantly wider axial ratio bandwidth. However, the additional feeding points will load the impedance of the opposite feeds because their null point is not at the same position (Kumar & Ray, 2003:316).

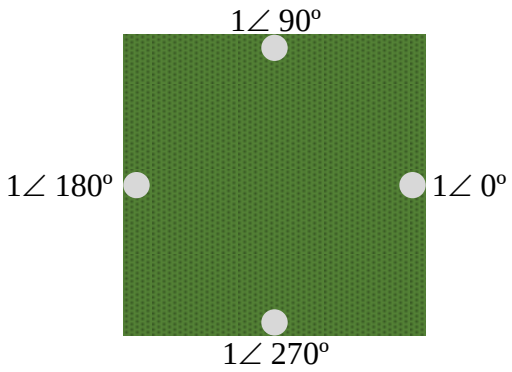

Figure 2-23: Four point fed microstrip patch antenna (Adapted from Kumar & Ray, 2003:315)

2.4.1.3. Sequentially rotated arrays

The sequentially rotated arrays can be achieved by using either linearly polarised patch elements or circularly polarised elements, which are governed by equations 2-14 and 2-15 where ψ represents the physical rotation of the elements and φ denotes the phase difference (Garg, *et al*., 2001:525). This is diagrammatically shown in Figure 2-24. A study that was conducted by Levine, Malamud, Shtrikman and Treves (1989:426) shows that the optimal gain can be obtained when elements are spaced at a range of 0.7 λ_0-0.9 λ_0.

$$\psi = (m-1)\frac{p\pi}{M} \qquad 2\text{-}14$$

$$\varphi = (m-1)\frac{p\pi}{nM} \qquad 2\text{-}15$$

Where:

p is an integer, $1 \leq m \leq M$

M is the total number of radiating elements and

n represents the number of modes

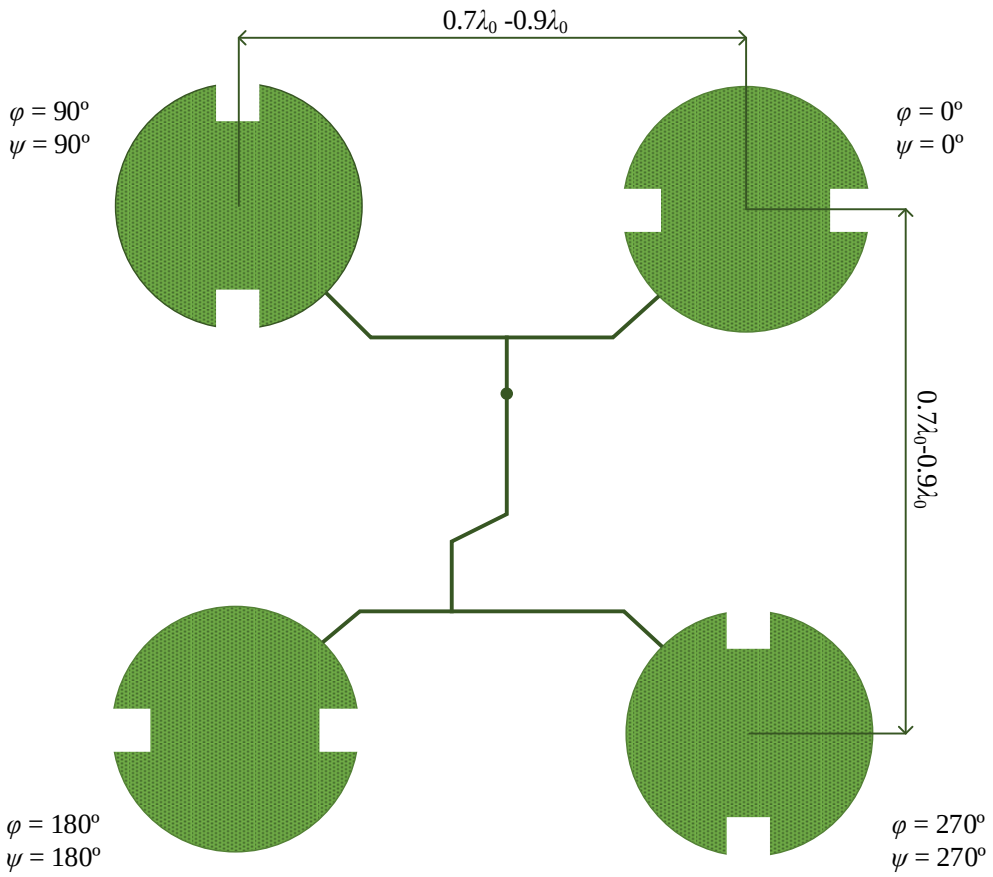

Figure 2-24: Typical sequential rotated patch array

In this configuration, the elements that are positioned at 0º and 90º have a quadrature phase difference. When they are mirrored about the horizontal axis, an additional quarter wavelength long feed line is added to realise the 180º and 270º phases.

Wider VSWR and AR bandwidths can also be achieved by using a planar multiple-resonators as shown in Figure 2-25. In this configuration, the central patch element is normally the one that is being fed, whilst the adjacent elements are parasitically coupled. The parasitic elements are coupled either by using a small gap between the elements or by direct coupling through a microstrip line. According to Kumar and Ray (2003:90), this configuration can yield a bandwidth of 5 % to 20 % for VSWR ≤ 2 and moreover; the axial ratio bandwidth can be further improved by cutting diagonal opposite corners of a square or rectangular patch, which are then sequentially rotated by 90º (see Figure 2-26). Equation 2-10 proves that the dimensions of an element define the cut-off frequencies of the modes for that particular element. For example, in a case of a four-

edge coupled planar antenna, the elements on the radiating edge will have different dimensions to those on the non-radiating sides, to make their resonant frequencies slightly different and yet close to each other as show in Figure 2-25 (a).

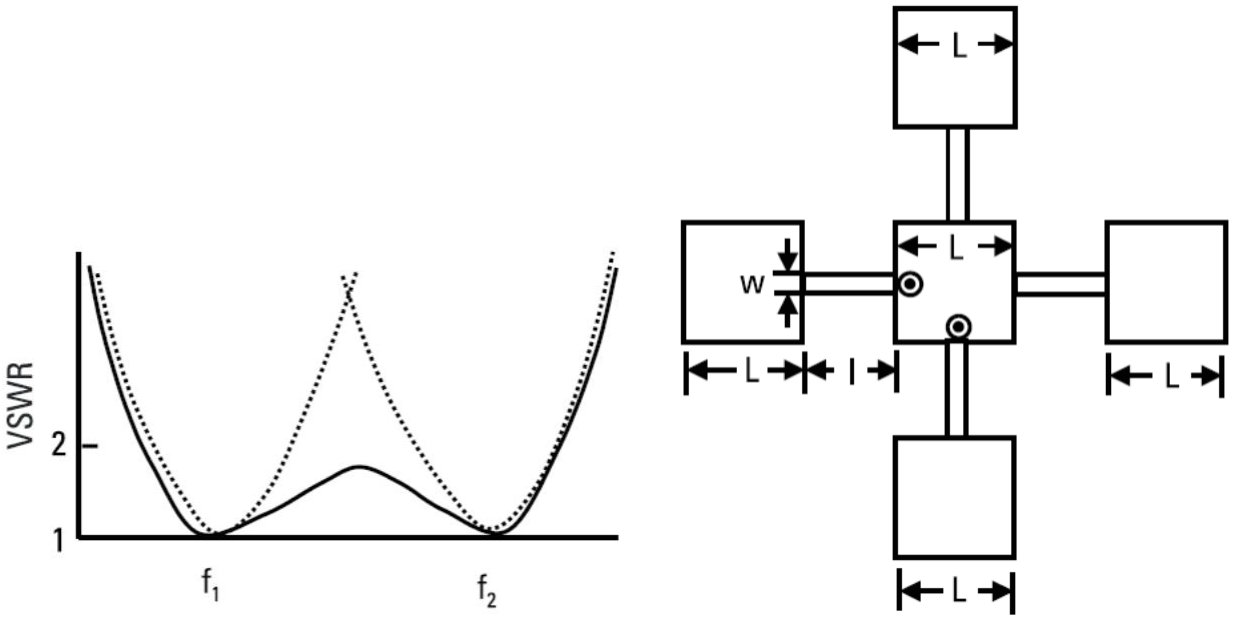

(a) (b)

Figure 2-25: (a) VSWR plot for two coupled resonators (b) Directly coupled multiple resonators (Adapted from Kumar & Ray, 2003)

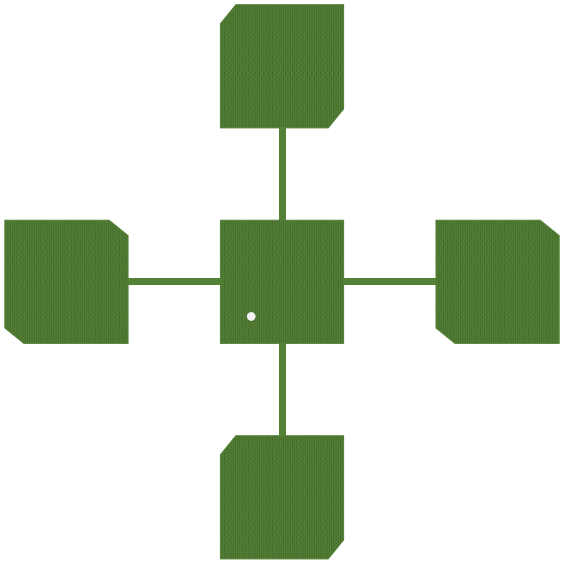

Figure 2-26: Sequentially rotated patch element for *AR* bandwidth widening

2.4.1.4. Stacked microstrip patch antennas

The stacked patches or electromagnetically coupled antennas as they are commonly known increases the overall height of the antenna but the size remains unchanged. This increase in antenna's height decreases the effective dielectric constant especially when there is an air gap or foam in between the patch layers, and this configuration allows the use of different substrate materials. Materials with high dielectric constants restrict the fields; as a result, the bottom substrate should have higher or equal dielectric constant as the substrate on top. This will create tightly bound fields, which will then be degraded by the effective height of the patch resulting in a lower *Q* value. The relative dielectric constant for this configuration is approximated by equation 2-16 with parameters defined in Figure 2-27 (Mendhe & Kosta, 2012:91). The method used to excite elements in the stacked microstrip antennas is almost the same as the one used in gap-coupled multiple resonators. The excitation can be made on the top or bottom element while the other element couples electromagnetically.

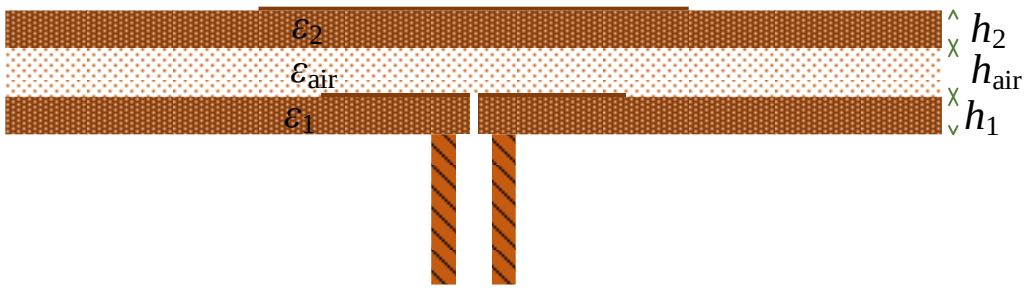

Figure 2-27: Cross-sectional view of a stacked patch antenna

$$\varepsilon_r = (h_1 + h_{air} + h_2)\left(\frac{\varepsilon_1}{h_1} + \frac{\varepsilon_{air}}{h_{air}} + \frac{\varepsilon_2}{h_2}\right) \quad 2\text{-}16$$

2.5 Feeding mechanisms

The feeding mechanism is one of the important design considerations because it can directly affect the performance parameters of the antenna. The microstrip patch antenna can be fed using different techniques, which are the probe feed, microstrip line feed, proximity coupled feed, and aperture coupled feed.

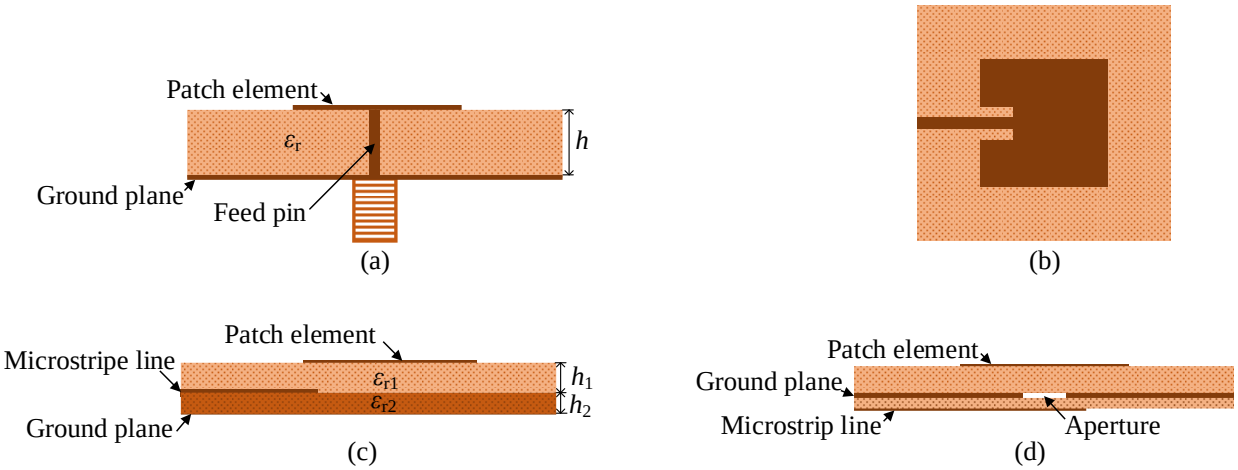

Figure 2-28: Feeding techniques of a microstrip patch antenna: (a) probe feed, (b) microstrip line insert feed, (c) proximity coupled feed, and (d) aperture coupled feed (Adapted from Volakis, 2007)

The probe and microstrip line feeds are classified as contact feeds. They both are easy to fabricate and are simple to match (Balanis, 2005:813). The probe feed shown in Figure 2-28(a) has a low spurious radiation but it limits the achievable bandwidth since the feed pin inductance increases with substrate thickness. The microstrip line insert feed as shown in Figure 2-28(b) is mostly used in array applications (Jackson, 2007) and it suffers from surface waves as well as spurious feed radiation as the substrate thickness increases. The proximity and aperture coupled feeding are non-contacting feeding techniques. The proximity feed, which is shown in Figure 2-28(c), has the largest bandwidth when compared to the other three feeding mechanisms (Balanis, 2005:815). However, it requires multilayers, which make its fabrication slightly more difficult and cost incurred can be high. The aperture coupled feed shown in Figure 2-28(d), has the capability to reduce the feed-line radiation but it suffers from back radiation.

Having considered almost all the necessary aspects essential in initiating the design process, the next step would be to put them into practice. Decisions taken in the next chapter, which entails the design process, will be greatly influenced by this literature study.

Chapter 3

X-Band Antenna Design and Analysis

3.1 Introduction

In chapter 2, antenna characteristics and various techniques that enhance the bandwidth of microstrip patch antennas were discussed. Some of these aspects are revisited in this chapter. The aim of this project was to design a circularly polarised microstrip patch antenna that will provide a proof of concept for F'SATI's future space missions. The antenna operates in the X-band at frequencies ranging from 8.025 GHz – 8.45 GHz. The design approach that has been followed is shown from the start to finish, and FEKO EM simulation software was used. Rectangular and circular shapes of the patch antenna have been used and were chosen for comparison purposes, as there are other shapes that could have been used to achieve the same results. A wider 3 dB axial ratio and a VSWR ≤ 2 bandwidth are the parameters of interest in this study.

3.2 Design and analysis

FEKO has a number of solvers that could be used depending on the application. These include the method of moments (MOM), multilevel fast multipole method (MLFMM), the finite element method (FEM), uniform theory of diffraction (UTD) and physical optics (PO). The method of moments technique was the numerical analysis used to perform the simulation since according to Table 3-1, MOM is ideally suited to the problem. This table is extracted from FEKO 2017 user's manual. The shaded circle implies that the solver technique is well suited for the problem while the clear circle indicates that the solver can be used even though it may not be well suited for the specific application.

Table 3-1: FEKO ideal solvers for different applications (Altair, 2017:10)

	Geometrically complex			*Electrically large*				
	MoM	FEM, FEM/MoM	FDTD	MLFMM	FEM/MLFMM	PO, MoM/PO, MLFMM/PO	RL-GO, MoM/RL-GO	UTD, MoM/UTD
Wire antennas	●		○	○				
Microstrip antennas	●	●	●	○	○			
Aperture antennas	●	○	○	○	○			
Reflector antennas	○	○	○	●	○	●	●	
Windscreen antennas	●			●				
Conformal antennas	●	●		●	●			
Broadband antennas	●	●	●	●	●			
Array antennas	●	●		●	●			
Lens antennas	○	○	○	○	○		●	
Radomes	○	○	○	●	●		●	
Antenna placement (radiation pattern)	●	○	○	●	●	●	●	●
Antenna placement (coupling)	●	○	○	●	●	○	○	○
Biomedical	○	●	●	○	●			
RADHAZ zones	●	●	○	●	●	●	●	○
Periodic structures FSS, metamaterials	●	○		○	○			
Scattering with plane wave source (RCS)	●	○	○	●	○	●	○	
Scattering with localised source	●	○		●	○	●	●	●
EMC/EMI shielding and coupling	●	●	○	●	○			
Propagation environment	○	○	○	○	○	○	○	●
Cable bundle coupling	●			●				
Waveguide components	●	●			○			
Connectors	●	●	○					
Microstrip circuits	●	●	●	○	○			

3.2.1. Nearly square patch antenna

The first type of antenna to be considered is the nearly square (rectangular) patch antenna (see Figure 3-1), where b represents the patch length, a is the width, W the size of ground plane, $p(x, y)$ the feed point and h the substrate thickness. The dimensions for this antenna were determined by making use of equations 2-9 and 2-12. An RT/duroid 6002 substrate with thickness h = 1.524 mm, dielectric constant ε_r = 2.94, copper thickness t = 0.035 mm and loss tangent tan δ = 0.0012 was used. The substrate was chosen according to the criteria required for material certified for space use and availability of the samples which were supplied by Rogers Corporations. The procedure that has been followed is described next.

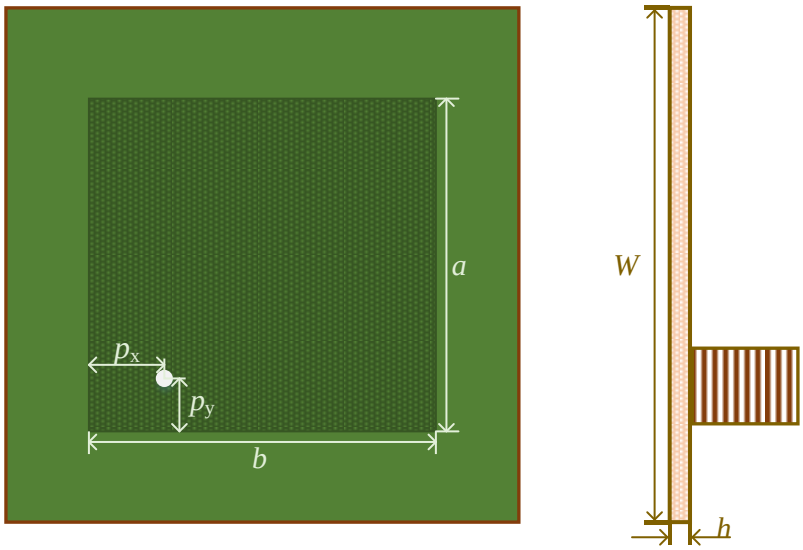

Figure 3-1: Nearly square patch antenna *b* > *a*

The cut-off value of impedance bandwidth in most antenna designs is −10 dB, which is equivalent to VSWR of 2:1. From Figure 2-13, the bandwidth of a substrate whose thickness h = 1.52 mm can be approximated to about 5 %. The quality factor (Q_t) corresponding to this bandwidth is 14.14, this was found by using equation 3-1. Once Q_t is known, the dimensions of the patch antenna can then be determined.

$$Q_t = \frac{\text{VSWR} - 1}{BW\sqrt{\text{VSWR}}} \qquad 3\text{-}1$$

FEKO's characteristic mode analysis (CMA) simulator was used to provide an indication of eigen modes that would likely be excited by using this geometry. Figure 3-2 shows the eigenvalue and modal significance in which one of them can be used to determine the possible resonant frequencies of the patch structure. If for example, the eigenvalue is zero or the modal significance is equal to one, then the antenna is likely to resonate at that particular frequency (Gallée, Bernabeu, Cabedo-Fabrès, Daviu & Nogueria, 2013). The plots show that the patch structure has modes that are resonating at lower frequencies and six modes were investigated. Only two of those modes namely mode 1 and mode 2 were found to be orthogonal (see Figure 3-3).

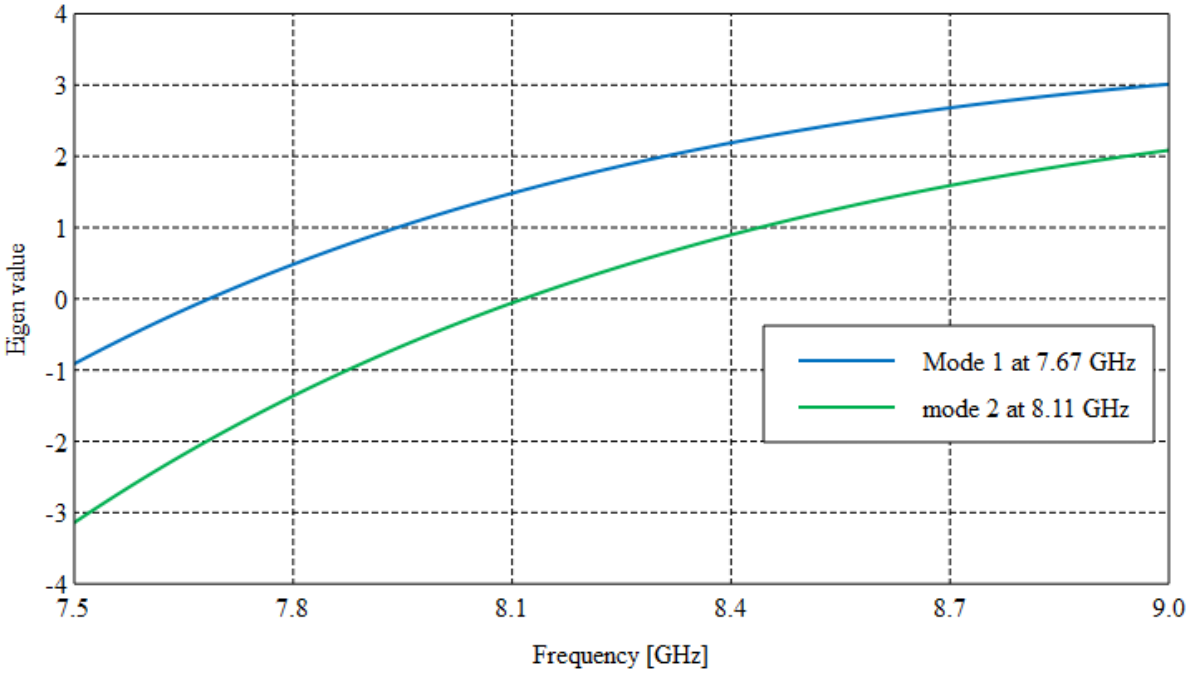

(a)

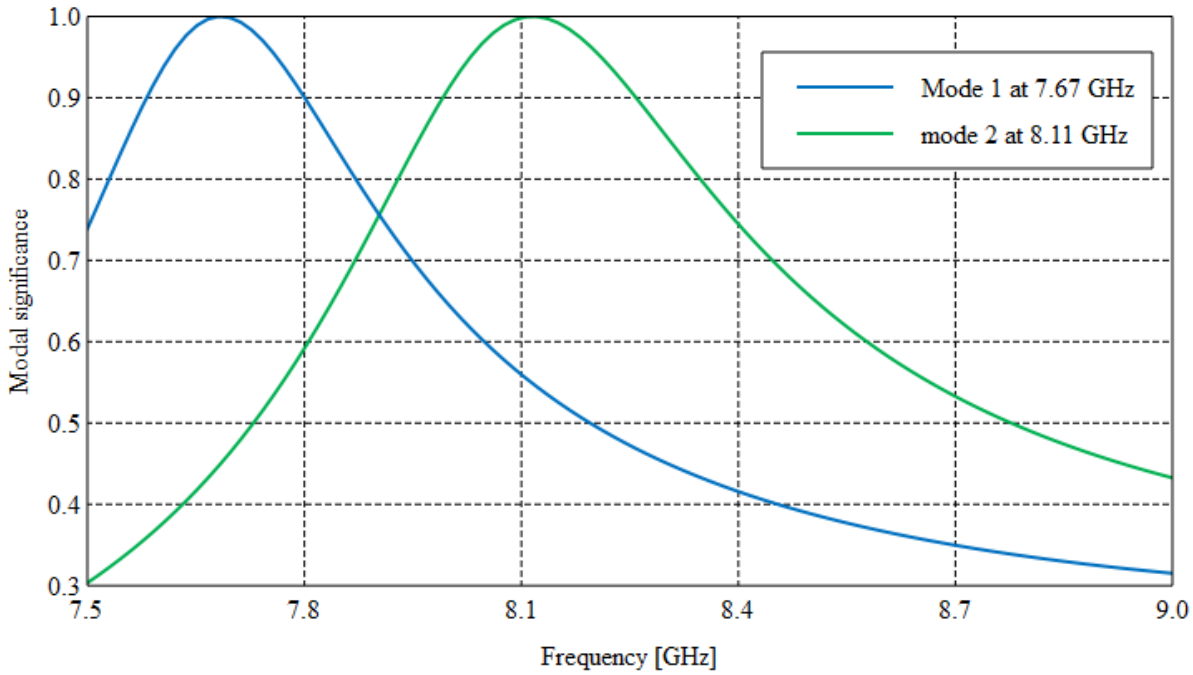

(b)

Figure 3-2: Orthogonal mode of the initial design: (a) Eigenvalue (b) Modal significance

Since the frequencies of the two orthogonal modes were lower than the desired frequencies, the patch dimensions were slightly modified to bring the two modal frequencies closer to the operating

frequency. The following optimal dimensions were achieved: a = 8.85 mm and b = 9.81 mm. To recall, the characteristic mode analysis does not require an excitation. For the purpose of this study, a single probe feeding technique was used and it needs to be carefully placed in order to excite both modes, otherwise the polarisation will be elliptical.

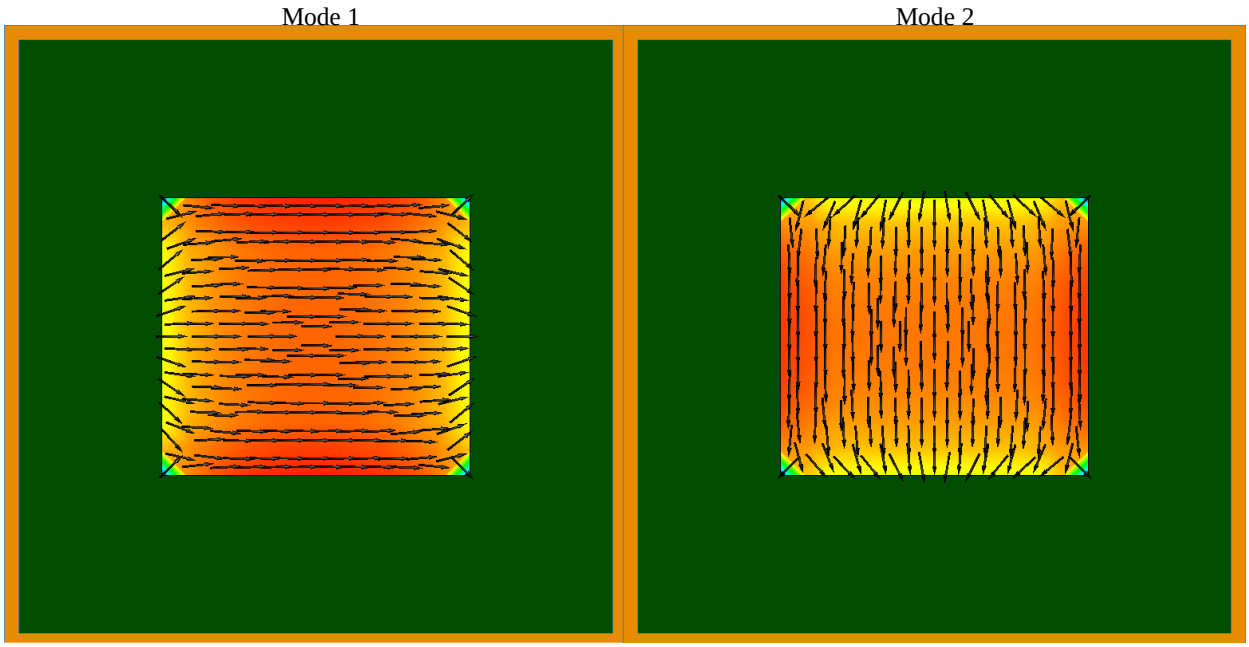

Figure 3-3: Orthogonal modes

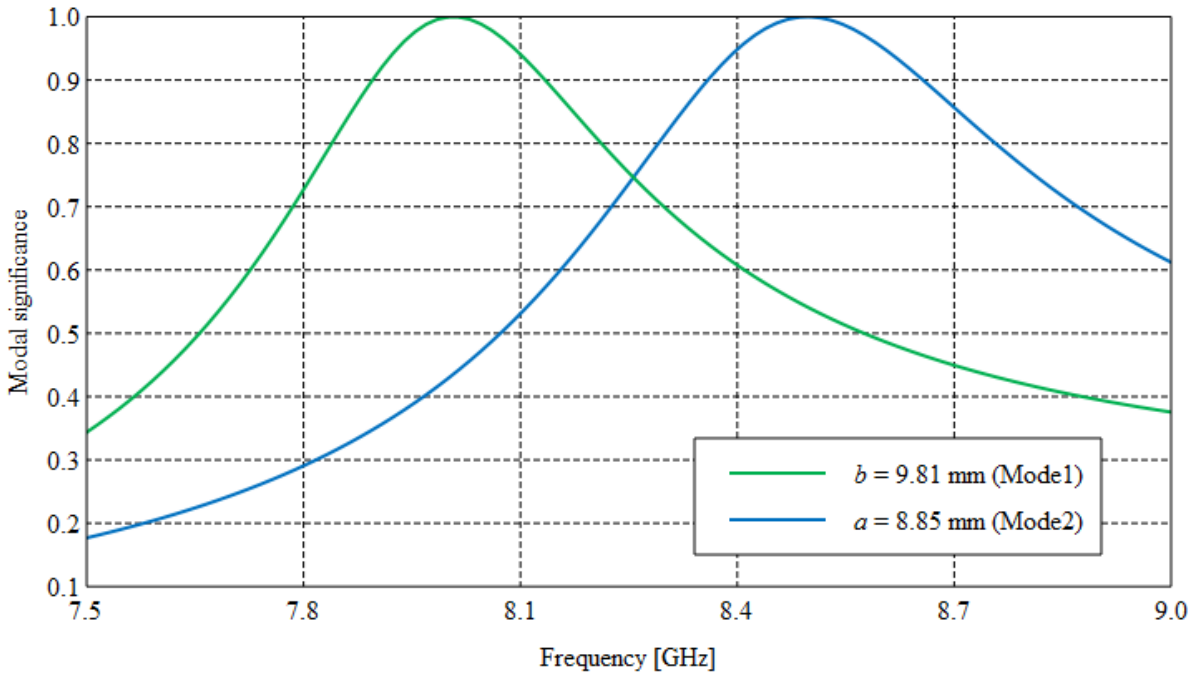

Figure 3-4: Characteristic modes of the optimal patch dimensions

Figure 3-4 shows that the centre frequency of the two modal frequencies is 8.25 GHz but the modal significance is very low. This means that the feed pin should be placed in a position such that most of the power is radiated. FEKO optimisation tool was used to vary the coordinates (p_x, p_y) of the feeding point while the other parameters were fixed. The feeding point is slightly off the diagonal axis to compensate for the impedance matching. The optimal patch dimensions are given in Table 3-2.

Table 3-2: Nearly-square patch dimensions

Parameter	Value [mm]
a	8.85
b	9.81
p_x	2.08
p_y	1.13
W	25
SMA-connector pin diameter	1.27

Figures 3-5 gives the results for the simulated VSWR. The nearly square patch antenna yields a bandwidth of about 10 % for a VSWR ≤ 2, which is slightly less than the theoretical bandwidth of 11 % calculated using optimal patch dimensions. This is the good indication that most of the power fed into the patch will be radiated. At 8.25 GHz, the impedance is very close to 50 Ω (Z_{in} = 49.83 + j 0.645 Ω), but elsewhere it is mostly inductive. This is shown in Figure 3-6. The axial ratio (AR) as depicted in Figure 3-7 quickly degrades as the frequency is swept off the operating frequency due the difficulty in maintaining proper excitation conditions. The AR at boresight is 0.29 dB, which signifies a near circular polarisation. It is worth noting that the VSWR bandwidth is larger than the AR bandwidth. This may not be useful for some applications. The improvement of AR bandwidth is detailed in the later sections of this chapter based on literature that has been discussed in the previous chapter.

Figure 3-8 shows a simulated gain, which peaks at 7 dBi and the antenna exhibits a pattern of approximately 76º half power beamwidth as illustrated in Figure 3-9. The cross polarisation on the broadside is far below −20 dBi, which implies that chances of having undesired radiation is very low. Figure 3-10 plots the radiation efficiency, which is 97 % at the centre frequency.

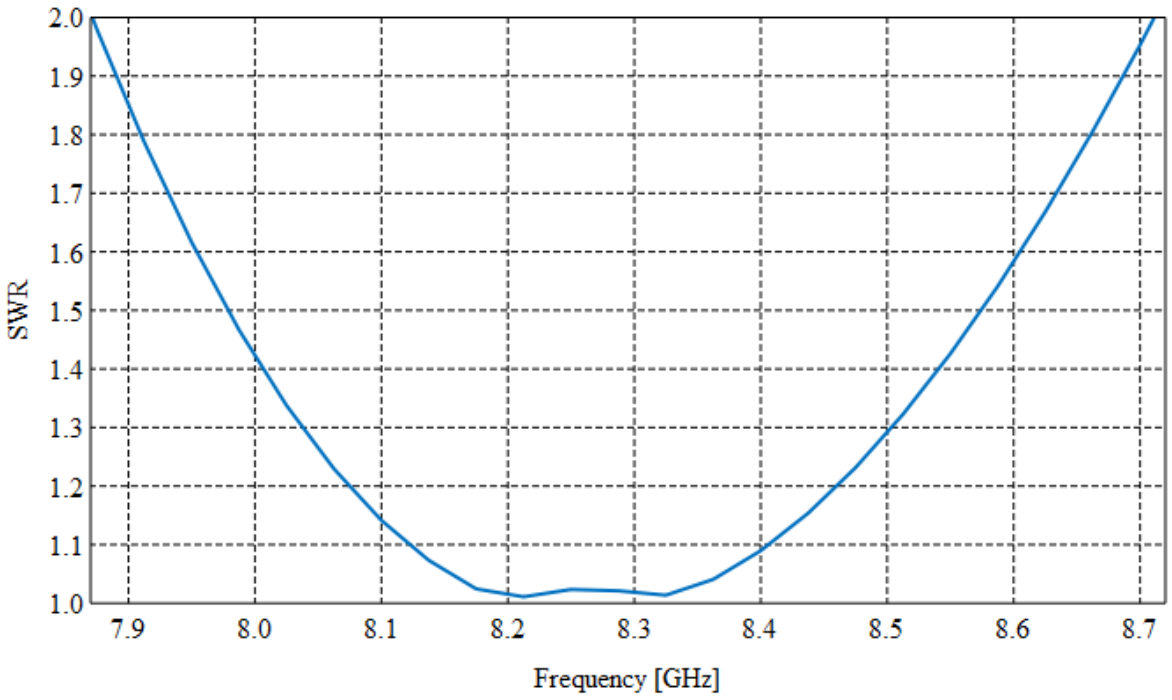

Figure 3-5: Simulated VSWR for the optimised nearly-square patch antenna

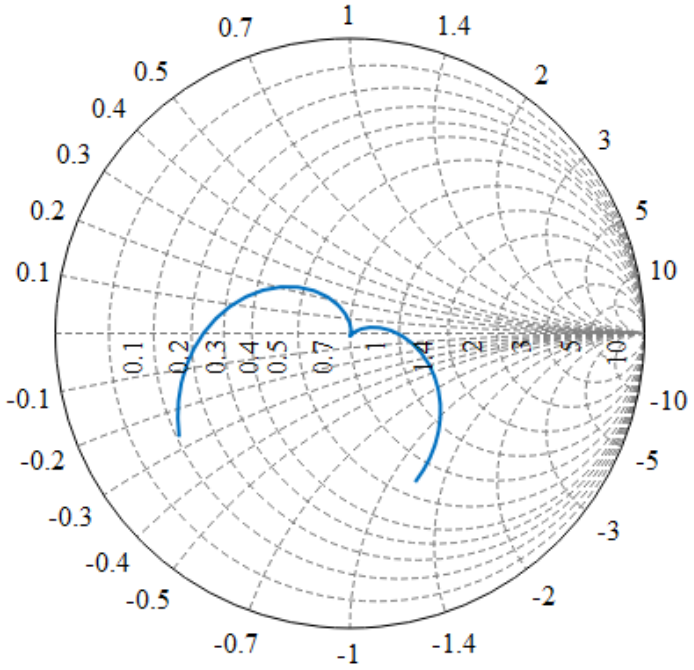

Figure 3-6: Simulated impedance of a nearly-square patch antenna

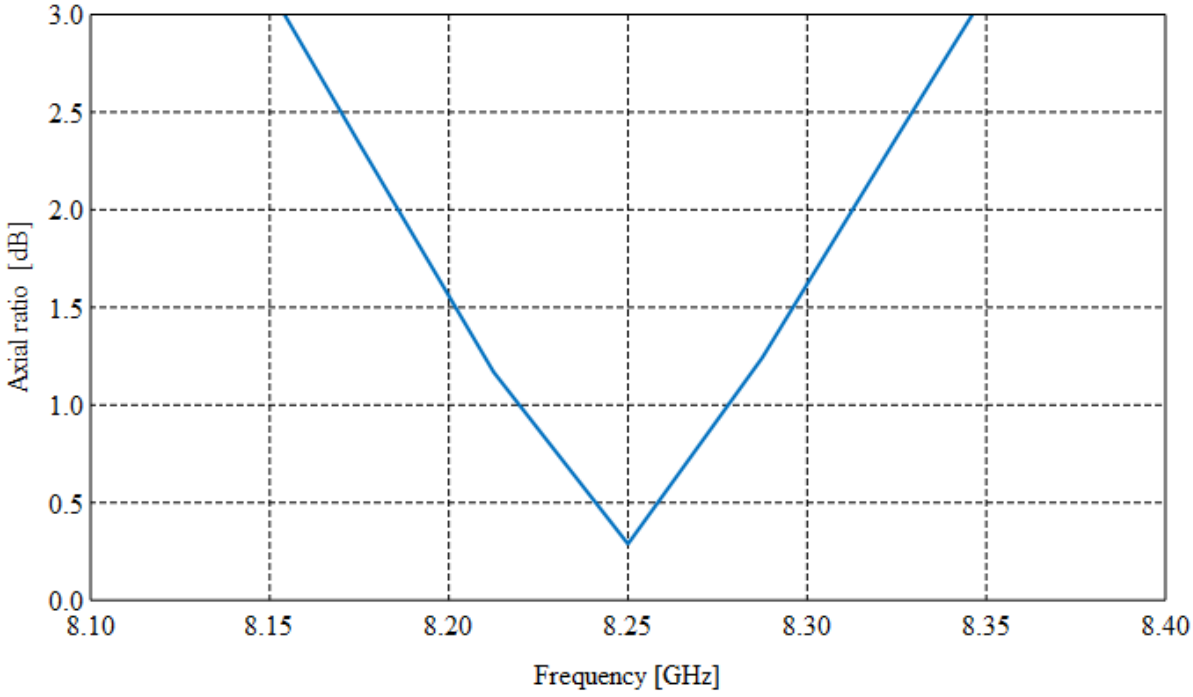

Figure 3-7: Nearly square patch antenna axial ratio (θ = 0°)

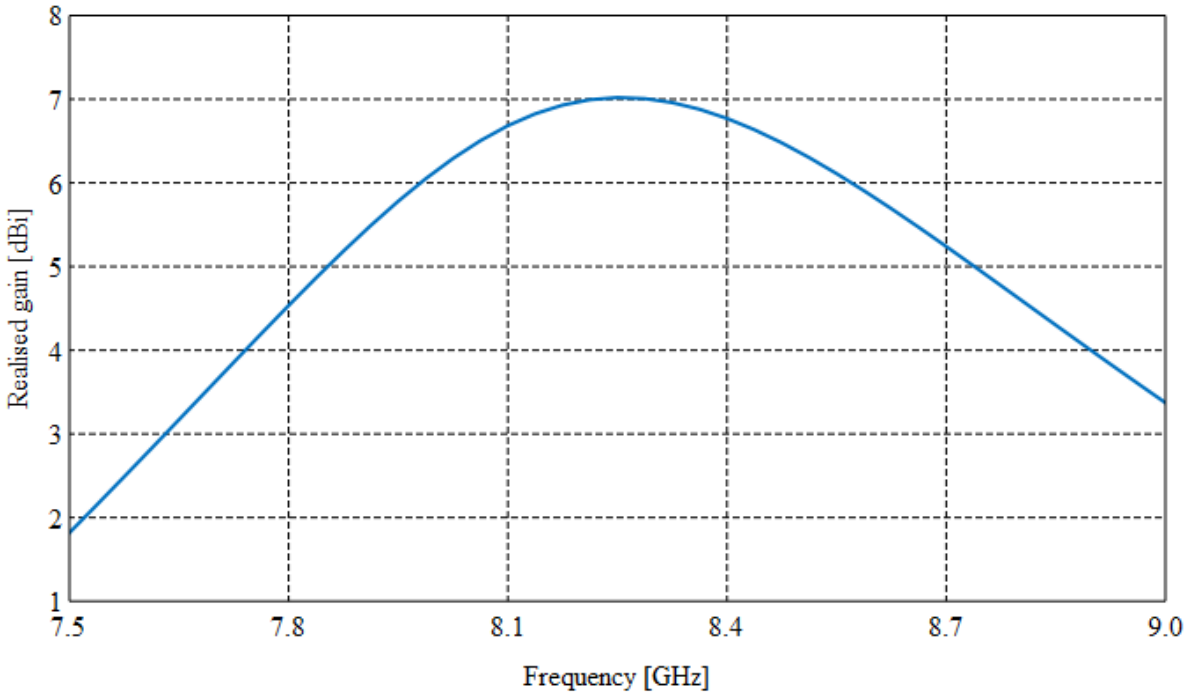

Figure 3-8: Realised gain over frequency for the nearly square patch antenna

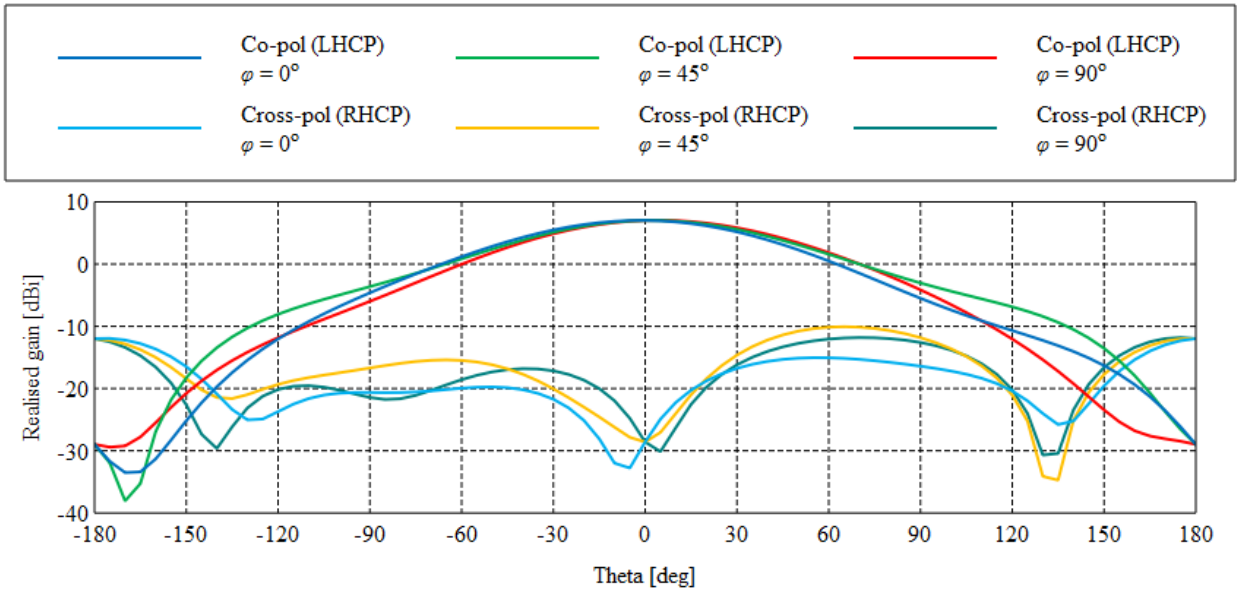

Figure 3-9: Simulated nearly square patch antenna pattern at 8.25 GHz

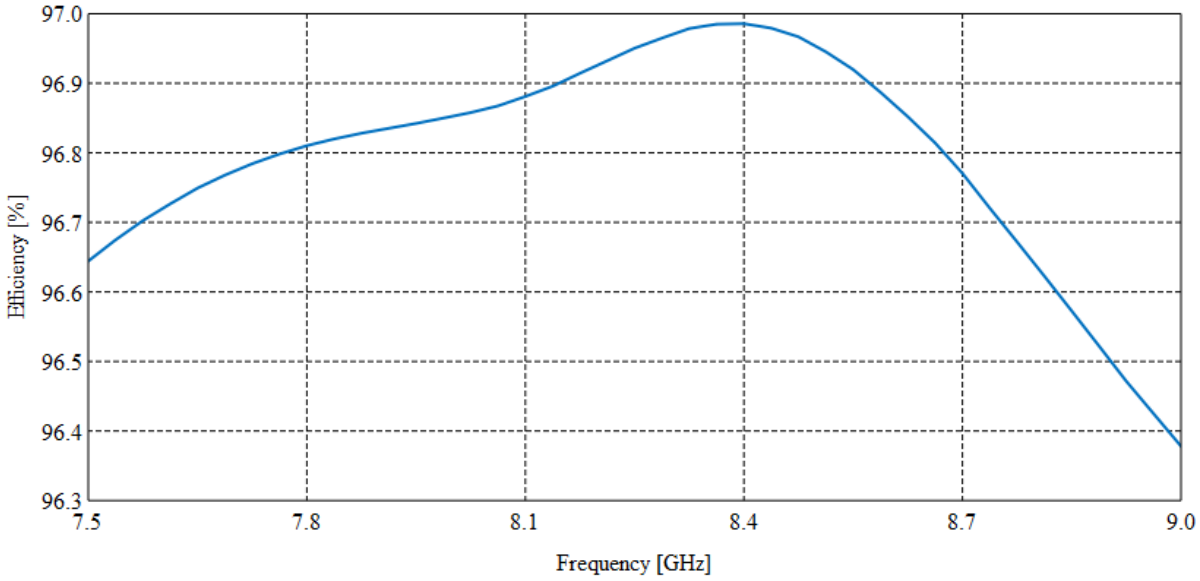

Figure 3-10: Simulated radiation efficiency of a nearly square patch antenna

A parametric study was conducted so that the performance sensitivity of the patch antenna can be analysed when one or all the parameters are varied. The analysis was made on patch dimensions and the following observations were made:

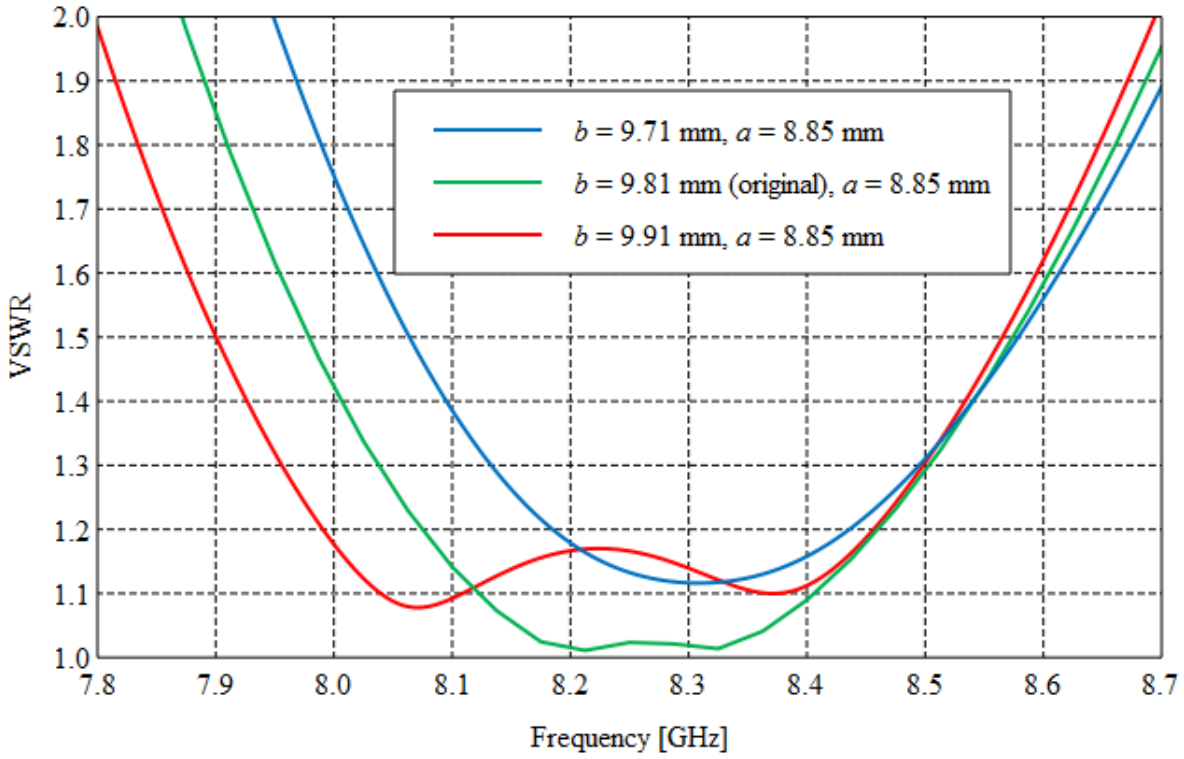

(a)

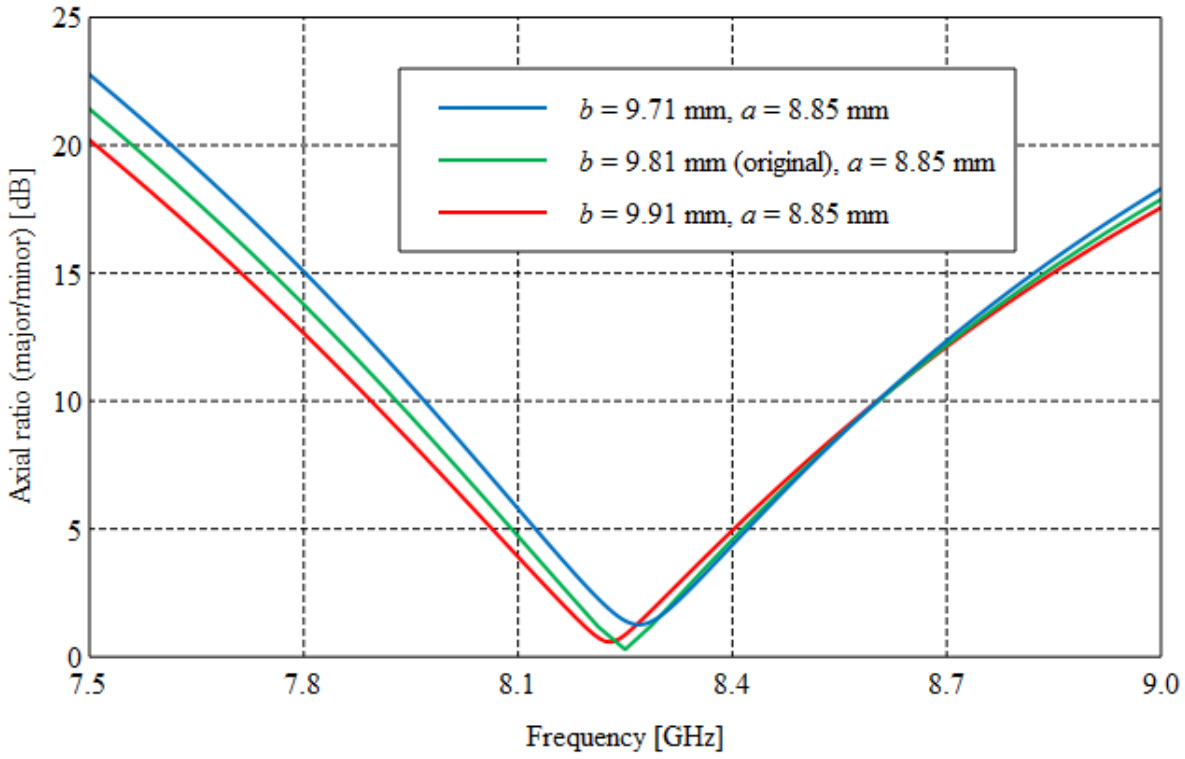

(b)

Figure 3-11: Performance study of a nearly square patch : (a) VSWR plots (b) Axial ratio

- If the patch length *b* is reduced to 9.71 mm, the fundamental cut-off frequency increases to a higher value resulting in a shift in VSWR plot. $b > a$
- For b = 9.91 mm, modal frequency associated to this parameter is reduced resulting in shift of VSWR to the left. The VSWR ≤ 2 bandwidth remains relatively the same.
- The width *a* was also changed by three values, which are 8.75 mm, 8.85 mm, and 8.95 mm. It was found that if the patch dimensions have 10 % or 12 % difference (separation) regardless of which side is being varied; the patch performance parameters will be similar if not identical. The axial ratio can be improved by modifying the feeding position.

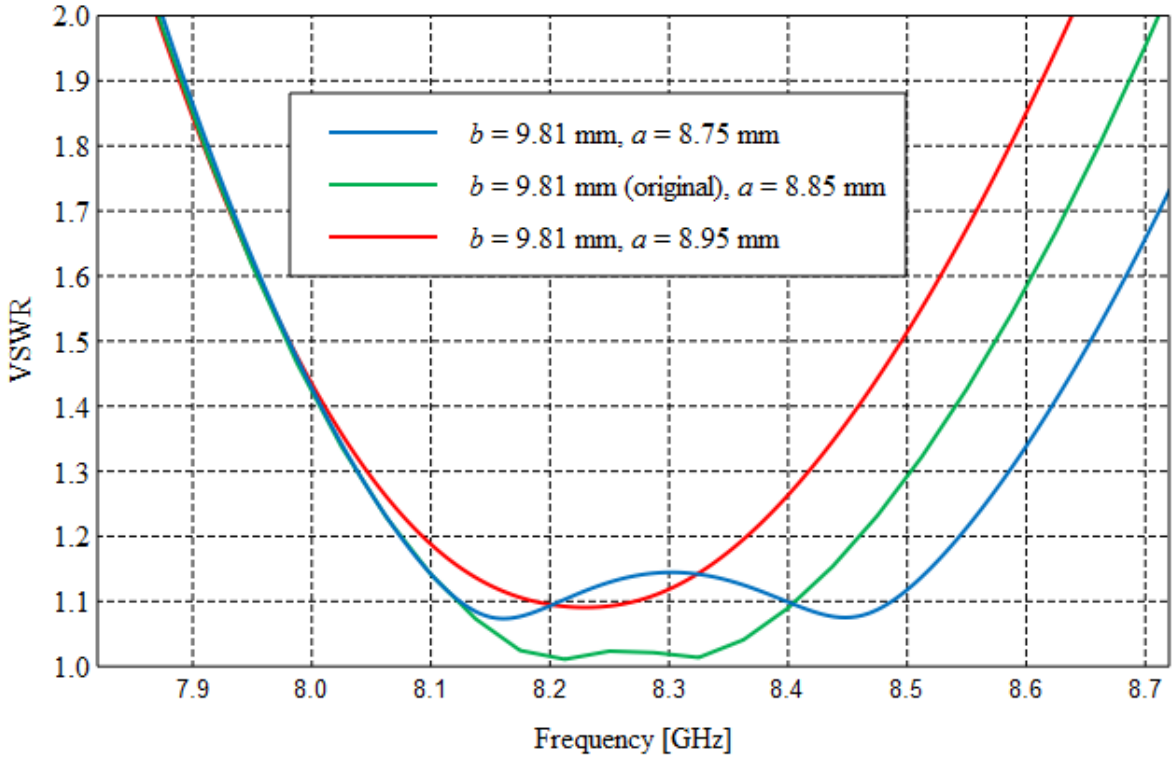

Figure 3-12: Performance study of the rectangular patch antenna for the varying width

$$\frac{\Delta f}{f_0} \approx \frac{b}{a} - 1 \qquad 3\text{-}2$$

Equation 3-2 provides an insight on how the bandwidth is modified by changes made on the dimensions of the patch. This is evident as Figures 3-11 and 3-12 show some slight change in the VSWR bandwidth. If for example, the length (*b*) of the patch element is increased, the value of a *Q* factor decreases. This implies that the bandwidth increases with an increase in length. This however, can hold for a certain range of values of the ratio of *b* to *a*. For instance, in the case of a nearly square patch antenna, this ratio ranges from 1.01 to about 1.1.

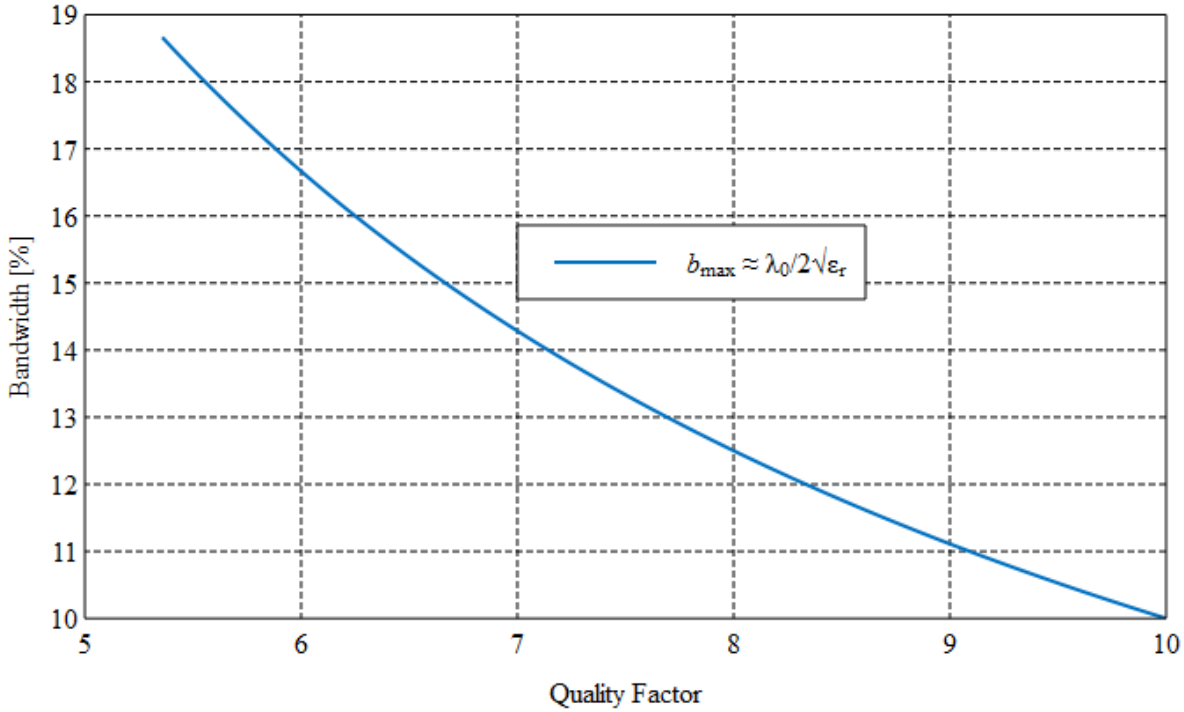

Figure 3-13: Normalised bandwidth vs. quality factor

3.2.2. Nearly square truncated patch antenna

The corner trimmed nearly square patch antenna was also modelled on the same RT/duroid 6002 substrate. The rectangular shape was chosen over the square shape because an acceptable return loss and axial ratio are achievable at the same frequency when this shape is used. The nearly square patch antenna in section 3.2.1 had its two diagonal corners trimmed by an area S^2. The perturbation modifies the field configuration of a rectangular patch cavity as they are now diagonal. This type of patch antenna is excited on the central axis as is shown in Figure 3-14 and the probe feed is used.

Table 3-3: Nearly-square truncated patch dimensions

Parameter	Value [mm]
a	10.02
b	9.37
p_y	2.53
S	1.85
W	25
SMA-connector pin diameter	1.27

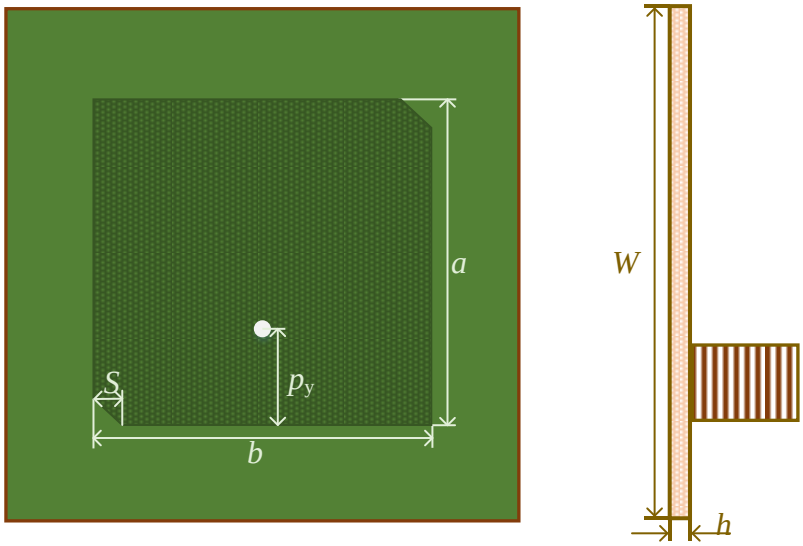

Figure 3-14: Truncated patch antenna

The input impedance of this truncated patch antenna is almost purely resistive (Z_{in} = 50.03 + j0.04 Ω), which means that the antenna is properly matched to 50 Ω SMA connector. Corresponding to the input impedance is the good VSWR of 1.01 at 8.25 GHz. This antenna exhibits very similar performance characteristics as the previous nearly square patch, which is fed on one of its diagonals and they are VSWR ≤ 2 bandwidth = 10 %, axial ratio = 0.04 dB, 3 dB bandwidth = 2.4 %, gain = 7 dBi and radiation efficiency = 97 %. The plots for these performance parameters are listed below. Even for this model, the VSWR bandwidth is wider than the AR bandwidth.

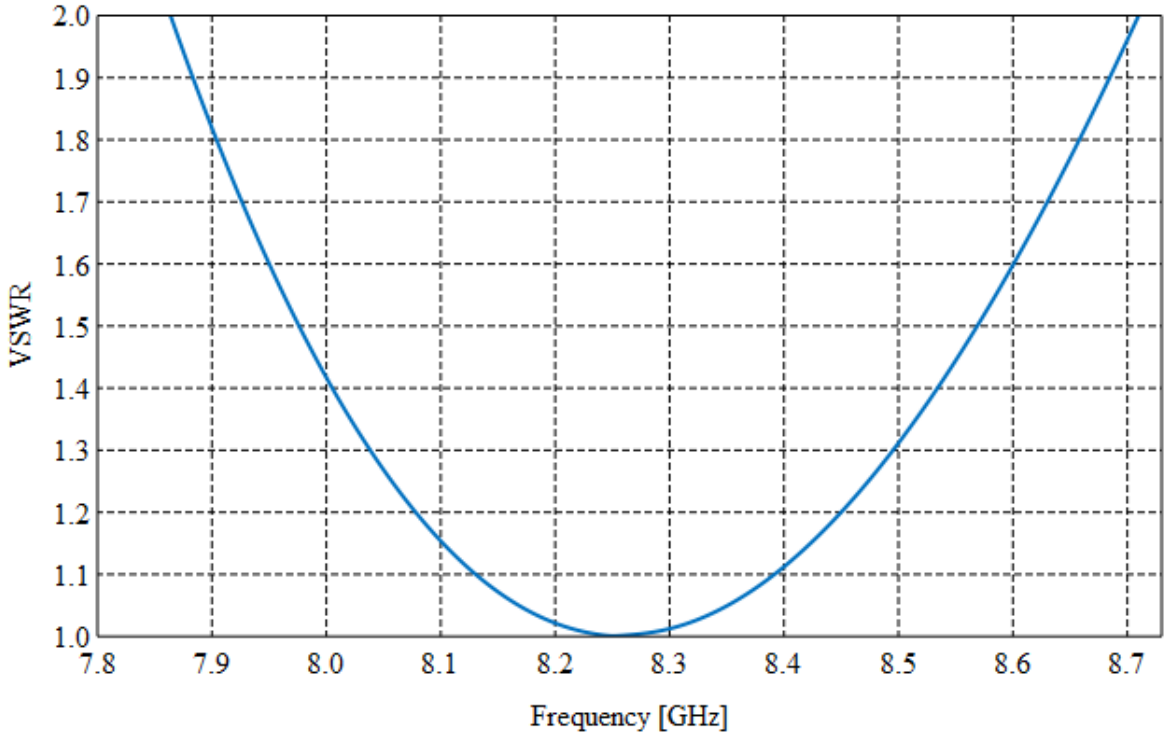

Figure 3-15: Simulated VSWR of the truncated patch antenna

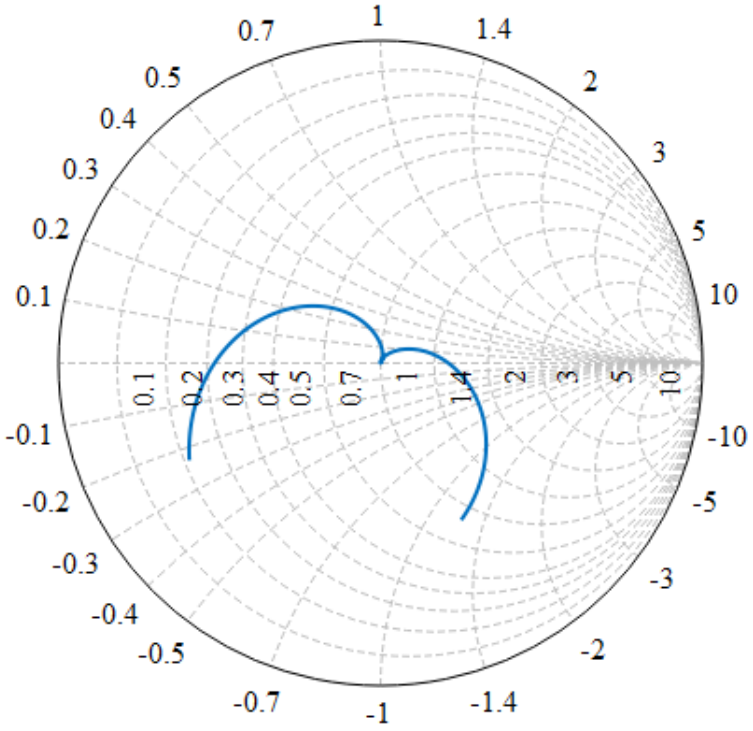

Figure 3-16: Input impedance of the truncated patch

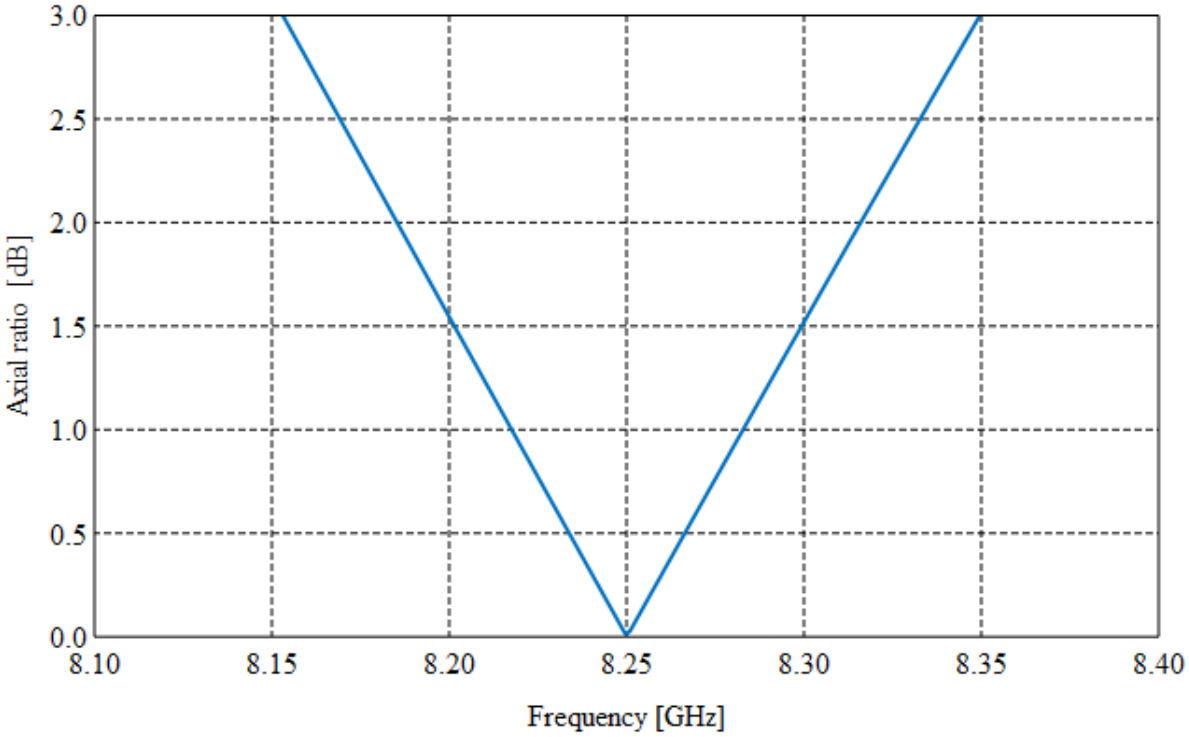

Figure 3-17: Simulated truncated patch antenna's axial ratio at boresight

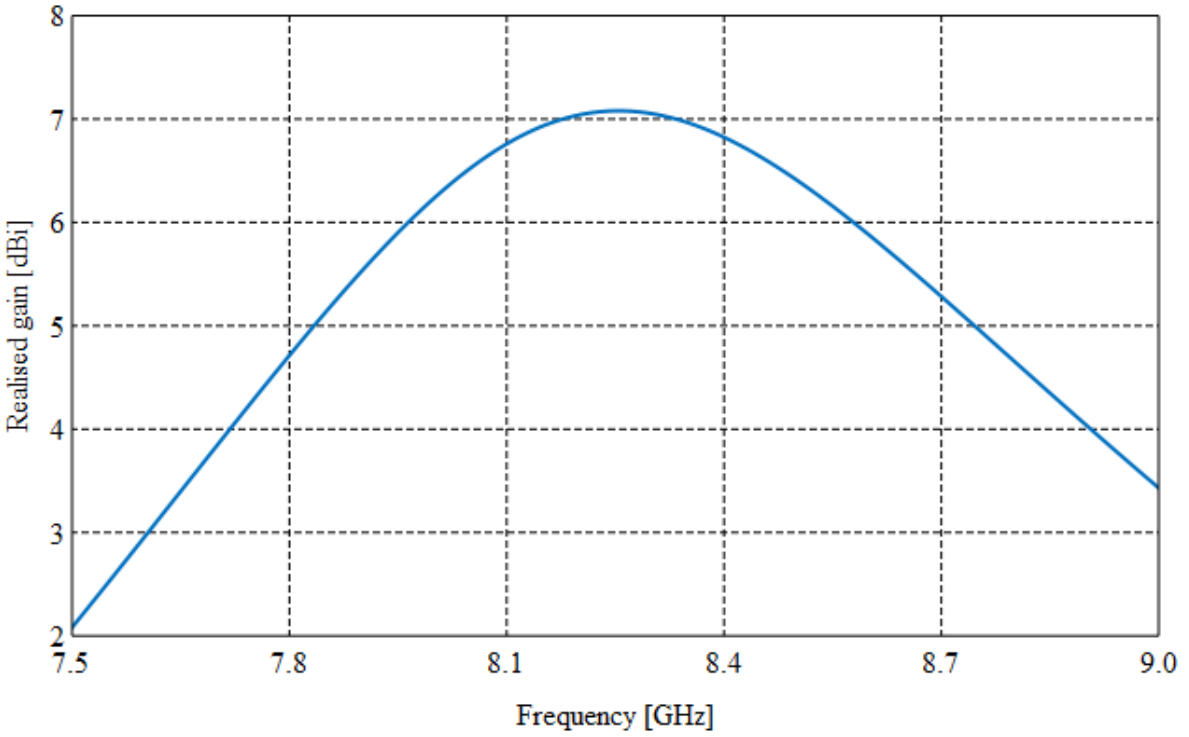

Figure 3-18: Realised gain over frequency of truncated patch antenna

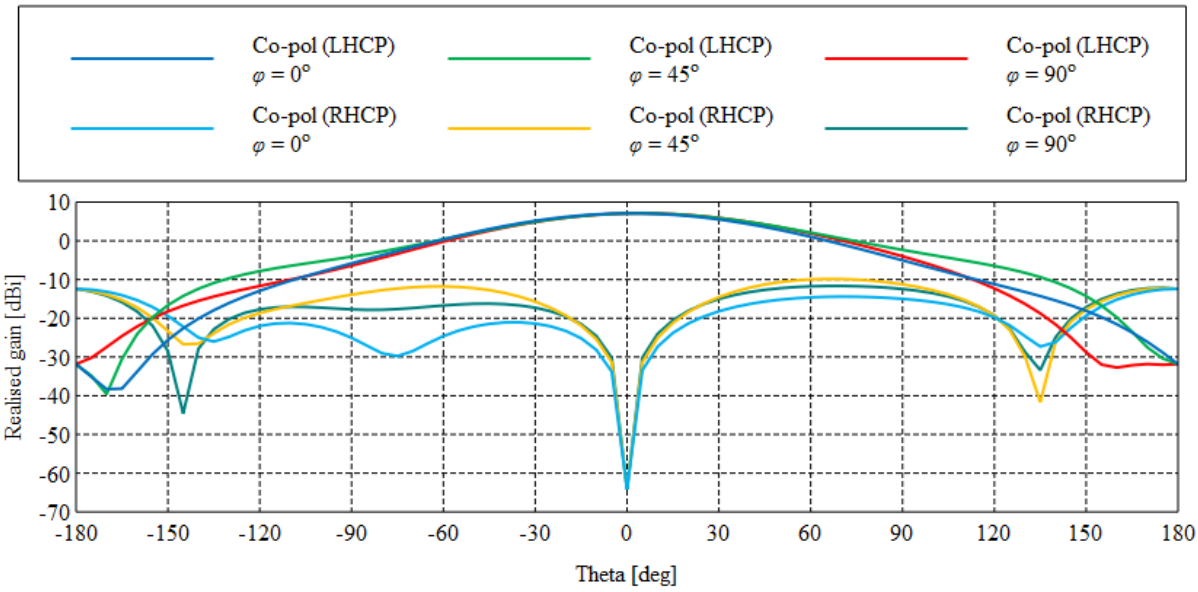

Figure 3-19: Simulated truncated patch antenna pattern at 8.25 GHz

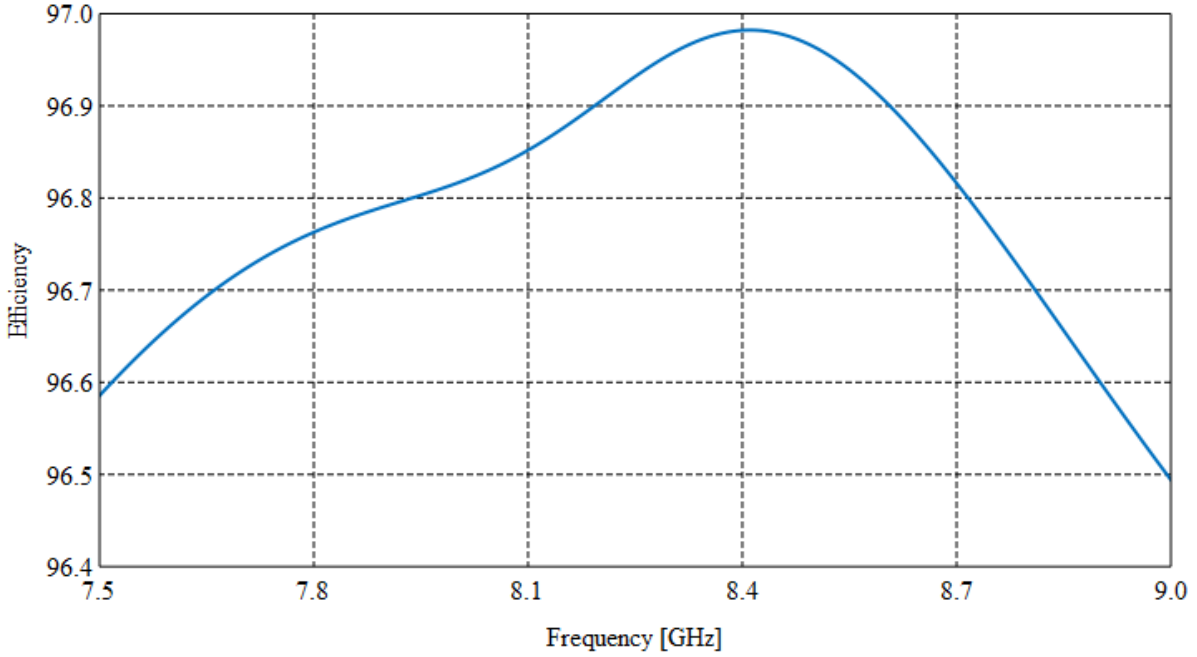

Figure 3-20: Simulated radiation efficiency of truncated patch

The modal frequencies of the truncated patch antenna can be modified by adjusting the length (*S*) or an area of the isosceles triangle cut on the opposite diagonal corners. The frequency of the unperturbed section remains relative constant while the perturbed diagonal frequency has a quadratic variation as indicated in Figure 3-21. Equation 3-3 is derived from Haneishi model (Garg *et al*, 2001:508), where (S^2) represents the total area of the perturbed section and *ab* is the area of the patch without perturbation.

$$\frac{\Delta f}{f_0} = 2\left|\frac{S^2}{ab}\right| \qquad 3\text{-}3$$

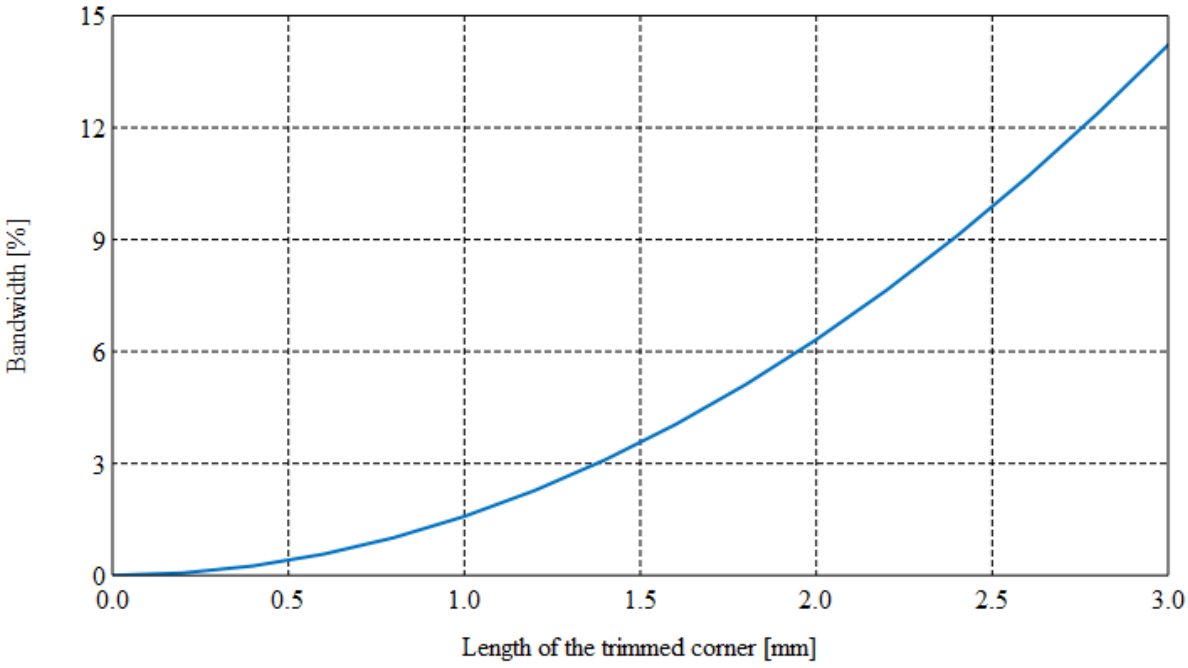

Figure 3-21: Normalised bandwidth vs. length of the isosceles cut

This approach can provide an understanding in the sensitivity analysis of a truncated patch antenna. A study of VSWR and AR bandwidths for certain values of *S* was made. Figure 3-22 below also proves that one modal frequency will be relatively constant whereas the other one varies with changes made to the cut on the opposite diagonal.

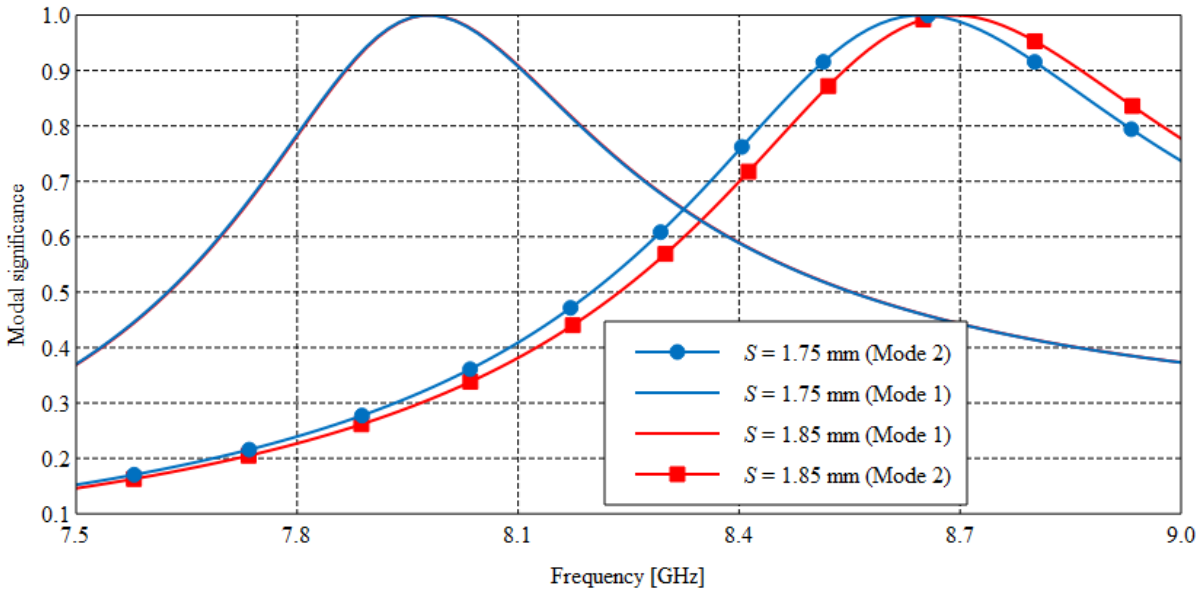

Figure 3-22: Modal analysis of truncated patch antenna

- When S = 1.75 mm, the upper mode is closer to the lower or fundamental mode. This slightly degrades the VSWR bandwidth. There is also a shift in the centre frequency of the AR bandwidth because the average modal frequency of the two orthogonal modes is modified.
- For S = 1.95 mm, the modes are farther from one another, consequently, the VSWR bandwidth slightly improves. In the case of an AR bandwidth, the centre frequency shifts towards the right. From this analysis, it can be deduced that the bandwidth can be controlled by the size of the chamfer cut on the diagonally opposite corners. The matching for both variations is degraded; however, this can be rectified by repositioning the feed pin.

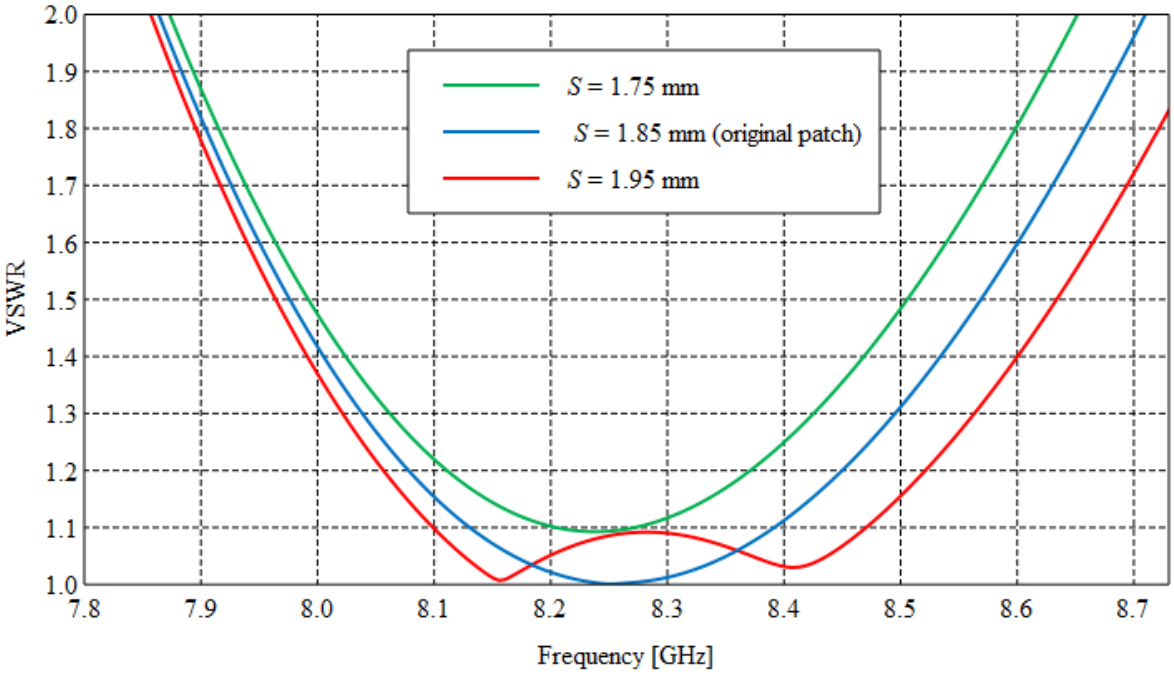

Figure 3-23: Analysis of a VSWR bandwidth of a truncated patch antenna

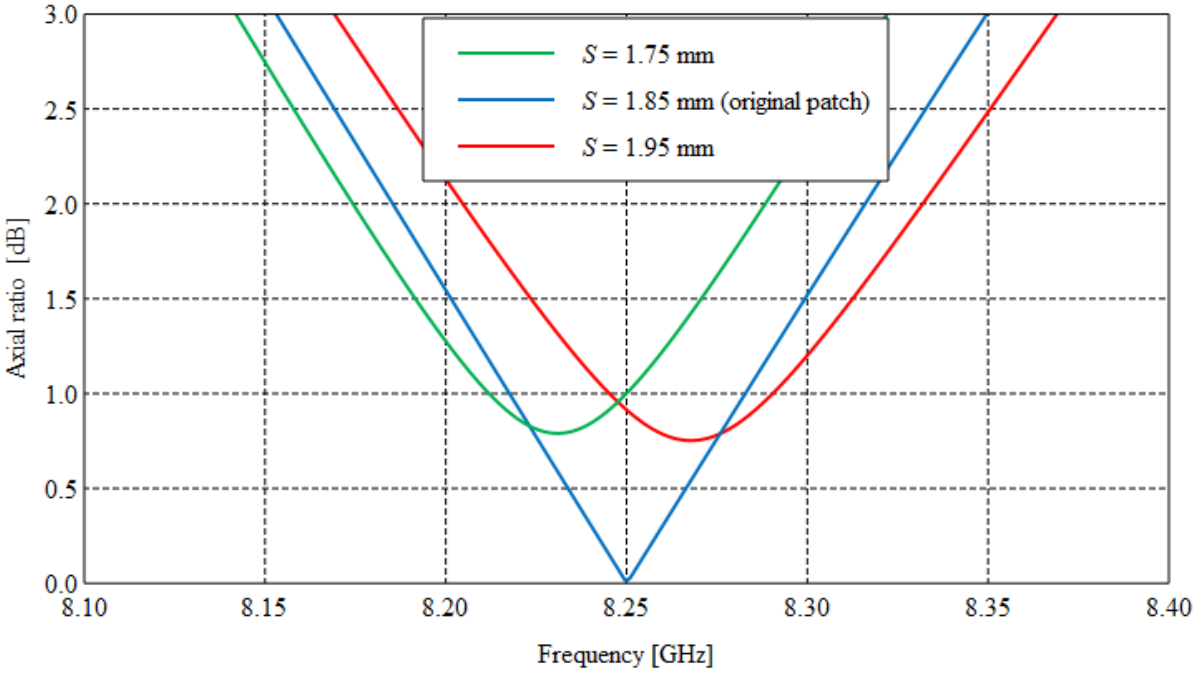

Figure 3-24: Truncated patch axial ratio bandwidth analysis

3.2.3. Circular patch antenna

The analysis of the circular patch antenna shown in Figure 3-25 is similar to the antenna types that were discussed in sections 3.2.1 and 3.2.2. However, unlike in the case of a rectangular or truncated patch antenna types, the modal frequencies are both varying and this can be clearly seen from equations 3-4 and 3-5 (Garg *et al*, 2001:514). This variation is greatly influenced by the dimensions of the slots and the patch radius. In this study, the slot dimension was fixed at 2 mm while the patch radius was varied between 5.4 mm and 6 mm. Equation 3-6 (Balanis, 2005:846) was used to determine the initial value of the patch radius.

$$f_a = f_0\left(1+0.4185\frac{\Delta S}{S}\right) \qquad 3\text{-}4$$

$$f_b = f_0\left(1-1.4185\frac{\Delta S}{S}\right) \qquad 3\text{-}5$$

$$a = \frac{10F}{\left\{1+\frac{2h}{\pi\varepsilon_r F}\left(\ln\left(\frac{\pi F}{2h}\right)+1.7726\right)\right\}^{\frac{1}{2}}} \qquad 3\text{-}6$$

Where $F = \dfrac{8.791\times10^9}{f_r\sqrt{\varepsilon_r}}$

f_a and f_b are the upper and lower modal frequencies respectively,

ΔS is the total area of perturbation,

S is the area of the circular patch,

h is the substrate thickness and

ε_r is the dielectric constant

The characteristic mode analysis relates to the above listed modal frequency equations in a manner that the modal frequency changes every time there is an alteration in the patch radius. This is shown in Figure 3-26. An elliptical shape was chosen to compensate for the feed pin inductance.

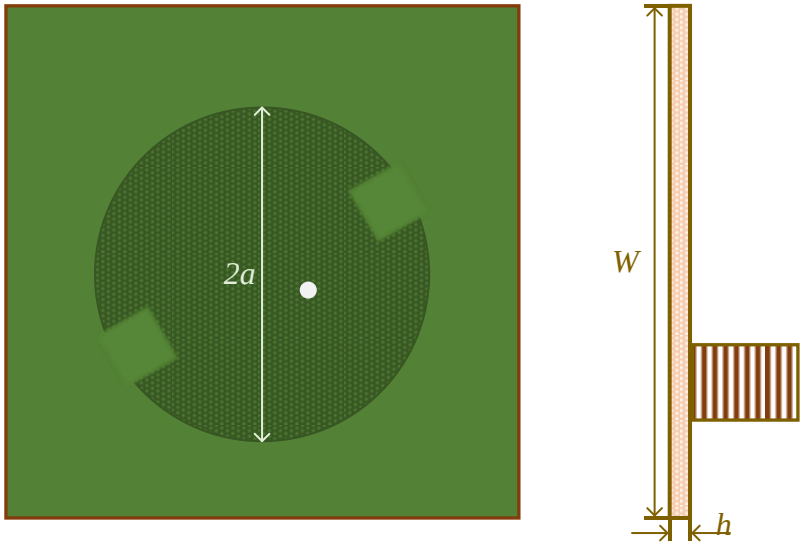

Figure 3-25: Circular patch

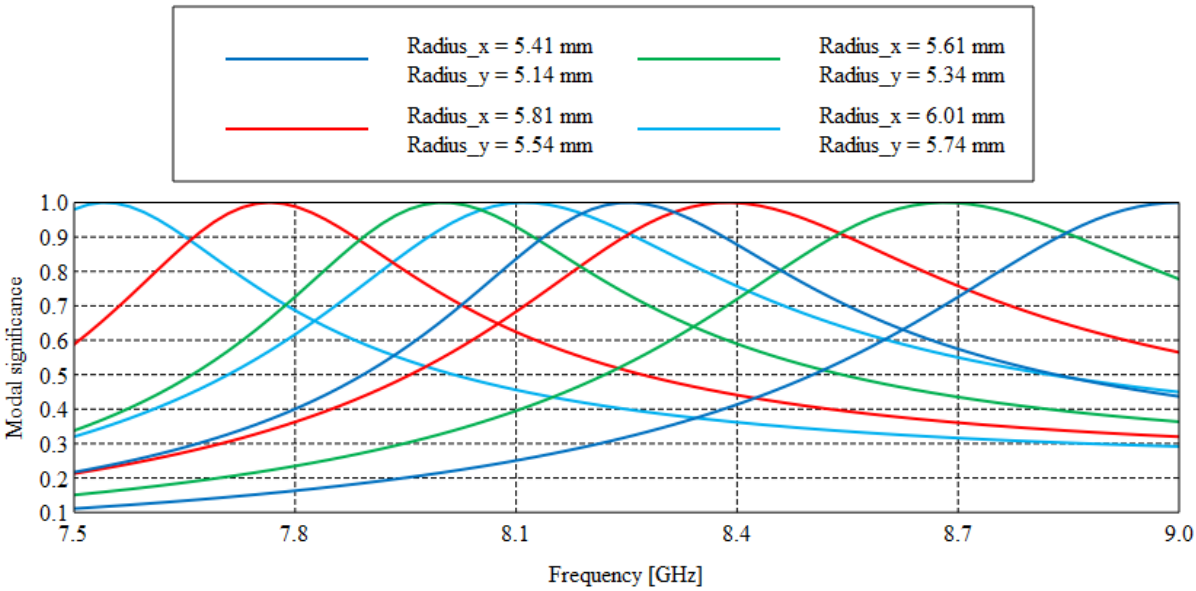

Figure 3-26: Circular patch modal analysis

The substrate properties are kept the same as before and the patch has a minor and major radius of 5.34 mm and 5.61 mm respectively with a 1.8 mm ×2.95 mm slots. The antenna yields the following performance parameters at 8.25 GHz as depicted in Figures 3-27, 3-28, 3-29, 3-30, and 3-31: VSWR ≤ 2 bandwidth = 10 %, gain = 7 dBi, 3 dB axial ratio bandwidth = 2.4 % and radiation efficiency = 97 %.

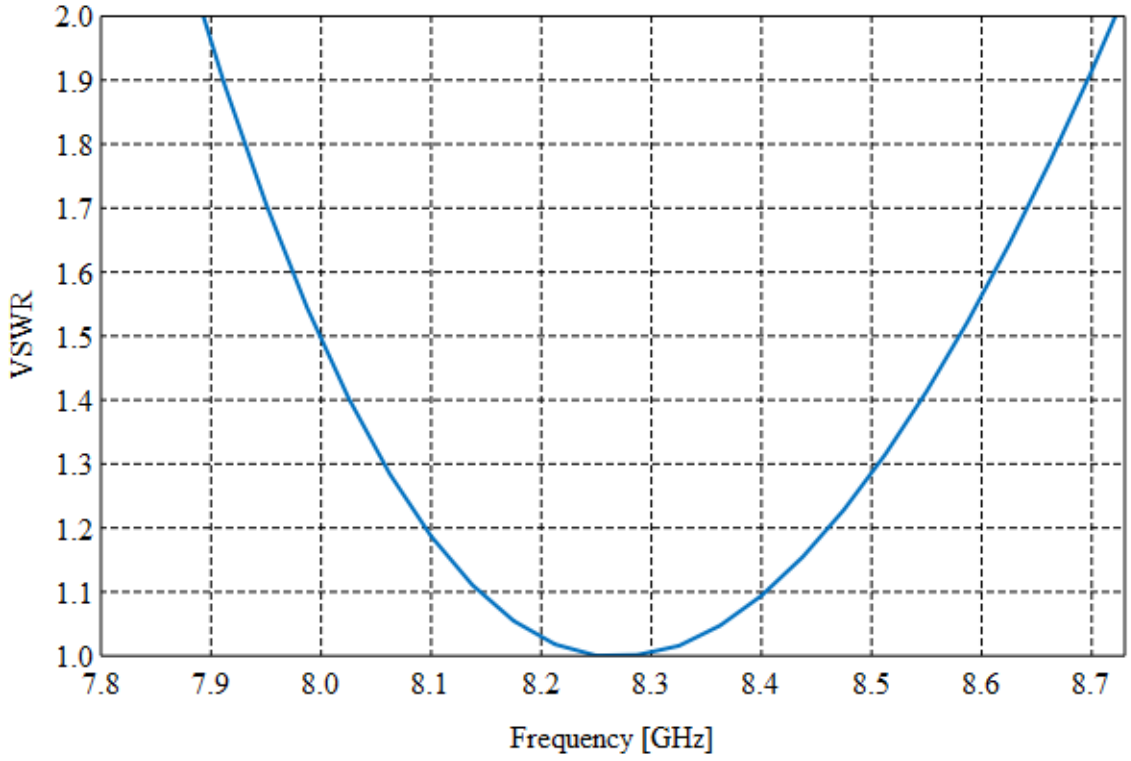

Figure 3-27: Circular patch VSWR plot

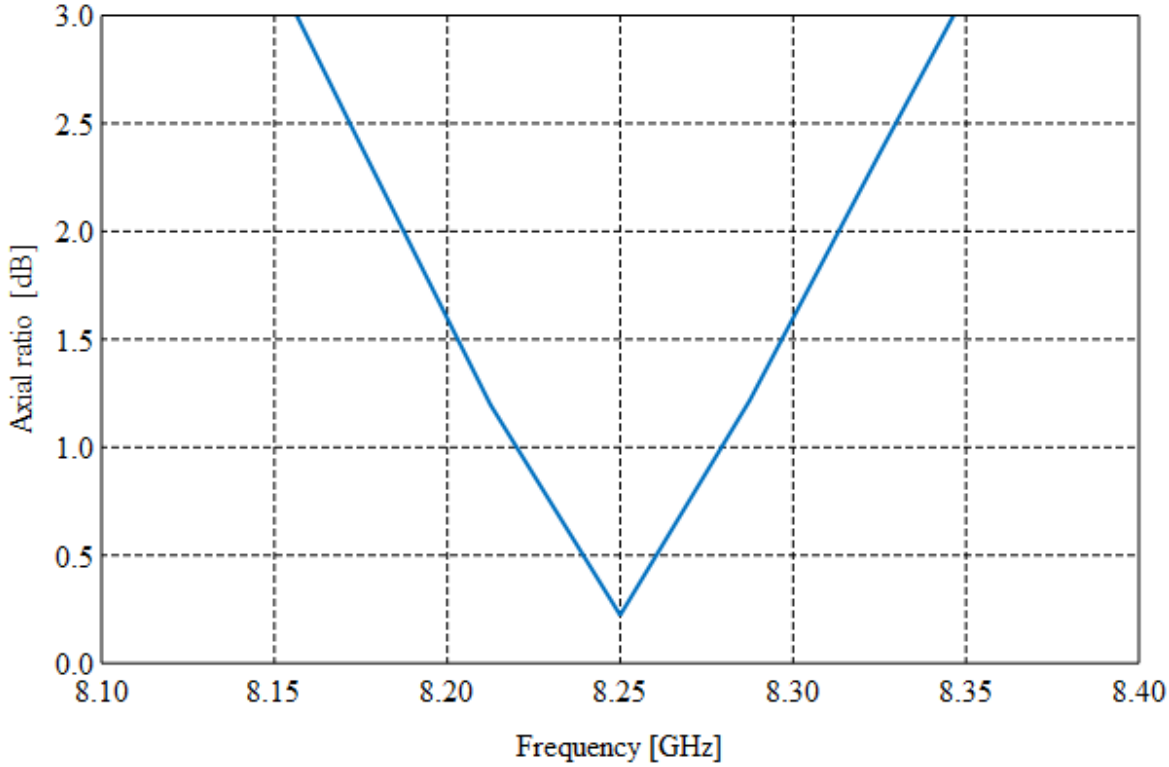

Figure 3-28: Circular patch axial ratio at boresight

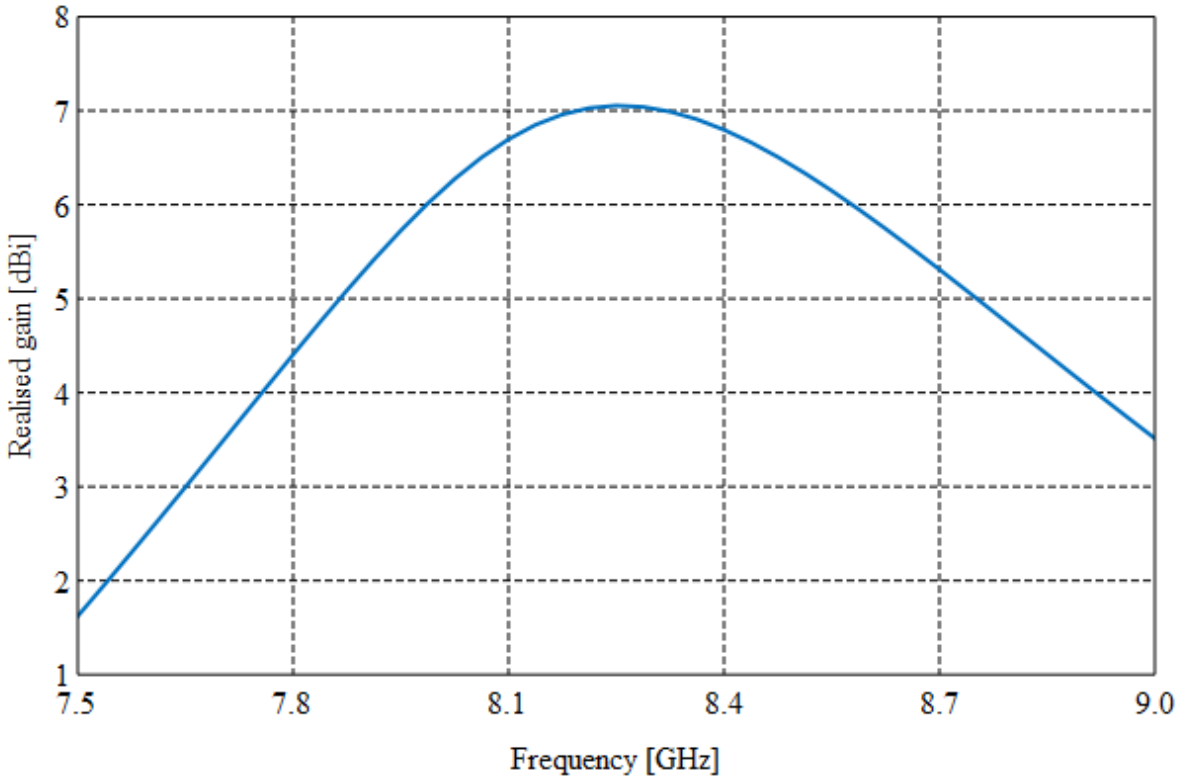

Figure 3-29: Circular patch antenna gain over frequency

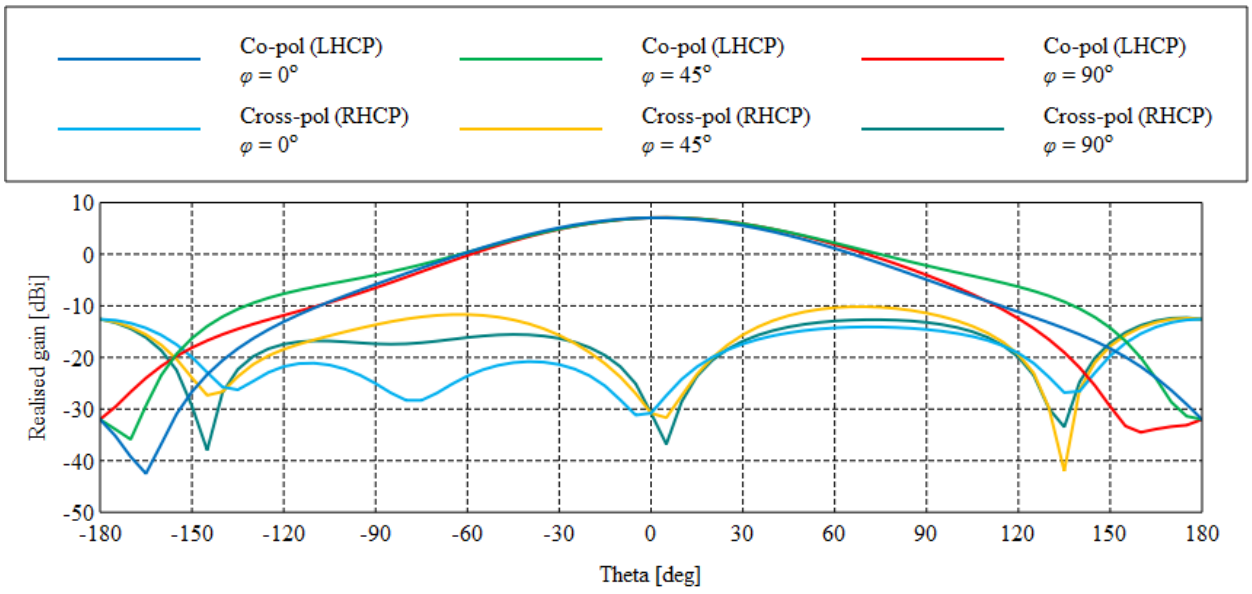

Figure 3-30: Simulated circular patch antenna pattern at 8.25 GHz

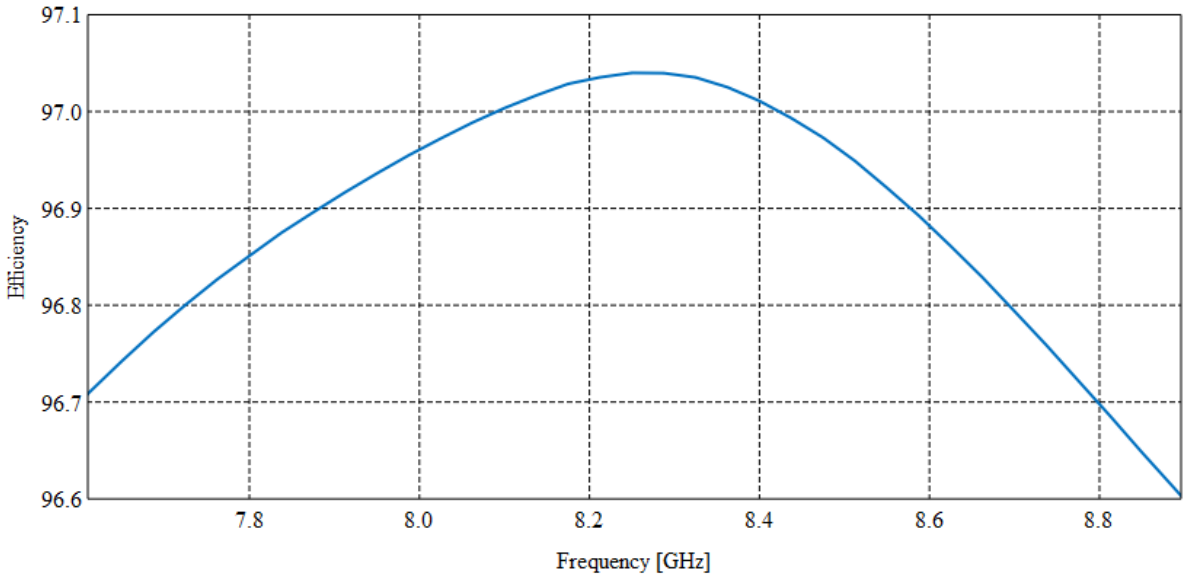

Figure 3-31: Radiation efficiency of a circular patch

Three different types of patch elements were considered and the 3 dB axial ratio characteristics did not satisfy the requirements needed for this specific antenna. In the previous studies that were made in sections 3.2.1, 3.2.2, and 3.2.3, it was found that the AR bandwidth quickly degrades as the frequency shifts away from the centre frequency. This is because the conditions needed for circular polarisation are no longer respected. A bandwidth enhancement technique can still use one of these elements, which can be systematically placed to achieve the desired objectives.

3.3 Bandwidth and gain enhancement

As it was stated that one of the main purposes of this research project is to look at possible ways that could broaden the bandwidth of a microstrip antenna, various techniques have been suggested in the literature but the size and the profile are the limiting factors. A 2×2 sequentially rotated patch array was considered based on its practicality for the intended application and its simplicity. The array makes use of circularly polarised circular patch elements designed in section 3.2.3. Each of these elements has an axial ratio that degrades quickly as the frequency is moved away from the resonant frequency and they are arranged to have an angular orientation of 0º, 90º, 180º, and 270º. According to Hall, Dahele, and James (1989:382), the rotation helps adjacent elements to cancel errors or mutual coupling resulting from the radiation polarisation impurity of each element,

which is fundamental in improving polarisation purity. Another important aspect of this design is to get the feeding line phase difference correct, which in this case is obtained by using different line length as diagrammatically shown in Figure 3-32. The patch was modelled on RT/duroid 5880 substrate with a height h = 0.79 mm. The use of thinner substrate was prompted by the fact that the size of feeding network specifically the width; thickens when substrate height is raised. Thus, this is the way to minimise the width size of the feeding network.

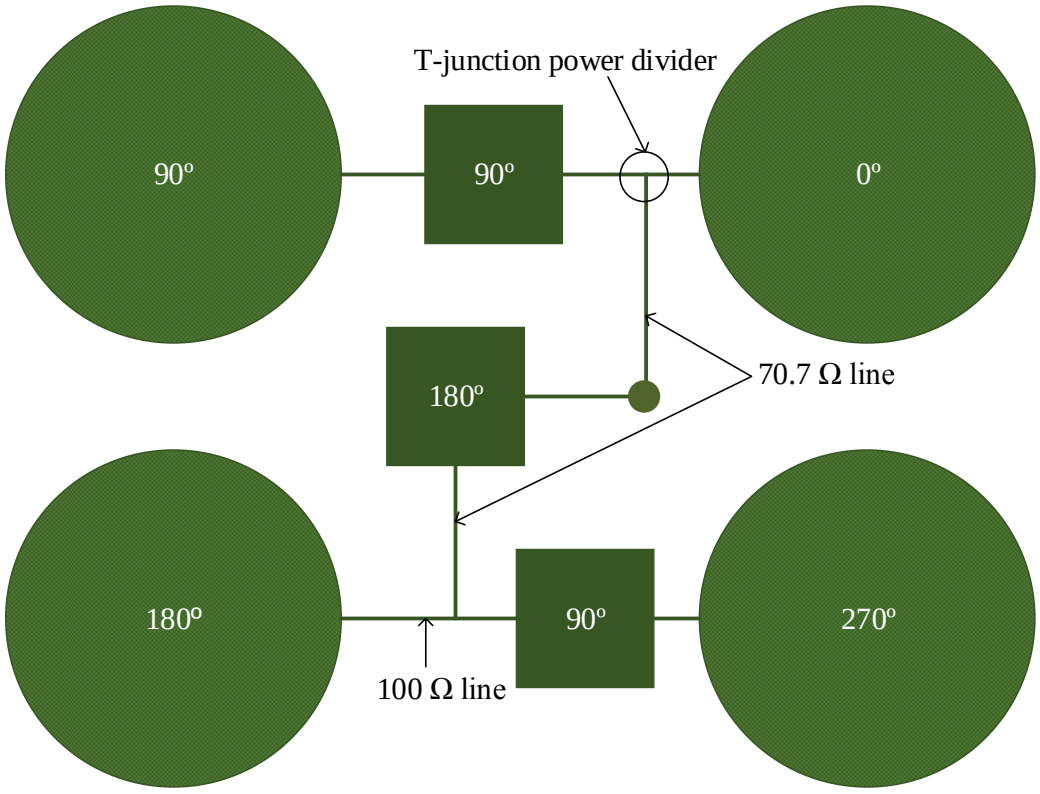

Figure 3-32: Sequentially rotated array feeding network

Figure 3-32 shows a feed network of a sequentially rotated patch array. This network is composed of a T-junction power divider that ensures an equal split of power at the intersection if the impedance of the T-arm is the same. In reference to Figure 3-32, the T-arm has an impedance of 100 Ω and the 90º phase is realised by the quarterwave transformer. The 180º phase is achieved by employing a half wavelength line on a 70.7 Ω transmission line.

3.3.1. Sequential rotated array

Figure 3-33 shows the optimal design of the sequential rotated patch antenna. An SMP connector with a pin diameter of 0.7 mm was used. The simulation results show an improvement of both the VSWR and axial ratio bandwidths.

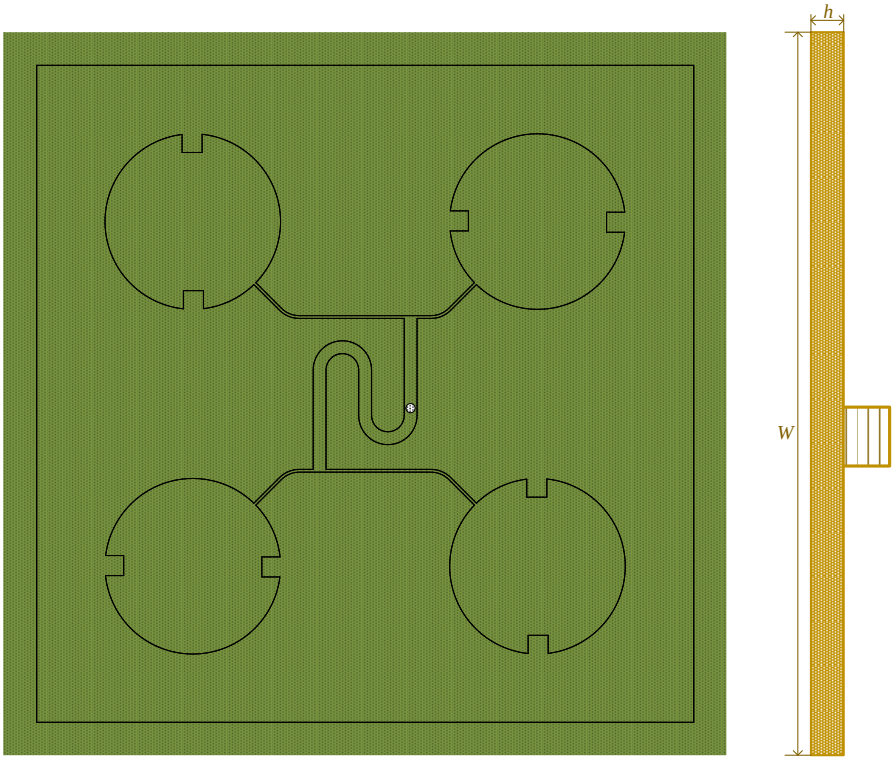

Figure 3-33: Sequential rotated patch antenna

Figure 3-34 plots the simulated VSWR, which indicates that the antenna yields a VSWR ≤ 2 bandwidth of more than 16 %, which increased by roughly 4 % when compared to that of single patch antenna. The 3 dB axial bandwidth has risen to 9.6 % from 2 %, gain = 12.95 dBi and radiation efficiency = 96 %, these are shown in Figures 3-35, 3-36 and 3-38 respectively. A directive pattern results from the array as is shown in Figure 3-37. This narrows the beamwidth by more than a half and there is formation of side lobes that could possibly lead to an undesired radiation.

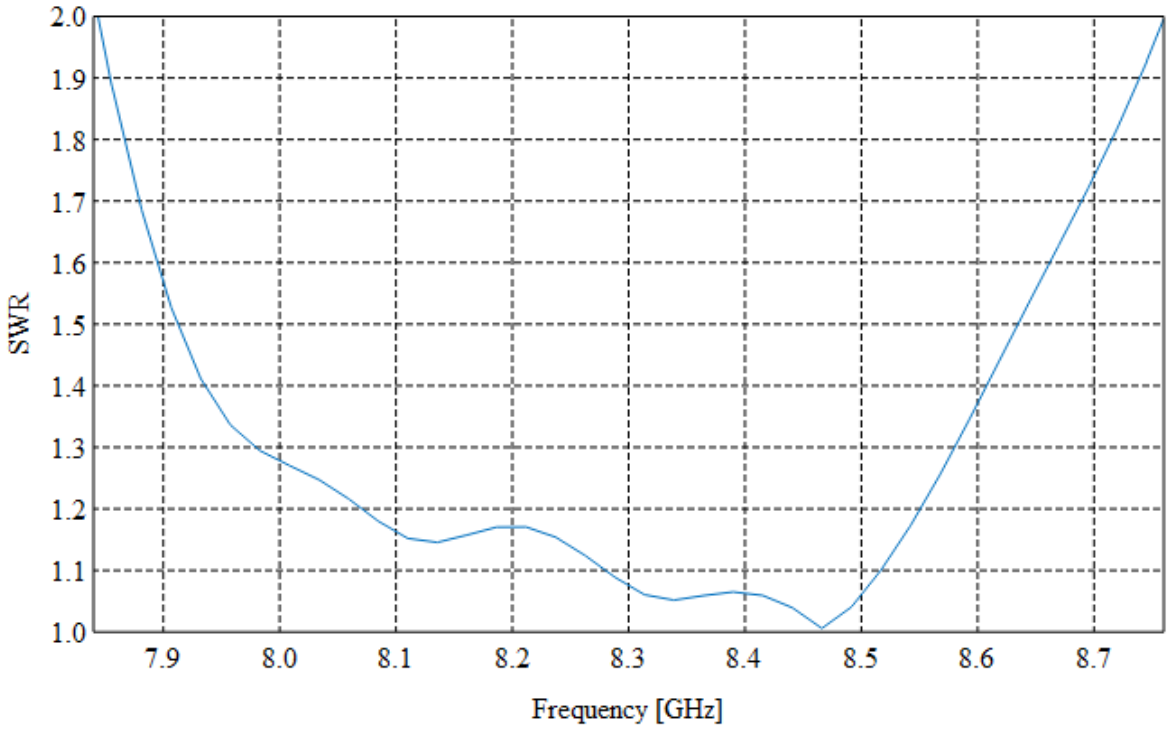

Figure 3-34: Sequentially rotated array VSWR plot

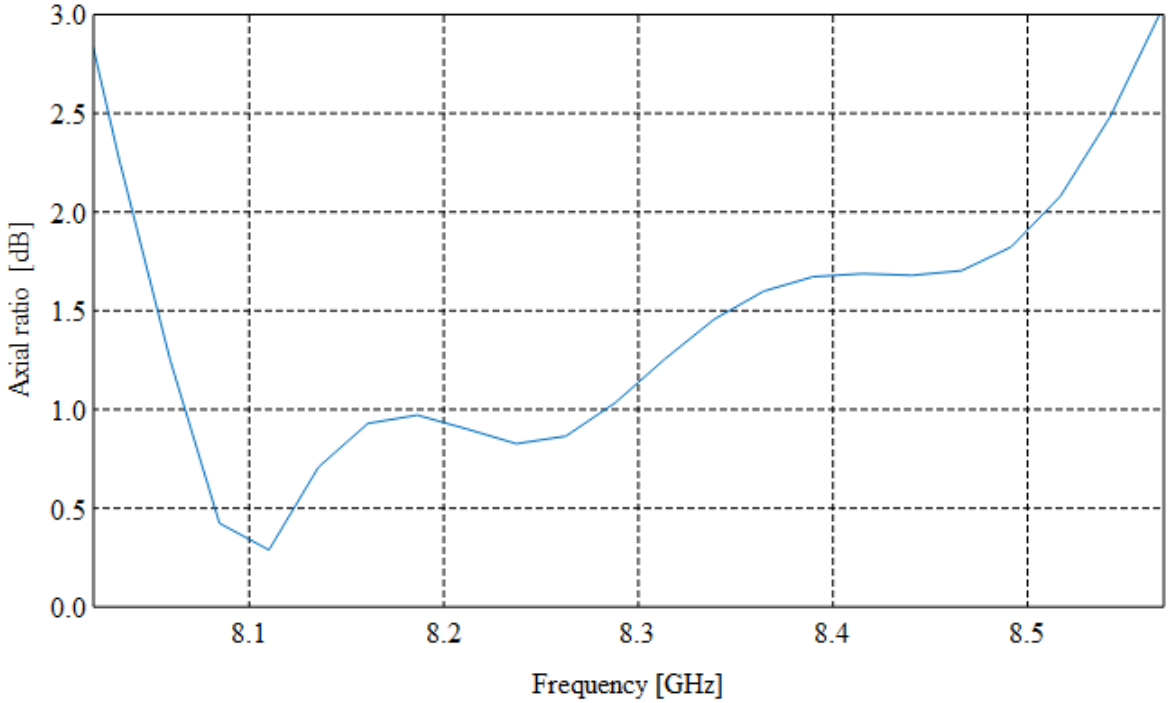

Figure 3-35: Simulated sequentially rotated patch antenna boresight axial ratio

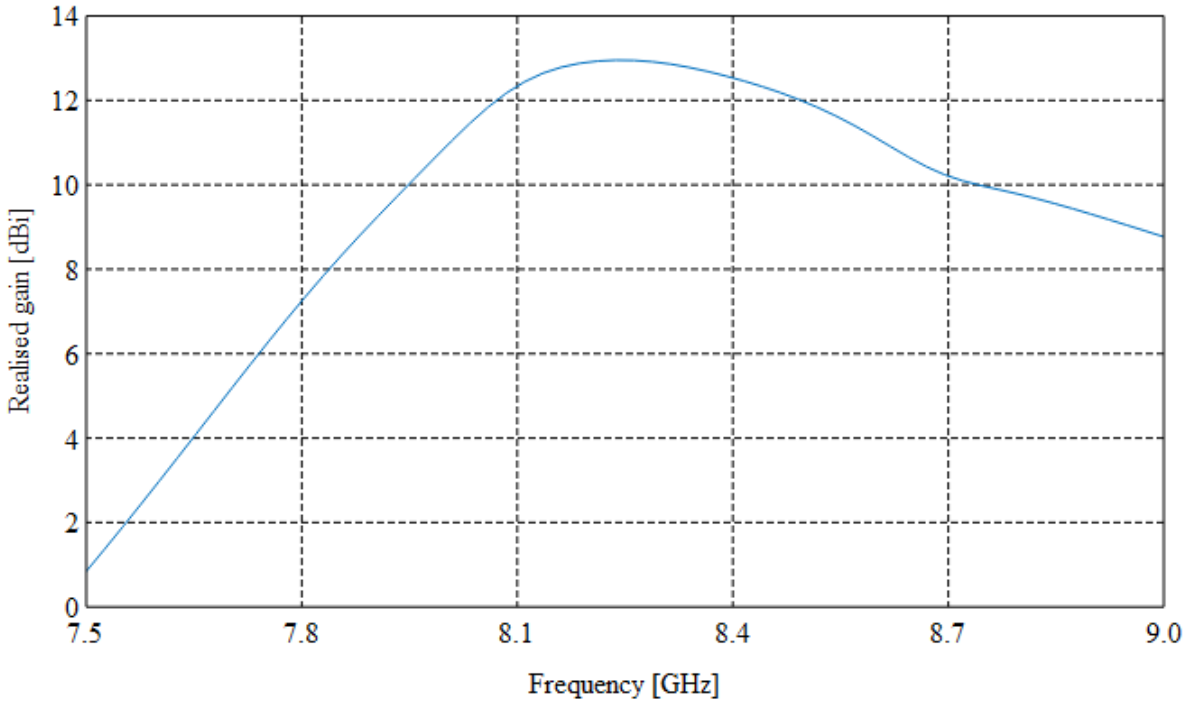

Figure 3-36: Gain over frequency of a sequentially rotated patch array

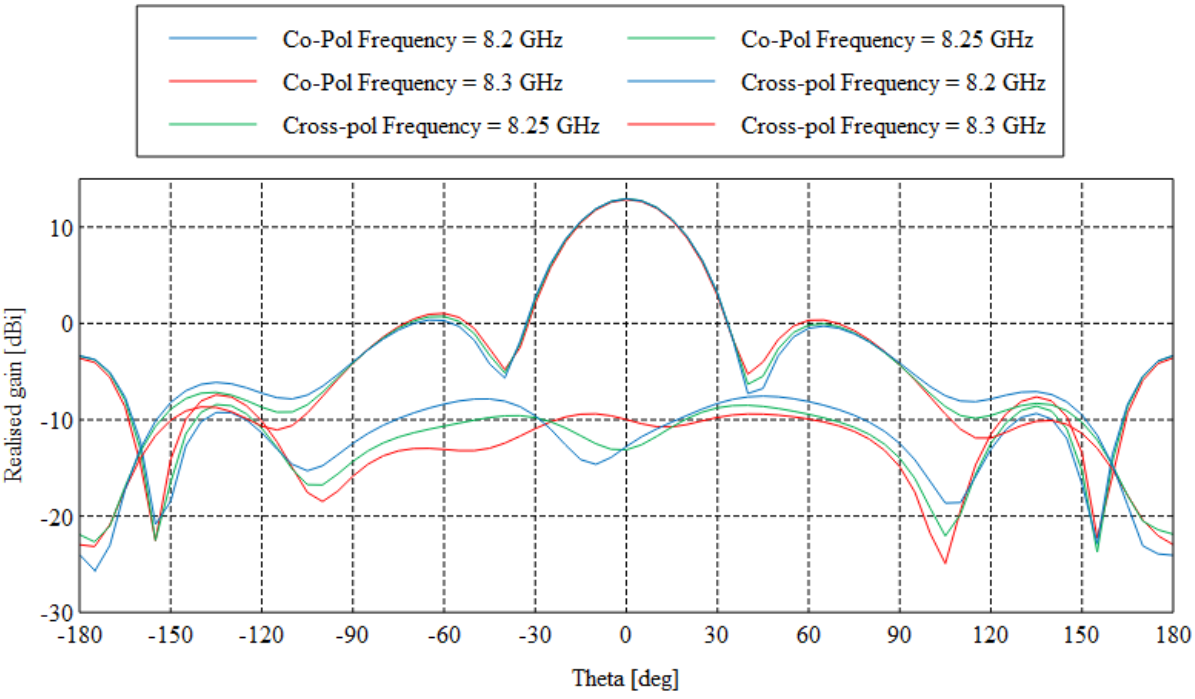

Figure 3-37: Sequentially rotated array patterns at different frequencies

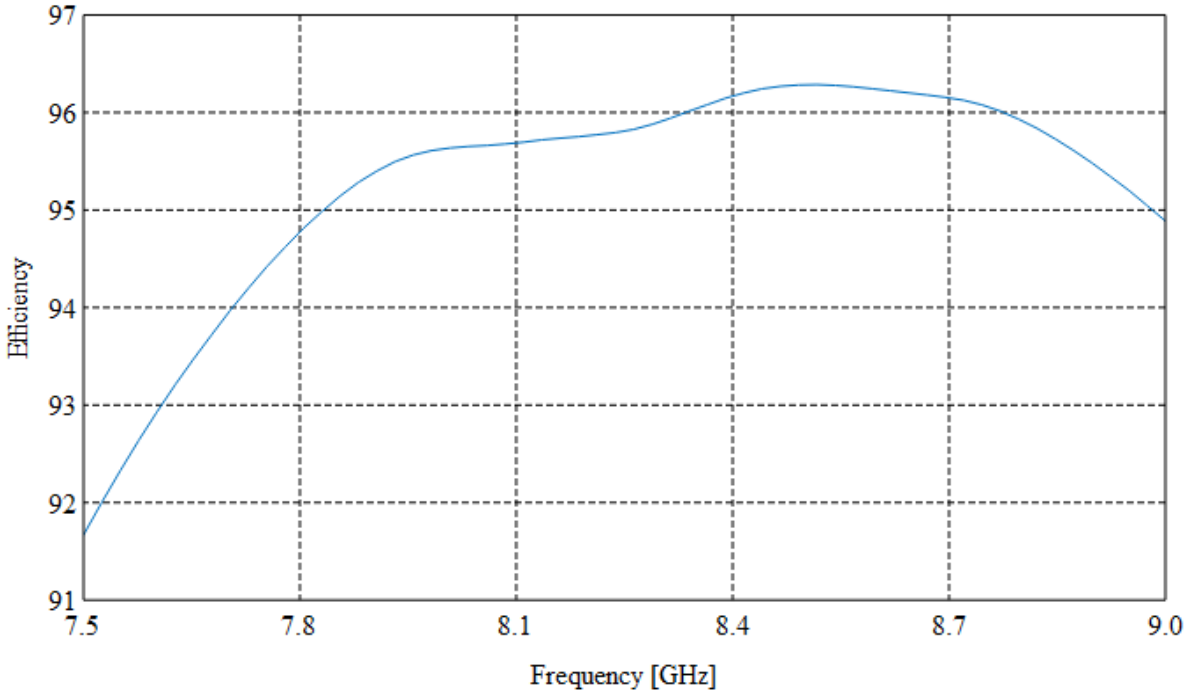

Figure 3-38: Sequentially rotated patch array radiation efficiency

Figures 3-39 and 3-40 show the comparison of some parameters of single patch elements to that of an array. From these figures, it can be deduced that the 2×2 patch array outperforms these elements, as it would be expected. The radiation pattern begins to form a directional pattern, which may result in undesired radiation caused by the side lobes, this is shown in Figure 3-41.

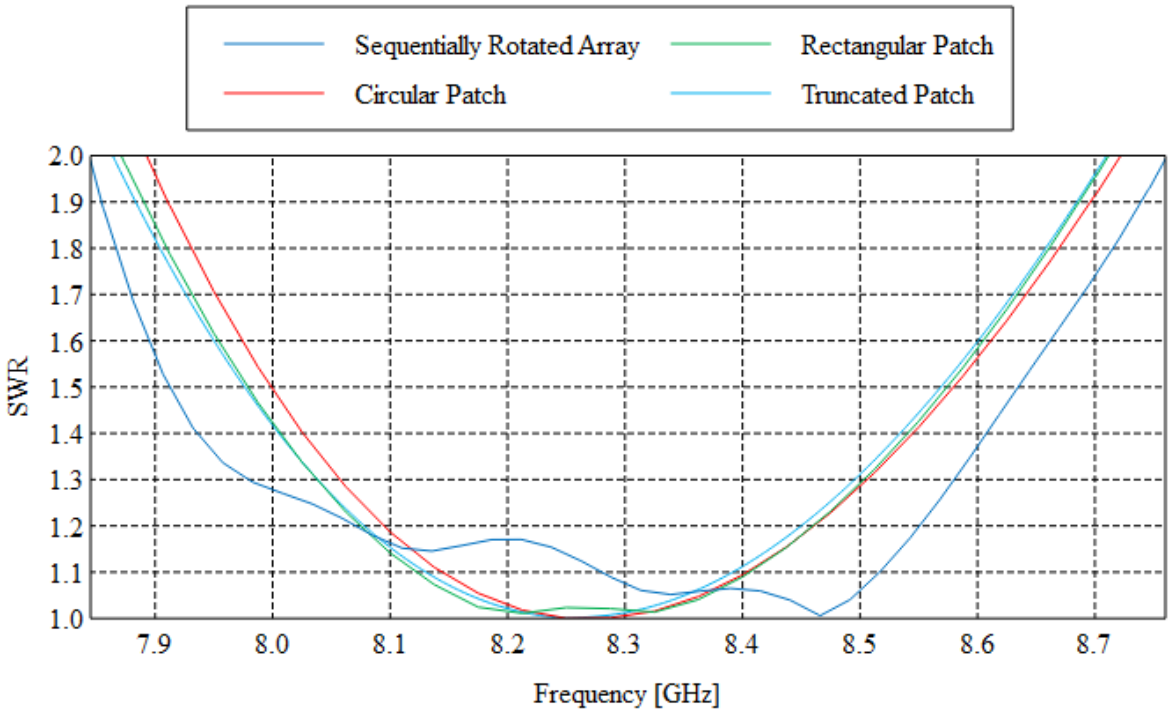

Figure 3-39: Comparison of simulated VSWR ≤ 2 bandwidth

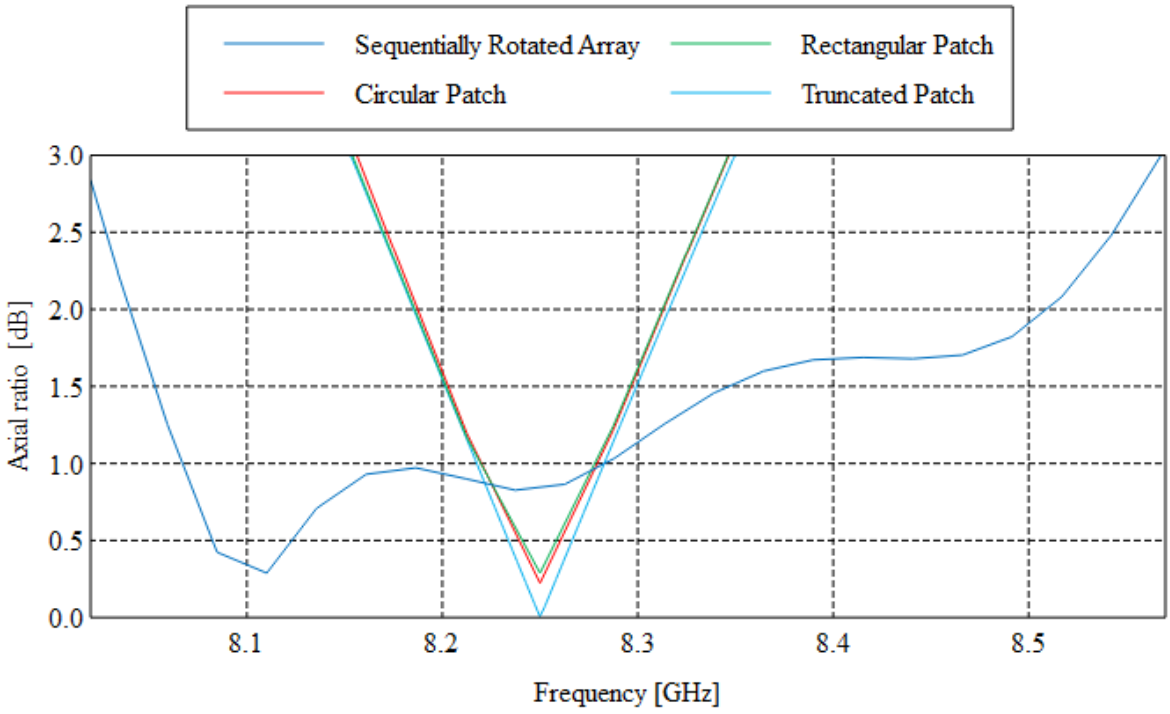

Figure 3-40: Comparison of 3 dB axial ratio bandwidth

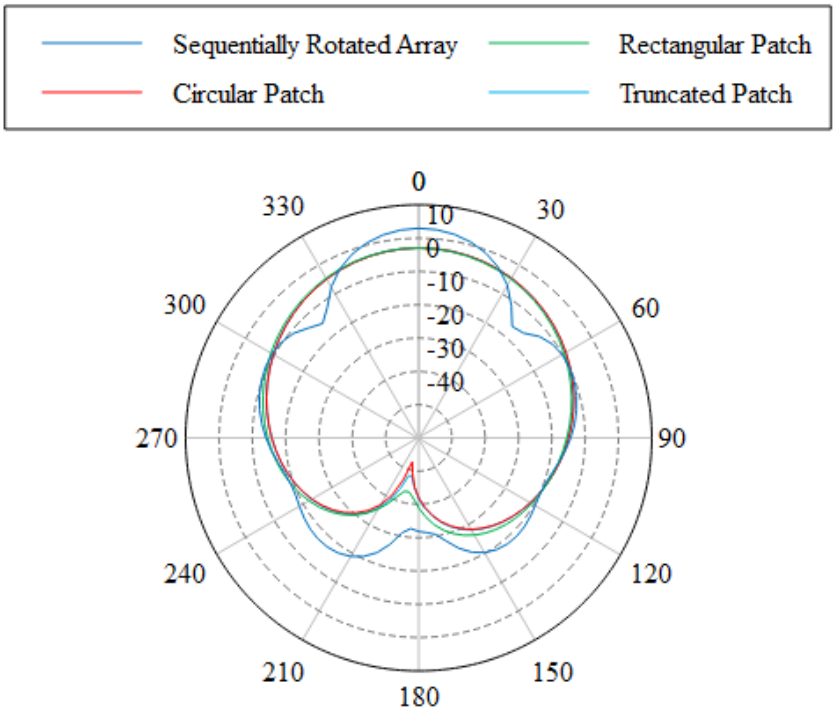

Figure 3-41: Sequentially rotated patch array radiation patterns at 8.25 GHz (ϕ = 0°)

3.4 Conclusions

In this chapter, different antenna characteristics were studied and the main parameters of interest were the VSWR ≤ 2 and 3 dB axial ratio bandwidths. Various patch antenna shapes namely nearly square patch, truncated patch and a circular patch were considered. As expected, the AR bandwidth for these elements did not meet the requirements set for this specific antenna. A bandwidth enhancement technique, which used a 2×2 array of sequentially rotated circular patch antennas, was used. The axial ratio bandwidth has improved greatly from 2 % to 9.6 %. These models were realised to verify the accuracy of simulated results. The measured results are presented in the next chapter.

Chapter 4

Prototypes and analysis of the measured results

4.1 Introduction

The X-band patch antennas were built and tested at the Cape Peninsula University of Technology's facilities. Final test measurements were made at Stellenbosch University. Figure 4-1 (a-d) shows the patch antenna prototypes. All single patch elements were fabricated on a 1.524 mm thick Roger's RT/duroid 6002 substrate material, which was the supplied sample. The patch antenna array was made on a 0.79 mm thick RT/duroid 5880 substrate material. This chapter verifies the accuracy of the models that were designed and analysed in FEKO.

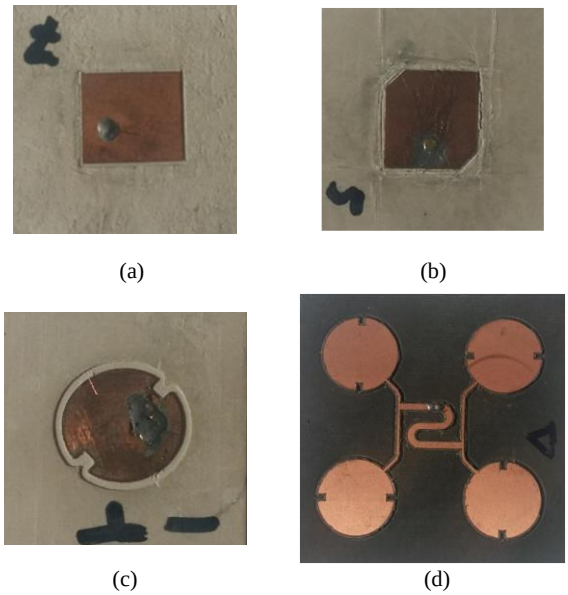

(a) (b)

(c) (d)

Figure 4-1: Antenna prototypes: (a) nearly square patch antenna (b) nearly square truncated patch antenna (c) circular patch antenna (d) sequentially rotated array

4.2 Analysis of the measured results

Before antenna measurements can be made, there are setups or equipment that needs to be first configured. This equipment is listed under heading 4.2.1. The common antenna measurements that define the performance of any antenna are radiation pattern, gain, voltage standing wave ratio, polarisation, and bandwidth.

4.2.1. Requirement

The following equipment is required for antenna measurements.

- Vector network analyser
- Source antenna
- Positioning system
- Test range (anechoic chamber)

A block diagram that represents a test setup of the equipment listed above is shown in Figure 4-2.

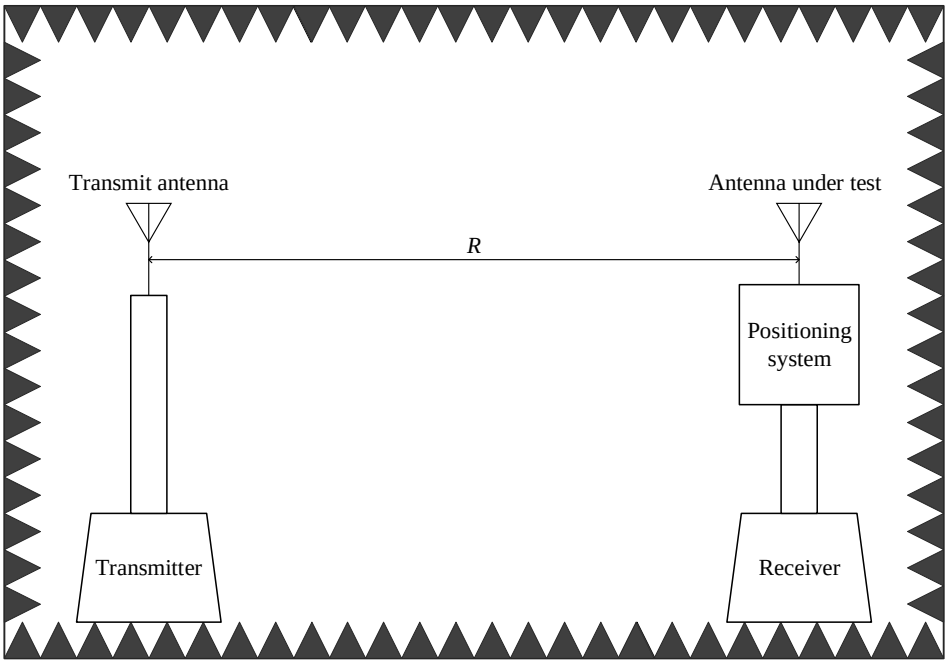

Figure 4-2: Antenna range measuring system

4.2.2. Setup

The vector network analyser (VNA) was calibrated for the desired frequency range. A two port calibration was done for the VSWR measurements and gain measurements. The VNA was used as both the transmitter and receiving device, therefore for a two port calibration, a 1.5 m cable was used to perform the through calibration since the two ports were distant. This normalises the forward transmission response to 0 dB for the selected frequency range.

4.3 Measured results

The measurements were done at Stellenbosch University and they are VSWR, gain, and pattern measurements.

4.3.1. Nearly square patch antenna

The antenna was manufactured and measured based on the optimal design presented in section 3.2.1, as displayed in Figure 4-1a. The model has dimensions of b = 9.96 mm and a = 9.03 mm with an average error percentage of 1.8 %. Figures 4-3 and 4-4 show the measured results for the VSWR and input impedance compared with simulated results. The shape of the measured VSWR plot exhibits similar characteristics when compared to the simulated results with a fractional bandwidth of 11.2 %, but is centred at a higher frequency of 8.4 GHz. The manufacturing process is one of the reasons the two models do not entirely correlate with one another. The FEKO model dimensions were changed to match those of the experimental model. The VSWR plots of these two models are similar and shifted to the same frequency point. This verifies that the manufacturing tolerances affects the antenna performance. Furthermore, the PCB machine cuts deep into the substrate around the edges of the patch element and thus affects the current distribution. The inductive properties of the input impedance (see Figure 4-4), can also alter the resonant frequency of the patch antenna. As seen in the figure, the patch antenna will resonate or radiate most of its energy to a point where there is least reactive component, in this case 8.4 GHz. In addition, the experimental model has a different input transmission line length when compared to the FEKO model, hence the rotation on the Smith chart.

The point with the circle on the Smith chart indicates that the sense of polarisation of electric fields is more circular there than any other point. The axial ratio plot shown in Figure 4-5 verifies this. The axial ratio is minimal at 8.4 GHz and is measured as 0.7 dB. Since the FEKO model and the built prototype are not exactly similar, the axial ratio at the desired frequency of 8.25 GHz is more than 3 dB, which implies that the fields are more elliptical. The normalised radiation pattern at 8.25 GHz shows differences in pattern measured at 0°, 45° and 90° plane cuts due to unequal amplitude of the fields resulting from high axial ratio. This is shown in Figure 4-6. The antenna radiates efficiently at 8.4 GHz and its pattern is uniform in all plane cuts (see Figure 4-7).

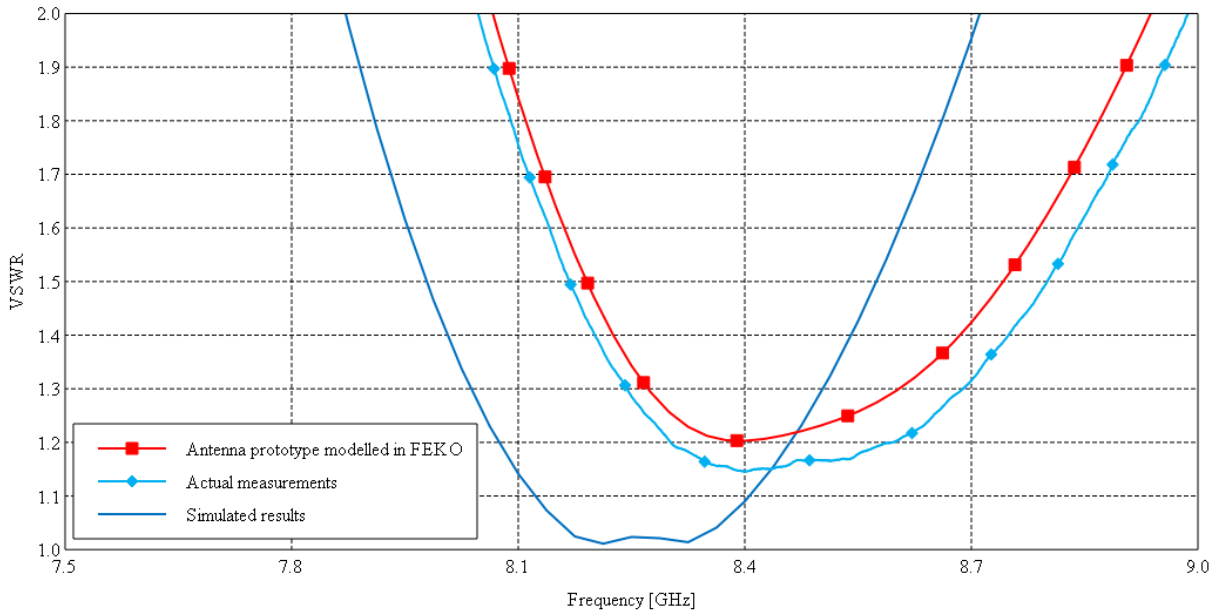

Figure 4-3: Comparison of the simulated and measured VSWR plots of a nearly square patch antenna

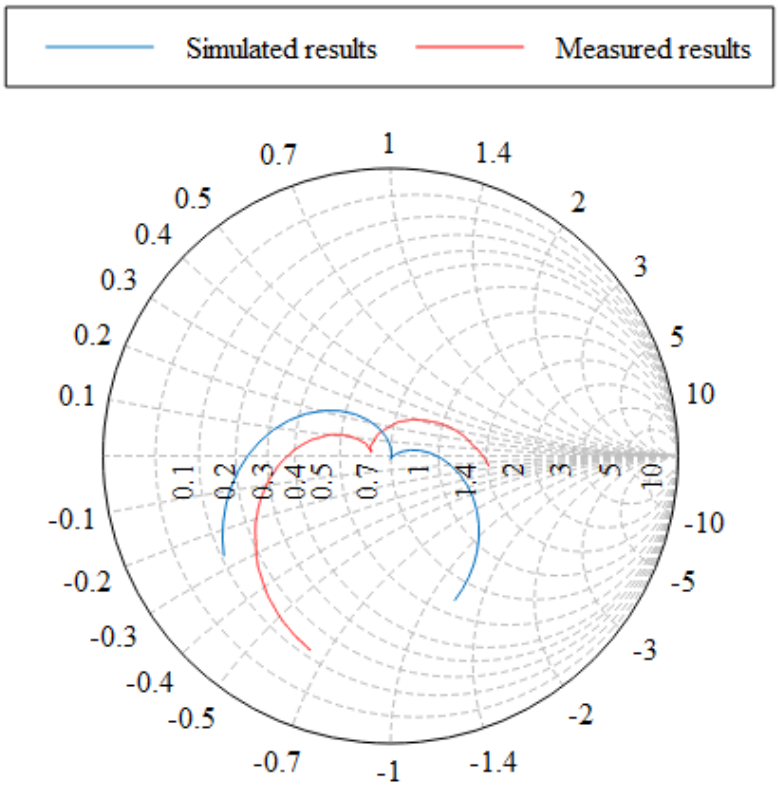

Figure 4-4: Simulated and measured impedances of a nearly square patch antenna

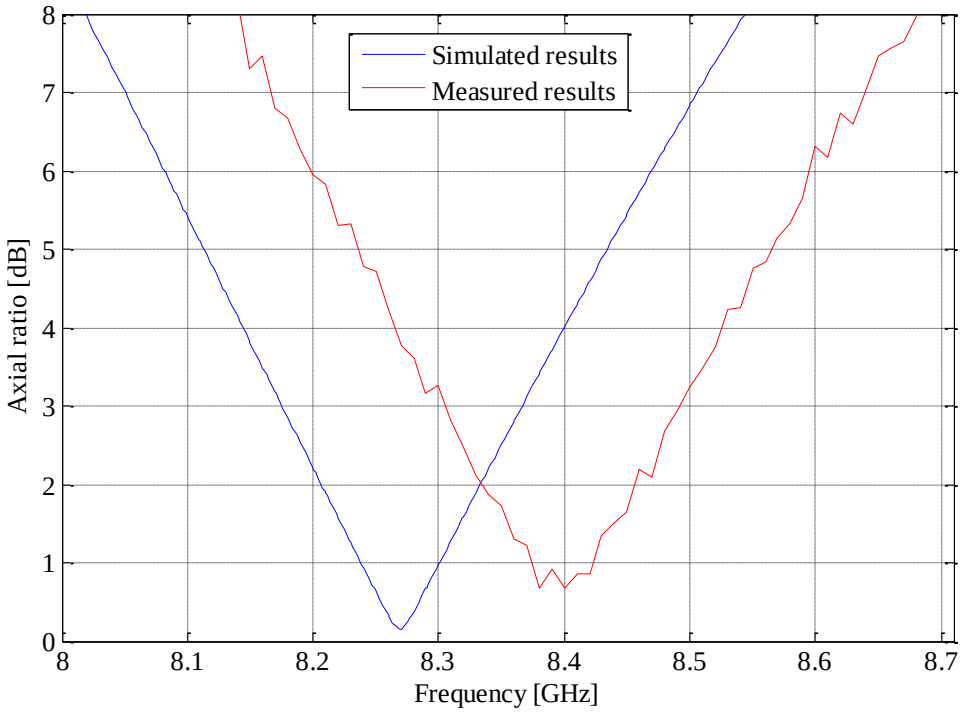

Figure 4-5: Comparison of simulated and measured boresight axial ratio of a nearly square patch antenna

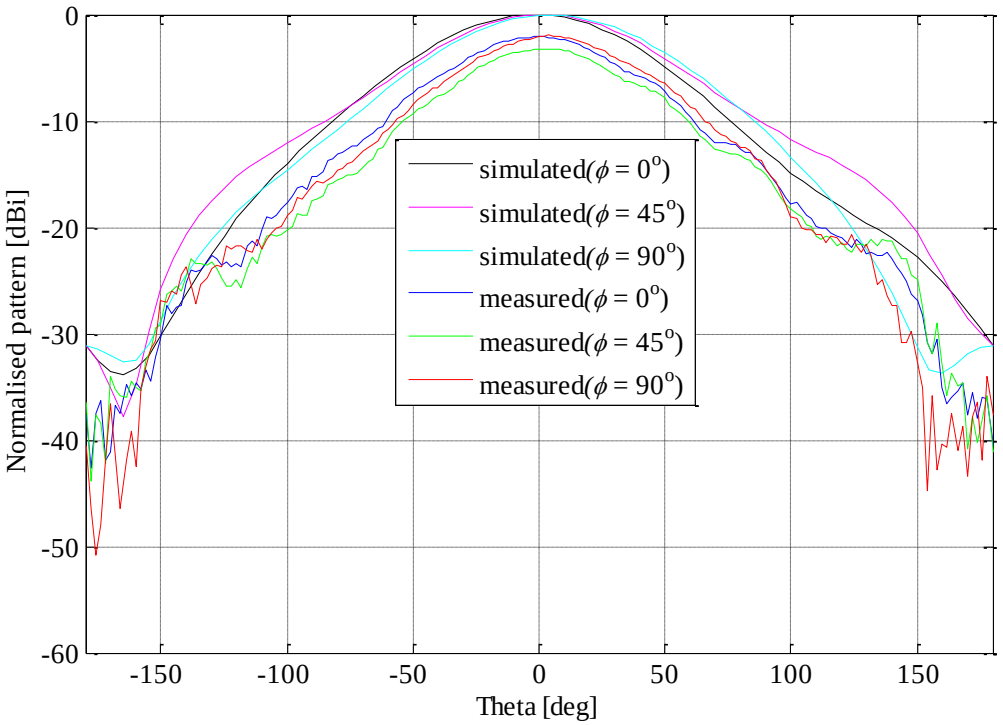

Figure 4-6: Normalised pattern of a nearly square patch antenna at 8.25 GHz

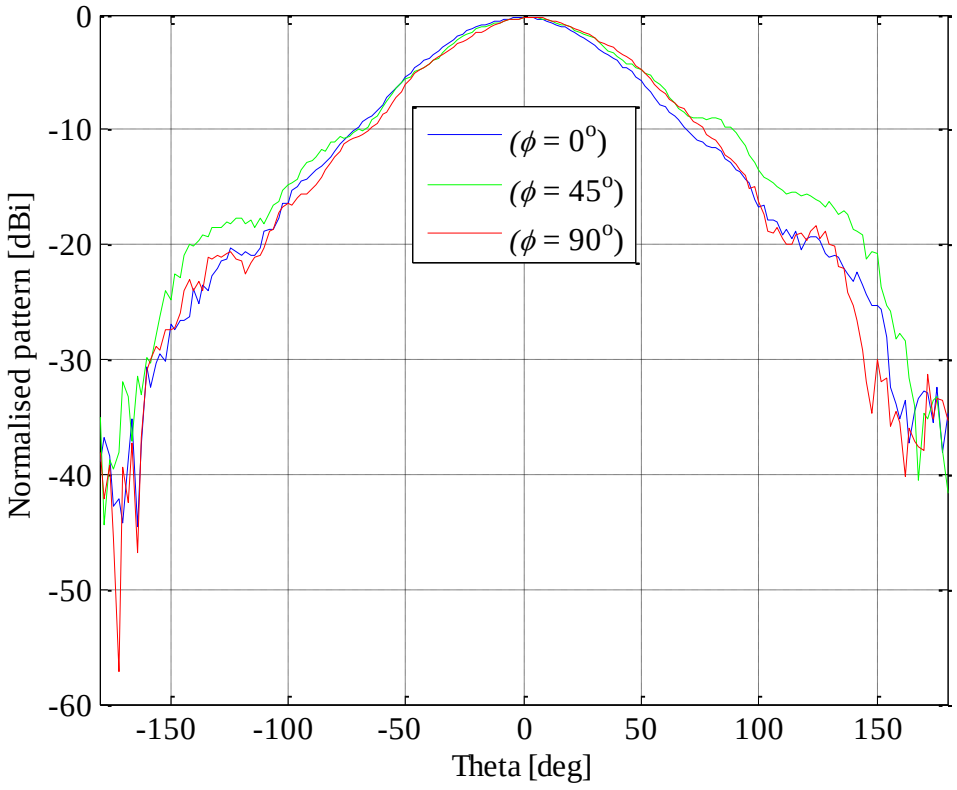

Figure 4-7: Normalised pattern of a nearly square patch antenna at 8.4 GHz

4.3.2. Nearly square truncated patch antenna

The experimental model of the truncated patch antenna is shown in Figure 4-1b. The antenna average tolerance error is summarised on Table 4-1. Once again, the FEKO model and the prototype do not yield the same performance results. As per simulations, the antenna is supposed to be resonating at 8.25 GHz instead of 8.5 GHz. Thus, the plots are shifted to this frequency as shown in the figures below. Looking at Figure 4-8, the VSWR plots have similar shape, however, due to high input reactance at 8.25 GHz (refer to Figure 4-9) the patch antenna is not properly matched to the 50 Ω SMA connector. Furthermore, the frequency point where the axial ratio is the best (Figure 4-10), the electric field is the same in all plane cuts implying that the fields are circularly polarised. The normalised pattern is shown in Figure 4-11. Due to time constraints, the gain measurements for the nearly square patch and nearly square truncated patch antennas were not performed. It was however, assumed that these antennas will have the same gain as the patch element discussed in section 4.3.3.

Table 4-1 Summary of the manufacturing tolerances for the truncated patch antenna

Parameter	FEKO model value [mm]	Prototype [mm]	Percentage error [%]
a	10.02	10.08	0.6
b	9.37	9.54	1.8
p_y	2.53	2.69	2.2
S	1.85	1.89	6.3
		Average	2.7

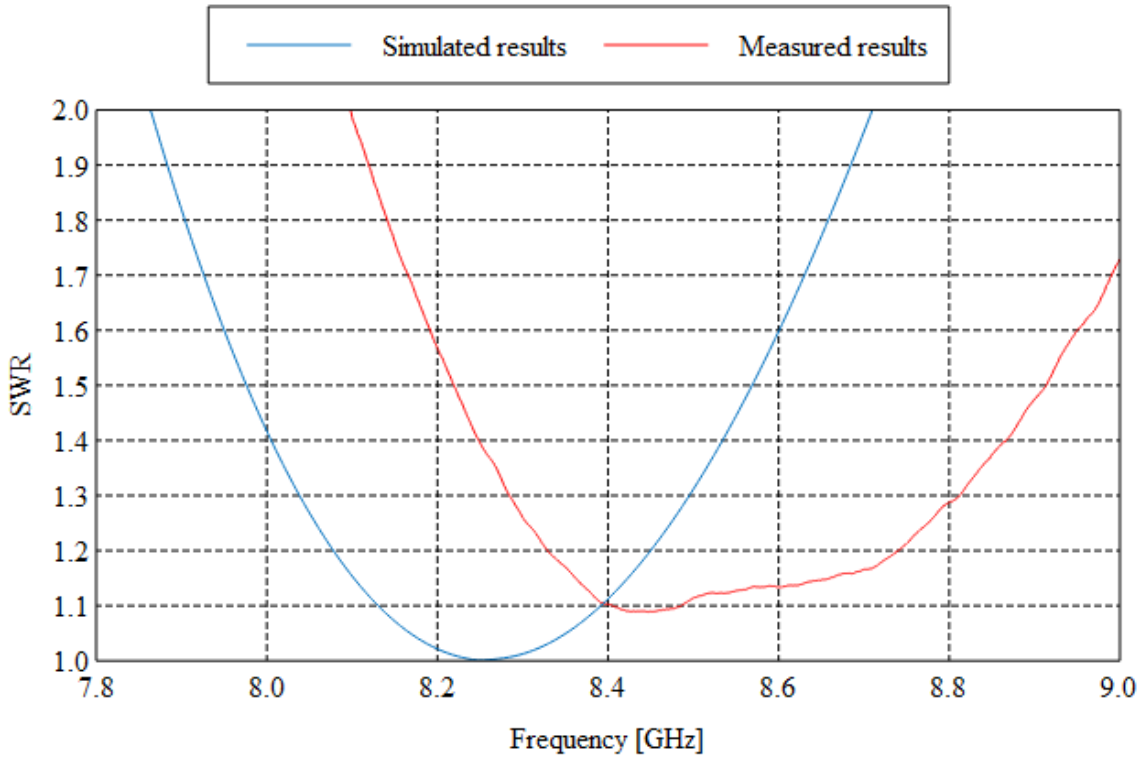

Figure 4-8: VSWR plots of the truncated patch antenna

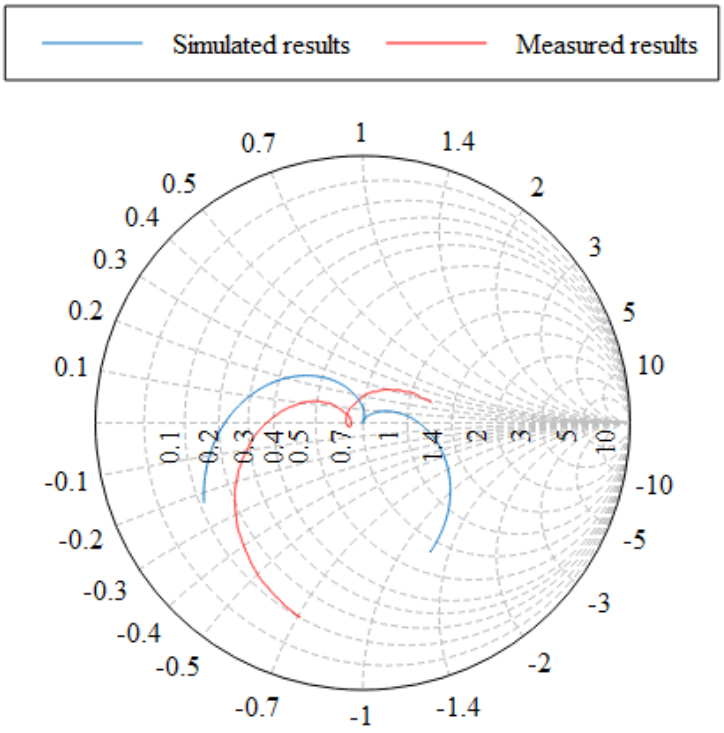

Figure 4-9: Input impedance of a truncated patch antenna

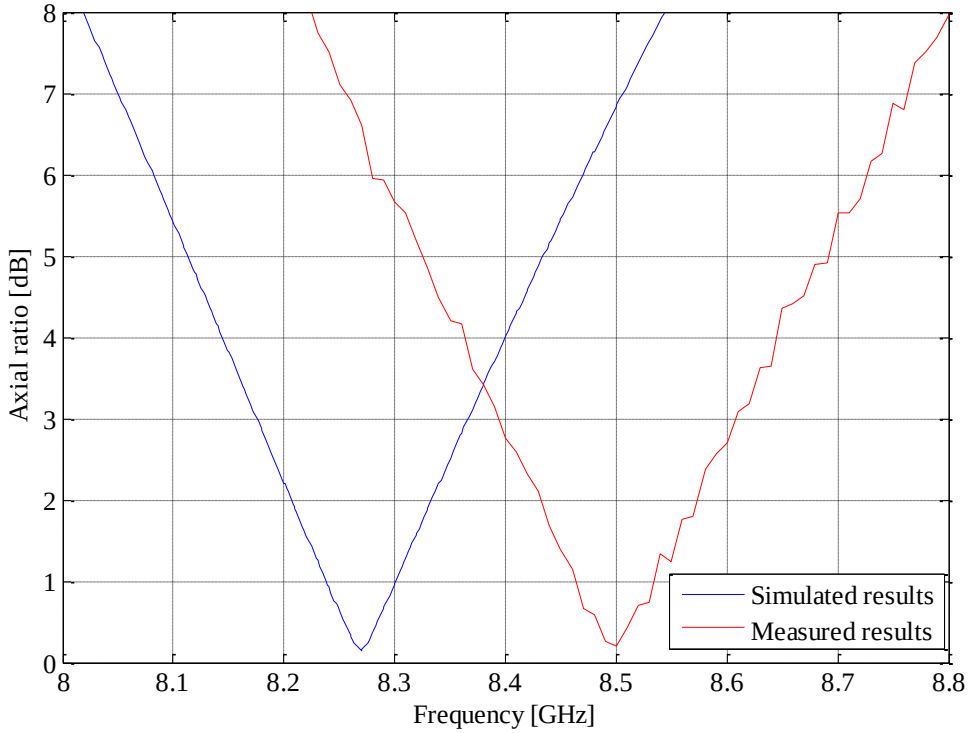

Figure 4-10: Truncated patch axial ratio at boresight

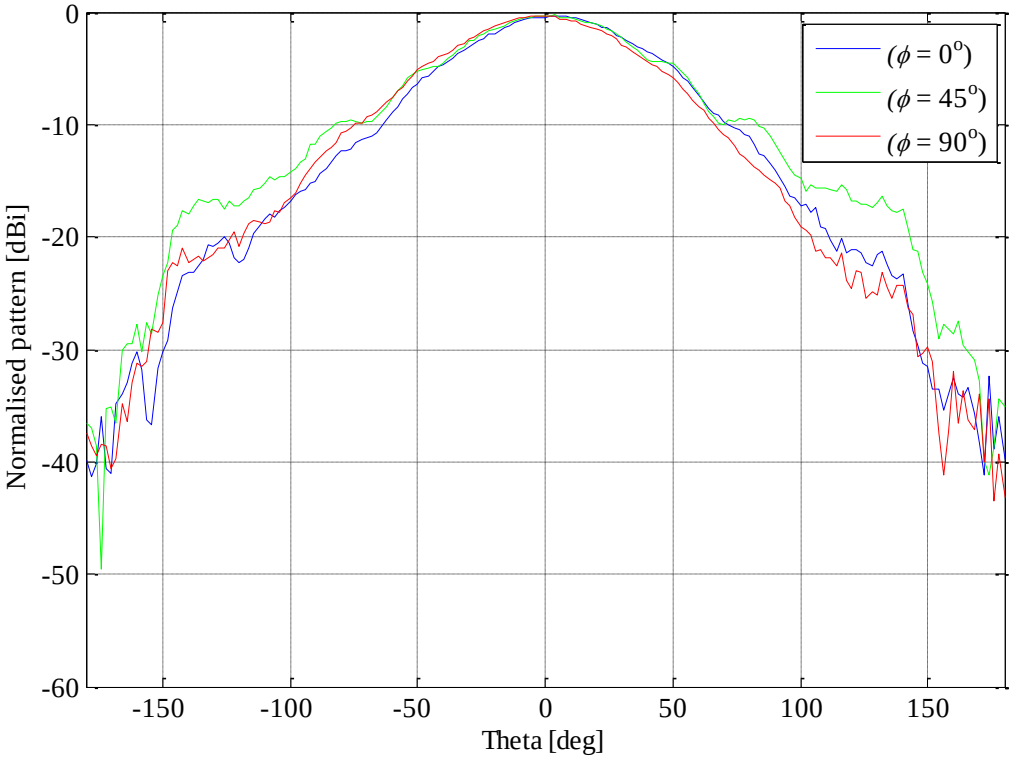

Figure 4-11: Normalised pattern of a truncated patch antenna at 8.5 GHz

4.3.3. Circular patch antenna

Figure 4-1c shows the circular patch antenna prototype. This model has the major radius and minor radius of 5.54 mm and 5.41 mm respectively with a 1.37 mm × 1.67 mm slot. The simulated and experimental VSWR plots are presented in Figure 4-12, with centre frequencies of 8.25 GHz and 8.41 GHz respectively. Again, the VSWR plot of the experimental model is off the desired resonant frequency of 8.25 GHz due to a high input reactance component. At 8.41 GHz, the input reactance is minimal but the real part is less than 50 Ω (Z_{in} = 42.8 + j1.11 Ω) resulting in higher VSWR. This is shown in Figure 4-13. The antenna yields a VSWR ≤ 2 bandwidth of 11%, which is the same as for the other two single patch antenna prototypes.

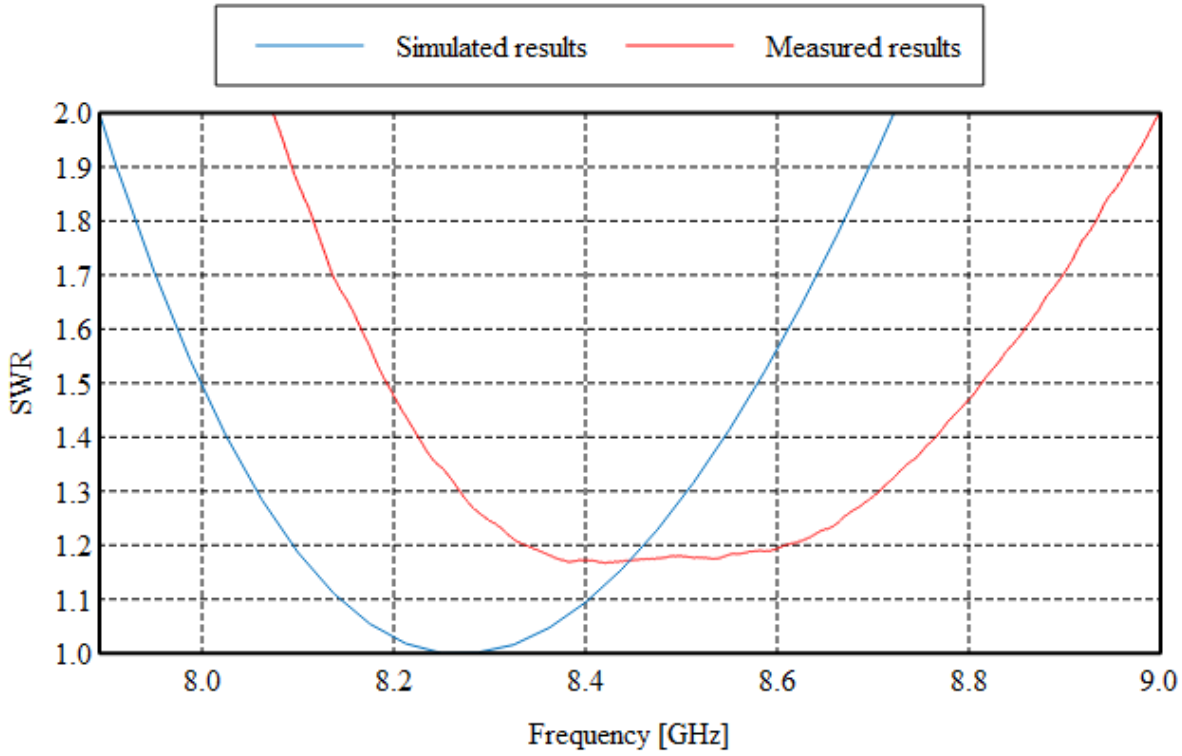

Figure 4-12: VSWR plots of circular patch antenna

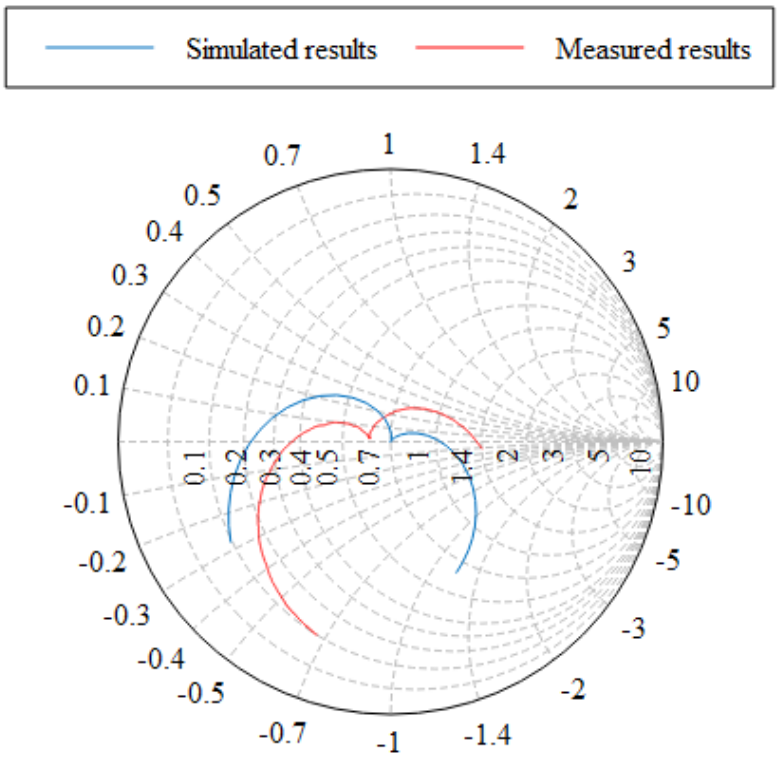

Figure 4-13: Circular patch input impedance

The axial ratio of the experimental model as depicted in Figure 4-14 is minimal at 8.41 GHz. This can also be verified by the normalised pattern plot of Figure 4-15 as the electric field in the three plane cuts that were chosen have the same amplitude for a specific beamwidth. The 3 dB AR bandwidth is approximated to 2.4 %. For the gain measurements, the gain transfer method was used since the gain of one antenna is known (Balanis, 2005:1033). This test method requires both the test and standard antennas to have their gain measured and thereafter, the difference in the gain can be compared to the known value of gain. Mathematically, this is described by equation 4-1.

$$G = G_K - (G_S - G_T) \text{ dB} \qquad 4\text{-}1$$

Where:

G_K is the given or known gain (NSI-RF-RGP-10 Antenna, refer to the appendix),

G_S is the measured gain for the standard antenna and

G_T is the measured gain for the antenna under test

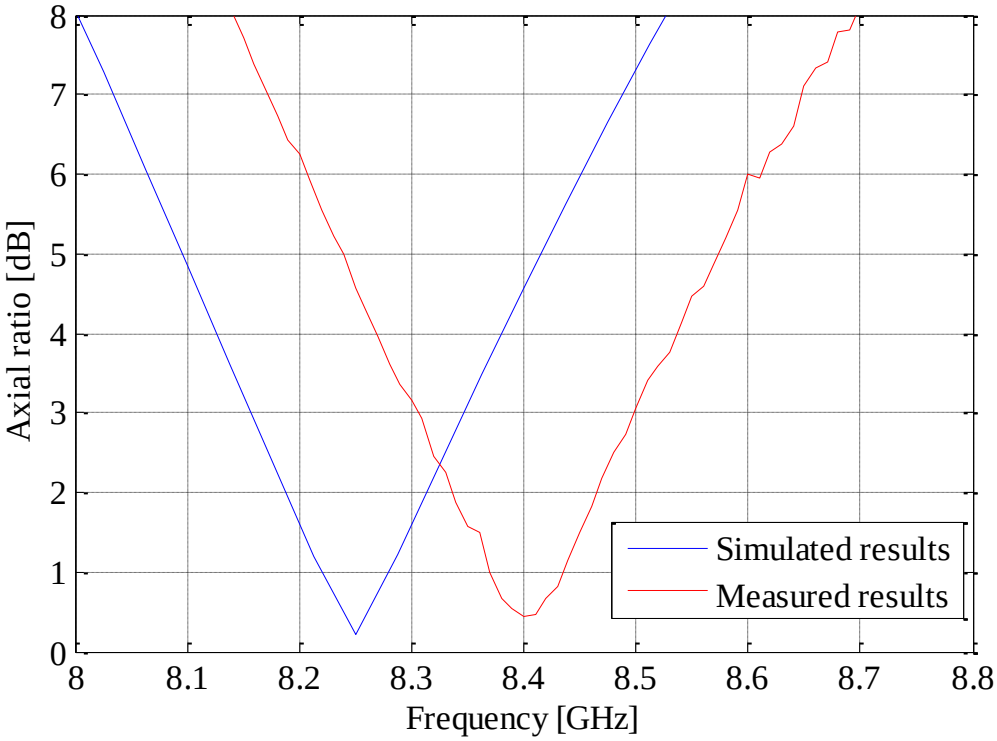

Figure 4-14: Circular patch axial ratio at boresight

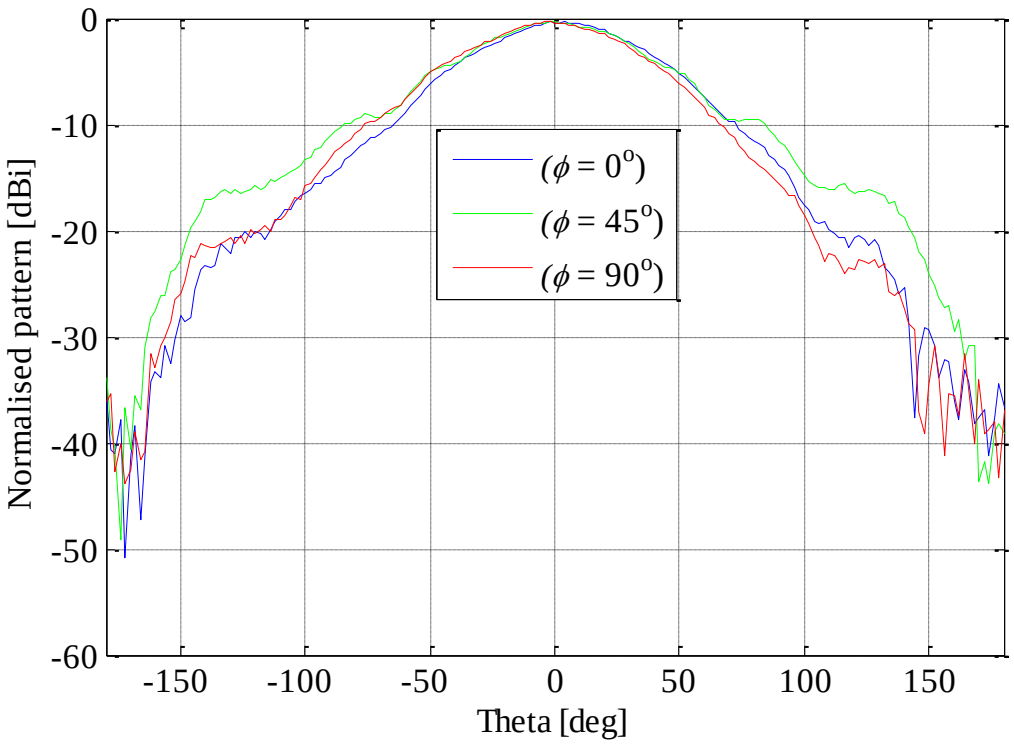

Figure 4-15: Normalised pattern of a circular patch at 8.4 GHz

Figure 4-16 presents a comparison of the LHCP gain of circular patch prototype and FEKO model. In this figure, it can be observed that the difference between the gain of the two antenna models is insignificant and the prototype gain peaks at 8.4 GHz. The ripples on the measured gain result from reflections within the cable and connectors. However, the results are still within the acceptable range.

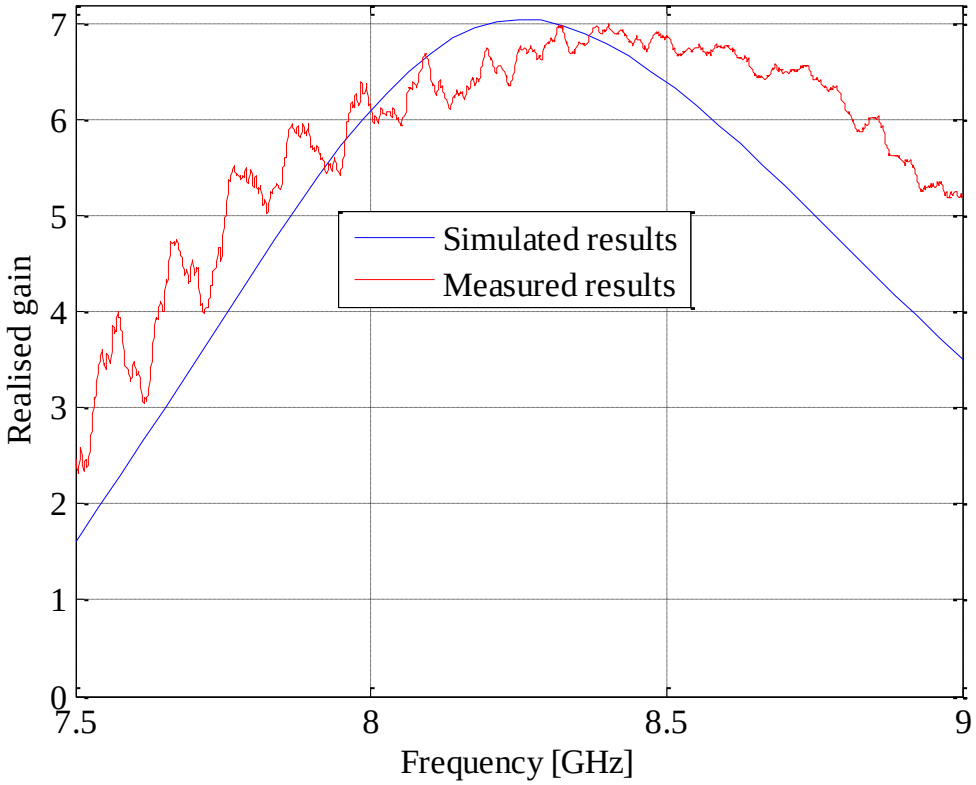

Figure 4-16: Comparison of simulated and measured gain of a circular patch antenna over frequency

4.3.4. Sequential rotated array

The sequential rotated 2×2 patch antenna array was realised on an RT 5880 Rogers substrate board as shown in Figure 4-1d. The patch has a radius of 6.84 mm with a 1.13 mm × 1.63 mm slot. Results, as measured on the prototype antenna are shown in Figures 4-17, 4-18, 4-19, 4-20, and 4-21. The measured VSWR plot presented in Figure 4-17 has modal frequencies at 7.81 GHz and 8.43 GHz, which results in a resonant frequency of 8.12 GHz. This frequency is lower than the specified resonant frequency. Figure 4-18 presents the impedance of this particular prototype on a

Smith chart. The small circle on the impedance plot indicates the frequency point with best axial ratio, which in this instance did not occur at the point with best matching.

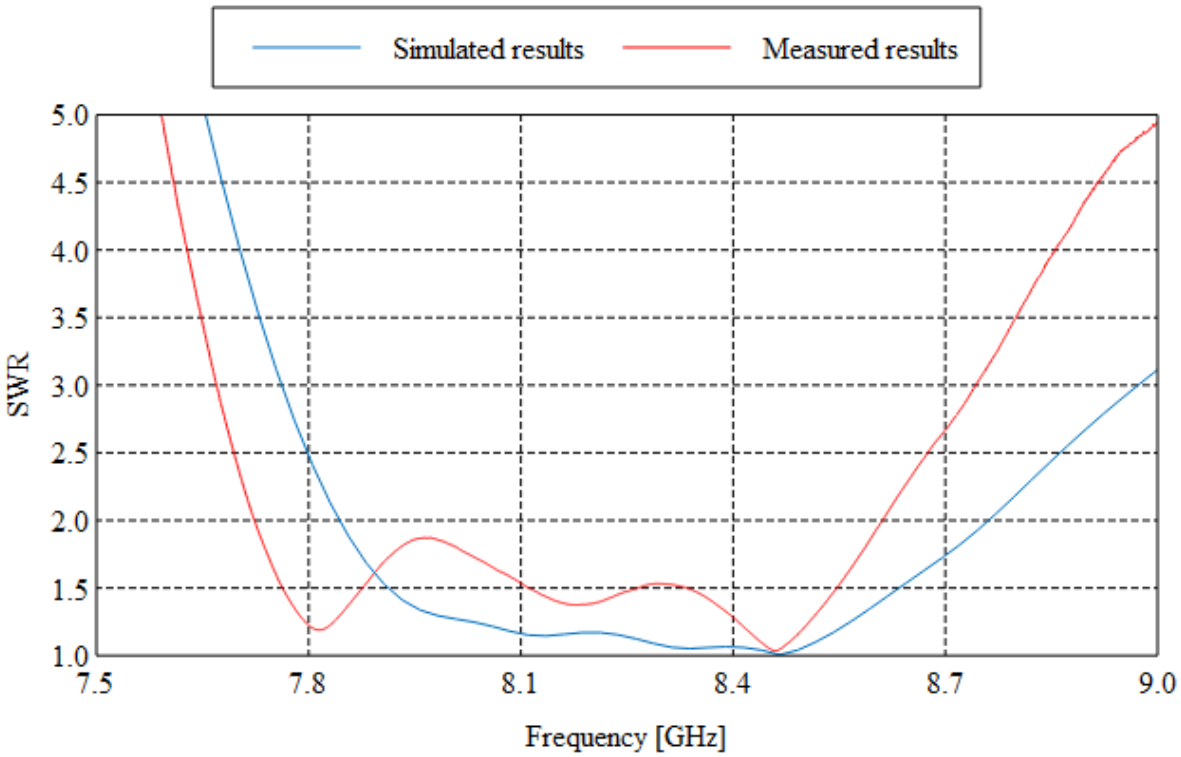

Figure 4-17: Sequential rotated array VSWR plots

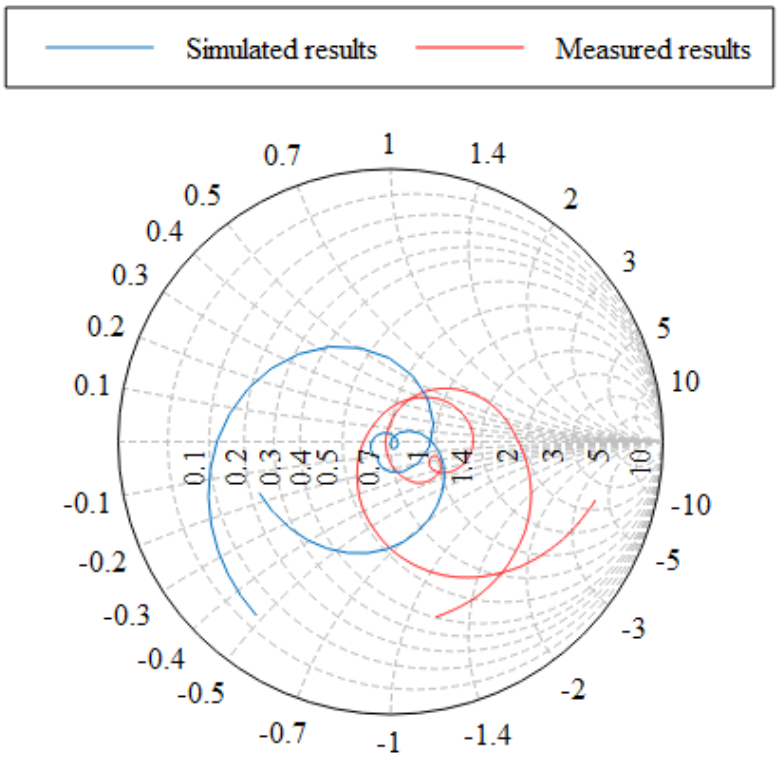

Figure 4-18: Input impedance of the sequential rotated patch array

The axial ratio is minimal at 8.12 GHz and the 3 dB axial ratio bandwith has increased significantly when compared to that of a single patch element. The normalised radiation pattern also confirms equal electric field magnitude for a specific beamwidth, which signifies circular polarisation. It is worth noting that the radiation pattern is more directive meaning that the energy is concentrated more in a specific direction. This narrows the pattern and results in higher gain. The gain measurement that is shown in Figure 4-21 was obtained using the gain transfer method. The maximum measured gain is 12 dBi at 8.12 GHz.

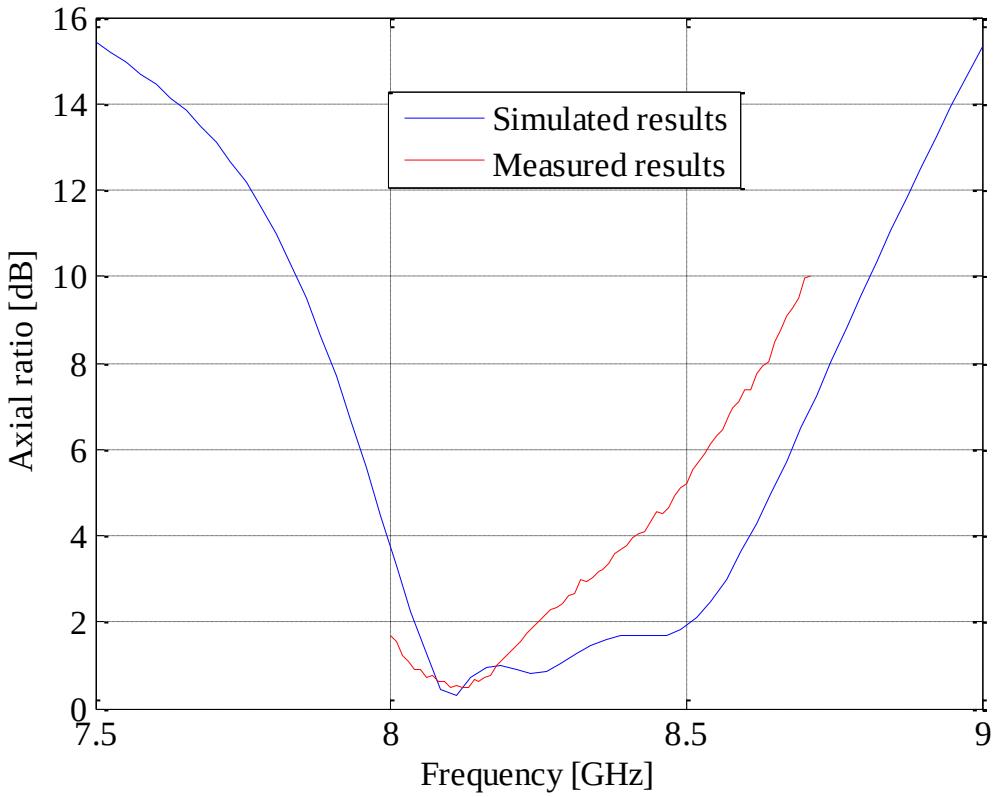

Figure 4-19: Sequential rotated array axial ratio measurements at boresight

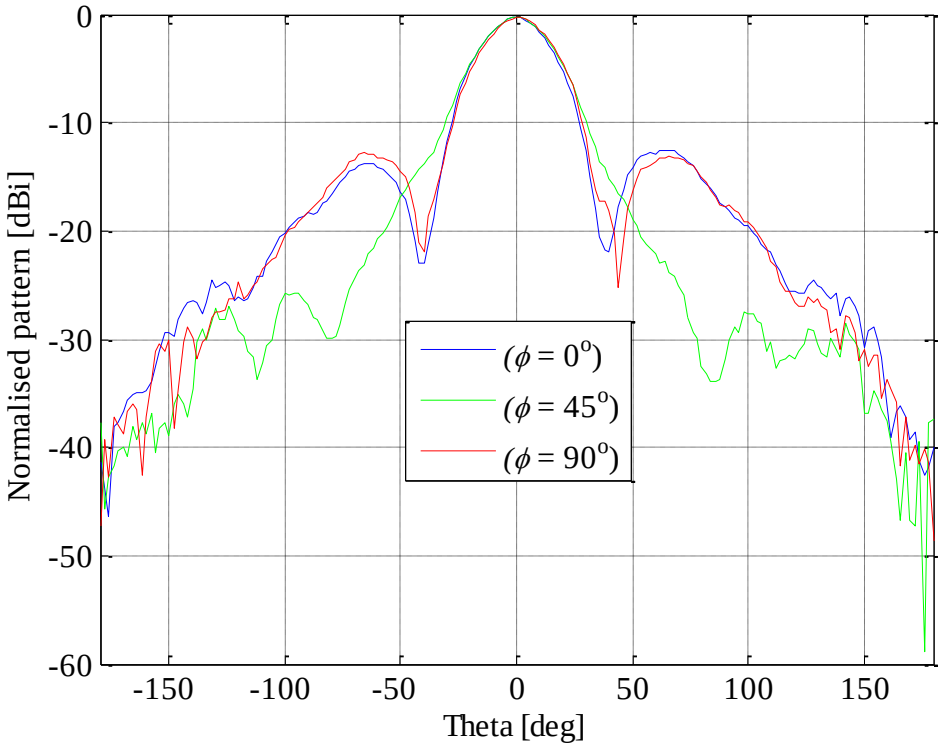

Figure 4-20: Normalised radiation pattern of the sequentially rotated array at 8.12 GHz

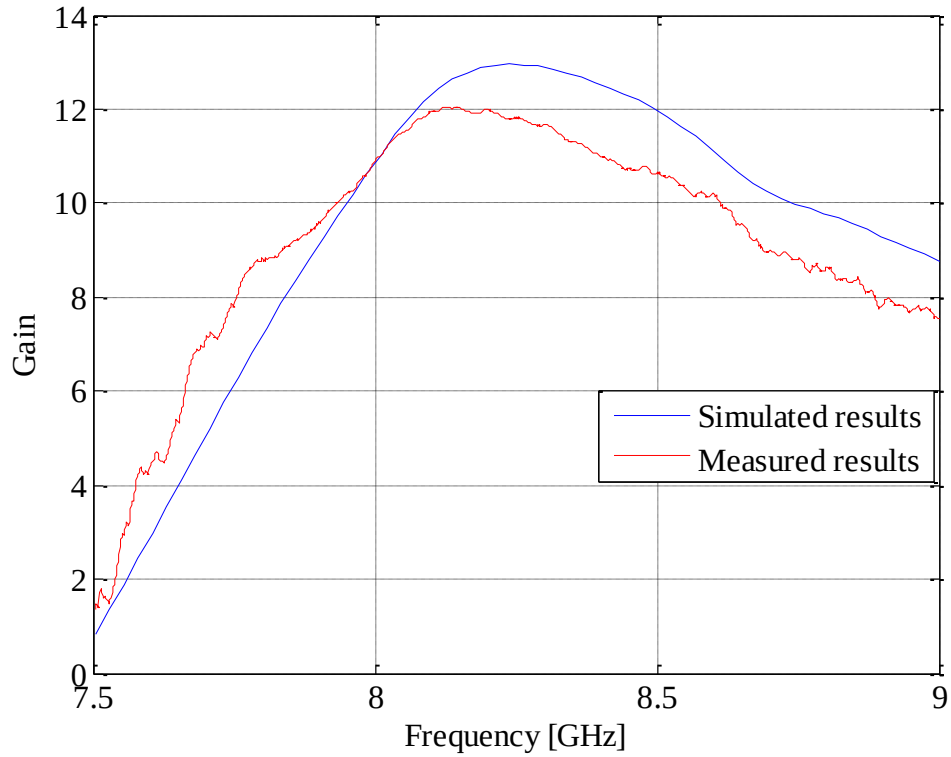

Figure 4-21: Sequentially rotated patch array gain over frequency

4.4 Conclusions

Chapter 4 has focused mainly on the experimental results of the antenna prototypes. The common antenna measurements, which are radiation pattern, gain, impedance matching, polarisation, and bandwidth, were analysed. The measurements were done at Stellenbosch University. The observation that was made was that the centre frequency had shifted to a higher value due to the manufacturing process. This was verified by simulations in FEKO. A follow up study will be made, where services of the professional PCB manufacturer will be used. Other than this, all the experimental antennas yield acceptable results.

Chapter 5

Conclusions and recommendations

5.1 Conclusions

The conformal patch antenna intended for use in satellite applications was designed, built, and tested. There were slight differences between the simulated and measured results due to manufacturing tolerances. Despite inaccuracies, the experimental model's performance was within the operable range. Future work will include improvements in the manufacturing process.

The single patch has a wide VSWR ≤ 2 bandwidth but the 3 dB AR bandwidth quickly degrades as the frequency is swept off resonance due to the impossibility of maintaining conditions needed for circular polarisation. The sequential rotated array has improved axial ratio bandwidth and gain compared to a single patch antenna. The array's narrower main beam may require an attitude determination and control system to point the antenna to the exact ground position.

5.2 Recommendations

- Rogers Corporation supplied the substrate material that was used to make the antennas. It is recommended that the performance of the antennas on low cost substrates are investigated as an alternative.
- The manufacturing process needs to be improved so that the accuracy of the FEKO models can be verified.
- A detailed parametric study is also essential to allow developing a technique that compensates for manufacturing tolerances.
- As the antenna needs to be mounted on a CubeSat, a mounting enclosure is required. This may have an effect on the antenna's performance and needs to be investigated.

Bibliography

Alexopolous, N.G., Broas, R.F., Sievenpiper, D., Yablonovitch, E. & Zhang, L. 1999. High-impedance electromagnetic surfaces with a forbidden frequency band. *IEEE Transactions on Microwave Theory and Techniques*, 47(11): 2059-2074, November.

Altair (2017). *FEKO: User manual.*

Bahl, I., Bhartia, P., Garg, R. & Ittipitoon, A. 2001. *Microstrip antenna design handbook.* London: Artech House.

Balanis, C.A. 2005. *Antenna theory analysis and design*. 3rd ed. New Jersey: Wiley.

Farr, D. & Henderson, B. 2014. Antenna design challenges for new-generation nano satellites. *Microwave Journal*: 24-34, August.

Gallée, F., Bernabeu, T., Cabedo-Frabrès, M., Antonino-Daviu, E. & Valero-Nogueria, A. 2013. Application of the theory of characteristic modes to the design of compact metallic strip antenna with multilayer technology (LTCC). *Proceedings of the 7th European conference on Antennas and Propagation*, 8-12 April 2013. Gothenburg: 1891-1895.

Gardelli, R., Albani, M. & La Cono, G. 2005. An efficient, fully-planar cavity backed module for smart array antennas. *2005 IEEE Antennas and Propagation Society International Symposium*:10-13, July.

Hall, P.S., Dahele, J.S. & James, J.R. 1989. Design principles of sequentially fed wide bandwidth circularly polarised microstrip antennas. *IEE proceeding*, 136(5): 381-389, October.

Hall, P.S. 1989. Application of sequential feeding to wide bandwidth, circularly polarised microstrip patch arrays. *IEE proceeding*, 136(5): 390-398, October.

Henry, G. 2014. *Spacecraft dynamic environment testing.* Washington: NASA.

Huang, J. 2006. Microstrip antenna: analysis, design and application. In William, I.A. (ed.). *Spaceborne antennas for planetary exploration*. New Jersey: Wiley.

Huang, J. 1986. A technique for an array to generate circular polarisation with linear polarised elements. *IEEE Transactions on Antennas and Propagation*, 34(9): 1113-1124, September.

Ippolito, L.J. 1999. *Propagation effects handbook for satellite systems design*. 5th ed. Virginia: NASA.

Jackson, D.R. & Alexopoulos, N.G. 1991. Simple approximate formulas for input resistance, bandwidth and efficiency of a resonant rectangular patch. *IEEE Transactions on Antennas and Propagation*, 39(3): 407-410, March.

Jackson, D.R., Williams, J.T., Bhattacharyya, A.K., Smith, R.L., Buchheit, S.J. & Long, S.A. 1993. Microstrip patch designs that do not excite surface waves. *IEEE Transactions on Antennas and Propagation*, 41(8): 1026-1037, August.

Jackson, D.R. 2007. Microstrip antennas. In Volakis, J.L. (ed.). *Antenna engineering handbook*. 4th ed. New York: McGraw-Hill.

James, J.R. & Hall, P.S. 1989. *Handbook of microstrip antennas.* London: Peter Peregrinus.

Jeun-Wen, W. & Jui-Han, L. 2003. 2×2 circularly polarised patch antenna arrays with broadband operation. *Microwave and Optical Technology Letters*, 39(5): 360-363, December.

Kristensson, G., Waller, P. & Derneryd, A. 2001. *Radiation efficiency and surface waves for patch antennas on inhomogeneous substrates*. Lund University, Lund.

Kumar, G. & Ray, K.P. 2003. *Broadband microstrip antennas.* London: Artech House.

Levine, E., Malamud, G., Shtrikman, S. & Treves, D. 1989. A study of microstrip array antennas with the feed network. *IEEE Transactions on Antennas and Propagations,*37(4): 426-434, April.

Levy, R. 1995. The relationship between dual mode cavity cross-coupling and waveguide polarisers. *IEEE Transaction on Microwave Theory and Techniques,* 43(11): 2614-2620, November.

Llombart, N., Neto, A. & De Maagt, P. 2004. Planar circularly symmetric EBG structures-design and analysis. *Proceedings of the 34th European Microwave Conference*, Amsterdam, 2004.

Lumini, F., Cividanes, L. & Lacava, J.C. da S. 1999. Computer aided design algorithm for singly fed circularly polarised rectangular microstrip patch antennas. *International Journal for RF and Microwave CAE 9,* 32-41, May.

Mabrouk, E. 2015. *What are SmallSats and CubeSats*?
[**Online**]. Available from:
www.nasa.gov/content/what-are-smallsats-and-cubesats
[Accessed 10/02/2017]

Martin, A.R. 1991. *Spacecraft/plasma interactions and electromagnetic effects in LEO and polar orbits.* Culham: Culham Laboratory.

Mendhe, S.E. & Kosta, Y.P. 2012. Stacked three layer rectangular microstrip patch antenna for ultra wide band applications. *Proceedings of international journal of Computer Science and communication,* 3(1): 145-147, June.

Milligan, T.A. 2005. *Modern antenna design.* 2nd ed. New Jersey: Wiley.

Narbudowicz, A.Z. 2013. *Advanced circularly polarised microstrip patch antennas.* A dissertation submitted in full fulfilment of the requirements for the Doctor of Philosophy: Electrical & Electronic Engineering in the faculty of Engineering at the Dublin Institute of Technology.

Nascimento, D.C., Schildberg, R. & Lacava, J.C. da S. 2008. Design of low cost microstrip antennas for Glonass applications. *Progress in Electromagnetics Research Symposium*: 199-202, July.

Nascimento, D.C. & Lacava, J.C. da S. 2011. Design of low-cost probe-fed micristrip antennas. In Prof. Nasimuddin Nasimuddi (Ed.), *Microstrip antennas*. InTech. Available from: http://www.intechopen.com/books/microstrip-antennas/design-of -low-cost-probe-fed-microstrip-antennas

Nivetha, K. & Monica, A. 2015. Microstrip patch array antenna for X-Band applications. *International Journal of Engineering Research & Technology*, 4(3): 543-545, March.

Oraizi, H. & Rezaei, B. 2011. Improvement of antenna radiation efficiency by the suppression of surface waves. *Journal of Electromagnetic Analysis and Applications*, 3(3): 79-83, March.

Pozar, D.M. & Schaubert, D.H. (eds). 1995. Microstrip antennas: *The analysis and design of microstrip antennas and arrays*. New Jersey: Wiley.

Reckeweg, M. & Rohner, C. 2015. *Antenna basics.* [**Online**]. Available from: https://www.rohde-schawrz.com/za/applications/antenna-basics-white-paper-230854-59777.html [Accessed 18/04/2017]

Stutzman, W.L. & Thiele, G.A. 2013. *Antenna theory and design*. 3rd ed. New Jersey: Wiley.

Whittlesey, A. & Garret, H.B. 2000. NASA's technical handbook for avoiding on-orbit ESD anomalies due to internal charging effects. *Proceeding of the 6th Spacecraft Charging Technology Conference, AFRL-VS-TR-20001578*: 131-134, September.

Wilke, R., Hamid, S., Schraml, K., Khunti, R. & Heberling, D. 2013. Multi-layer patch antenna array design for Ka-band satellite communication. *2013 SBMO/IEEE MTT-S International Microwave & Optoelectronics Conference*, August.

Zhang, X. & Zhu, L. 2016. Gain-enhanced patch antennas with loading of shorting pins. *IEEE Transactions on Antennas and Propagation*, 64(8): 3310-3318, August.

Appendix

NSI-RF-RGP-10 Antenna Properties

Product description

NSI-RF-RGP-10 is a 0.75 - 10 GHz Dual Ridged Waveguide Horn suitable for use as a near-field measurement probe for spherical near-field systems. The wide bandwidth of this probe allows it to replace several standard Open Ended Waveguide (OEWG) Probes, eliminating the need to change probes frequently. The probe is delivered with typical measured probe correction data from NSI to serve as the probe model for the SNF near-field measurement process.

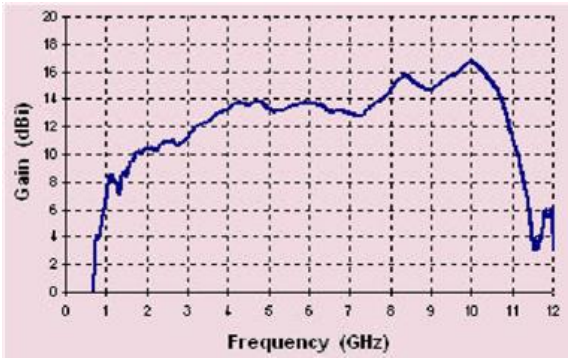

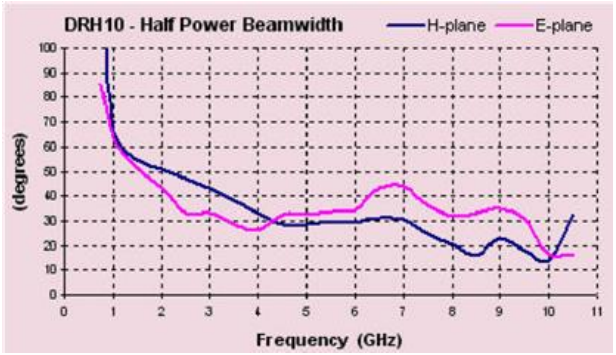

Features

- Broad Frequency Band 0.75 - 10 GHz
- Connector N(f)
- NSI SNF Pattern Calibration Files (typical)
- Includes mounting flange and outline drawing
- VSWR max < 1.6:1
- Gain 3 - 16 dBi
- Cross polarization > 25 dB
- Maximum input power 100 W CW, 200 W peak

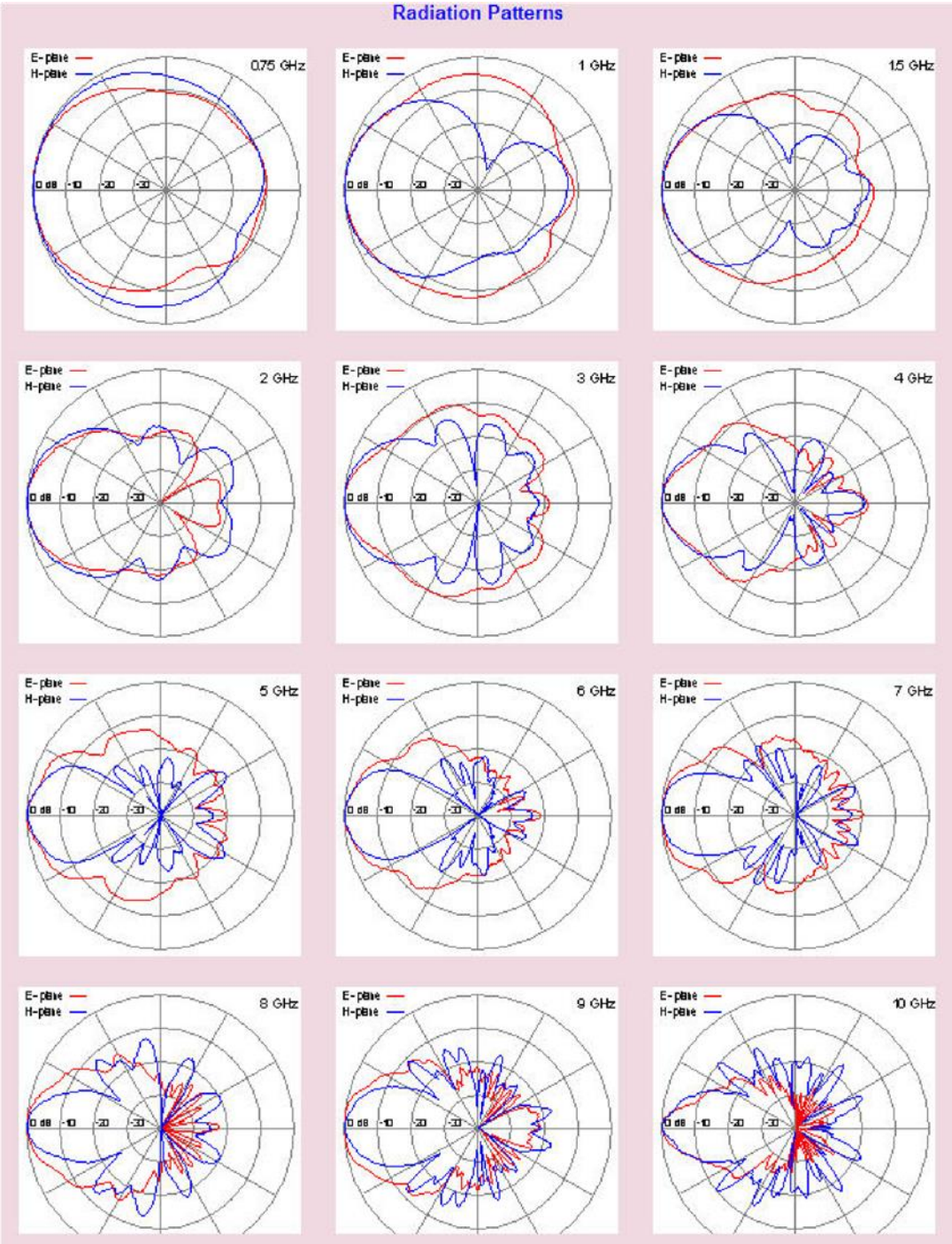
Radiation Patterns
E-plane
H-plane
0.75 GHz
1 GHz
1.5 GHz
2 GHz
3 GHz
4 GHz
5 GHz
6 GHz
7 GHz
8 GHz
9 GHz
10 GHz
0 dB
-10
-20
-30